UNIVERSITÉ DE MONTRÉAL

UNBALANCED THREE-PHASE LOAD-FLOW USING A POSITIVE-SEQUENCE LOAD-FLOW PROGRAM

JAIME PERALTA
DÉPARTEMENT DE GÉNIE ÉLECTTRIQUE
ÉCOLE POLYTECHNIQUE DE MONTRÉAL

MÉMOIRE PRESENTÉ EN VUE DE L'OBTENTION
DU DIPLÔME DE MAÎTRISE ÈS SCIENCES APPLIQUÉES
(GÉNIE ÉLECTRIQUE)
AOÛT 2007

Your file Votre référence
ISBN: 978-0-494-36929-6
Our file Notre référence
ISBN: 978-0-494-36929-6

UNIVERSITÉ DE MONTRÉAL

ÉCOLE POLYTECHNIQUE DE MONTRÉAL

Mémoire intitulé:

UNBALANCED THREE-PHASE LOAD-FLOW USING A POSITIVE-SEQUENCE LOAD-FLOW PROGRAM

présenté par: PERALTA Jaime
en vue de l'obtention du diplôme de: Maîtrise ès sciences appliquées
a été dûment accepté par le jury d'examen constitué de:

M. OLIVIER Guy, PhD., président
M. MAHSEREDJIAN Jean, PhD., membre et directeur de recherche
M. DE LEON Francisco, PhD., membre et co-directeur de recherche
M. ROY Gilles, M.Sc.A., membre

DÉDICACE

À ma très chère femme est mes merveilleuses filles

À mes chers parents

ACKNOWLEDGEMENTS

I would like to express my appreciation to all people who made possible the realization of this research project. A special acknowledgment has to be done to the company CYME International Inc., which has contributed to this research with financial, technical and very specialized professional support. I really appreciate the confidence of its President, Mr. Marc Coursol, who believed and trusted in the benefit of this research.

I would like to thank the research co-director Dr. Francisco De Leon from CYME, who has shown me how comprehensive and interesting power systems steady-state analysis domain can be. He collaborated with proper orientation, valuable information, ideas, and useful hints, all of them gathered along many years of experience doing research and writing papers about topics related to this domain and others.

Without any question, the most valuable and significant acknowledgment is addressed to Dr. Jean Mahseredjian, research director. A great professional and a remarkable person, who trusted my potential as a researcher and encouraged me to undertake this challenge. He was a great collaborator and I really appreciate and value having worked with him.

I would like to express my gratitude to Luce Pelletier of CYME International for her valuable contribution in proofreading and formatting several versions of a difficult manuscript. She did a lot more than correcting the typographical errors and improving the quality of the format, she suggested changes that have improved the readability of the final document.

I would like to thank again CYME International Inc. for all the support and for allowing me to become part of its permanent staff. It is a real pleasure for me, and I am very proud of being part of such a great team. Finally, and most importantly, I would like to express infinite acknowledgment to my loving family who, with love and patience, allowed me to overcome all difficulties found in this long path that I have chosen to take.

SUMMARY

Most of the existing commercial transmission load-flow packages have the capability of solving large balanced transmission systems using little computer memory and time processing. These tools are very efficient and accurate when a three-phase system can be represented by its positive-sequence equivalent circuit. Distribution systems are mostly unbalanced and radial, which makes the utilization of fast iterative sweep solvers for their analysis very attractive. The efficiency reached by most commercial load-flow software overcomes the lack of accuracy and precision caused by the modeling simplifications and assumptions made by both transmission and distributions simulation software. Typical system features and assumptions are: uncoupled devices, balanced loads, perfect line transposition, implicit neutral wire conductor and ground representation, and weakly meshed distribution systems. However, the interest for modeling more accurate real networks and solving complex integrated transmission-distribution systems has substantially increased among the operating and planning power system specialists.

The contribution of the present research work consists in the development of a multi-phase load-flow algorithm with the capability to model any coupled device and network features found in power systems along with to solve all the complexities mentioned above. The proposed methodology utilizes a positive sequence-based commercial load-flow solver. It relies on the use of positive-sequence equivalent circuits to represent all multi-phase electro-magnetically coupled devices found in transmission and distribution networks. Although uncoupled device models have previously been developed, none of those models has been implemented in an integral load-flow algorithm capable of solving complex composed transmission-distribution systems.

The simulation results were validated with the EMTP-RV load-flow package, which is the only commercial load-flow package known to the author that is capable of modeling and solving large and complex multi-phase networks. The validation test cases proved that the proposed algorithm has good numerical accuracy and robustness. The efficiency attained for large networks is comparable to the standard simulation performance exhibited by EMTP-RV.

CONDENSÉ EN FRANÇAIS

1 INTRODUCTION

La plupart des analyses d'écoulements de puissance dans les réseaux électriques sont exécutées pour des réseaux équilibrés, permettant une représentation monophasée ou de séquence positive des lignes, des transformateurs, des charges et autres dispositifs. Cependant, il existe des cas pour lesquels cette représentation n'est pas assez précise, comme c'est souvent le cas avec des systèmes de distribution non équilibrés, ou des systèmes de transmission où les lignes ne sont pas transposées et pour lesquels l'accouplement électromagnétique ne peut être négligé. Par conséquent, une représentation plus précise de tous les composants trouvés dans les réseaux électriques est fortement souhaitable et nécessaire pour surmonter ces complexités.

Beaucoup de méthodologies d'écoulement de puissance et de solutions numériques ont été proposées ces dernières années, certaines d'entre elles ont été mises en application dans différents logiciels commerciaux, mais aucune d'elles n'a été développée pour résoudre des configurations peu communes que l'on retrouve souvent dans les systèmes de distribution comportant le fil de neutre et la représentation de la terre.

2 OBJECTIF ET MÉTHODOLOGIE

L'objectif du présent travail est de développer un algorithme qui permette de résoudre des écoulements de puissance multiphasés non équilibrés pour des systèmes de transmission et de distribution, en utilisant un programme existant d'écoulement de puissance monophasé à séquence positive. La méthodologie utilisée propose une représentation monophasée et électromagnétiquement désaccouplée de tous les composants habituellement présents dans les réseaux électriques tels que les générateurs, les lignes de transmission, les câbles, les transformateurs, les compensateurs shunt, les charges, et les dispositifs de réglage de tension.

La méthodologie suivie dans cette recherche considère en premier lieu la modélisation de chacun des composants des réseaux multiphasés dans une représentation monophasée, ce qui implique la modélisation de tous les accouplements électromagnétiques présents dans chacun de ces composants. En second lieu, un algorithme d'écoulement de puissance est développé pour résoudre ces réseaux équivalents monophasés. L'algorithme, écrit dans Fortran-95, est basé sur la méthodologie conventionnelle d'écoulement de puissance à séquence positive de Newton-Raphson.

Finalement, étant donné qu'une validation des résultats est exigée, l'outil d'écoulement de puissance multiphasé du logiciel EMTP-RV [1] a été employé à cet effet dû à sa renommée de performance et d'efficacité. En outre, le solutionneur itératif d'écoulement de puissance pour systèmes de distribution CYMDIST [2] a été également utilisé pour comparer l'exactitude et l'efficacité de la méthodologie proposée pour des systèmes équilibrés et parfaitement transposés.

3 CONTRIBUTION DU PROJET DE RECHERCHE

La contribution principale de cette recherche consiste au développement d'un programme dans un environnement de séquence positive capable de modéliser:

- Générateurs et transformateurs avec différents raccordements.
- Lignes multiphasées électromagnétiquement couplées et découplées avec des hauts et bas rapports *R/X*.
- Lignes de un, deux, trois et quatre fils comprenant la représentation explicite de fil de neutre et de la terre.
- Réseaux radiaux et fortement bouclés comprenant des lignes transposées et non transposées.
- Charges non équilibrées à puissance, courant et impédance constantes reliées en delta ou en étoile ainsi que des charges branchées entre phases, phase et neutre et phases fusionnées.

- Ample rangée de tensions : des extra hautes tensions aux tensions résidentielles de distribution.

Bien que les dispositifs à tension commandés, tels que les régulateurs automatiques de tension ou les condensateurs à tension commandés, n'aient pas été inclus dans la portée de cette recherche, ils peuvent être facilement incorporés au moyen d'un processus itératif. Ainsi, ces dispositifs n'imposent pas une limitation à la méthodologie développée.

La plupart des limitations de convergence dans les solutionneurs d'écoulement de puissance itératifs au balayage arrière-avant (« Backward-forward sweep ») non équilibrés, disparaissent avec la méthodologie proposée dans ce travail, ce qui correspond à une des contributions principales de ce travail de recherche. Bien que le temps de simulation de la méthodologie proposée demeure encore élevé comparé aux méthodes itératives rapides pour de grands systèmes, la capacité d'obtenir des résultats précis est une contribution valable; particulièrement en considérant l'augmentation de la performance dans l'exécution du calcul et la capacité de mémoire des actuels processeurs.

Il existe présentement dans l'industrie, plusieurs outils commerciaux qui offrent la possibilité de résoudre des systèmes équilibrés de transmission ou des systèmes de distribution non équilibrés avec ses lignes idéalement transposées, mais peu d'entre eux peuvent résoudre des systèmes multiphasés complexes et des systèmes de transmission et de distribution composés. L'algorithme présenté dans cette recherche est une méthodologie appropriée et facile à implémenter pour résoudre ces systèmes complexes.

4 SOMMAIRE DU RAPPORT

Le chapitre 2 présente une description complète des plus importantes méthodologies d'écoulements de puissance triphasés et des solutions numériques. La portée et les limitations de ces techniques sont également discutées. Une attention particulière est portée aux méthodologies de solution utilisées par les logiciels d'écoulement de puissance EMTP-RV et CYMDIST. Dans le chapitre 3, les modèles équivalents monophasés désaccouplés de différents dispositifs des réseaux sont dérivés. La méthodologie et la structure de l'algorithme d'écoulement de puissance triphasé sont

présentées dans le chapitre 4. Un cas d'épreuve simple est présenté à la fin de ce chapitre afin de mieux comprendre la fonctionnalité de l'algorithme développé. Le chapitre 5 décrit trois cas d'épreuves utilisées à des fins de validation. Les résultats recueillis d'EMTP-RV, CYMDIST et l'algorithme développé sont comparés et discutés. Bien que la validation de l'exactitude de la méthodologie proposée soit le but principal de cette validation, un cas additionnel d'épreuve est inclus à la fin du chapitre 5 pour comparer la performance et la robustesse de la méthodologie proposée aux deux outils commerciaux utilisés.

5 CIRCUITS ÉQUIVALENTS MONOPHASÉS DES DISPOSITIFS TRIPHASÉS MUTUELLEMENT COUPLÉS

La méthodologie originellement proposée dans [35] et [37] comporte une représentation électromagnétiquement découplée de tous les composants des réseaux. Cette représentation monophasée découplée peut être facilement dérivée et comprise en termes de la théorie de graphiques élémentaires, et une fois cela fait, les éléments des branches peuvent être déterminés par inspection pour la majorité des cas. Les éléments découplés résultants peuvent être facilement ajoutés à la matrice d'admittance du réseau, indépendamment de la taille du système, après application de l'inversion d'une petite matrice d'impédance primitive symétrique. Cette méthode est exacte et numériquement stable, et elle s'est montrée robuste pour les systèmes de transmission et de distribution autant théoriques que pratiques.

A. Représentation des lignes et des câbles

Une ligne triphasée équilibrée est typiquement représentée par son impédance série à séquence positive, en plus de deux admittances parallèles (modèle π). Dans la méthodologie proposée, une section de ligne triphasée est représentée par 21 lignes, où 15 d'entre elles représentent la matrice d'impédance et les 6 autres, les accouplements mutuels capacitifs tel qu'indiqué dans la figure 3.2.

La matrice d'admittance $\boldsymbol{Y_{Bus\_L}}$ pour la ligne triphasée, montrée dans la figure 3.2, est formée en multipliant l'inverse de la matrice d'impédance primitive $\boldsymbol{Z_{prim}}$ par sa matrice

d'incidence nœud-branche [37] correspondante. La matrice résultante est montrée dans l'équation (3.15).

Le modèle de ligne à trois fils, dérivé auparavant, peut représenter soit une ligne triphasée, une ligne biphasée avec le fil neutre, ou une ligne monophasée avec le fil de neutre et la terre.

Le modèle de ligne à deux fils peut représenter une ligne biphasée ou une ligne monophasée avec le neutre ou la terre, donc il est extrêmement utile pour l'analyse de réseaux de distribution. Sa représentation est semblable à celle de la ligne à trois fils mais le nombre de lignes artificielles est de 6. Pour le cas d'une section de ligne triphasée à quatre fils, qui peut représenter une ligne triphasée avec le fil de neutre ou la terre, ou une ligne biphasée avec le fil de neutre et la terre, le nombre de lignes artificielles est de 28. Ce modèle peut être dérivé de la même façon que pour le modèle de ligne triphasée. Cette même méthodologie peut aussi être appliquée pour représenter les modèles de sections de câbles multiphasés couplés.

B. Représentation de transformateurs

La méthode pour modéliser le transformateur a été proposée en premier par Chen dans [39]. Celui-ci calcule fondamentalement la matrice d'incidence constituée par le raccordement d'unités de transformateurs monophasés. Tous les modèles typiques de raccordements de transformateur peuvent être dérivés avec cette méthodologie, y compris les raccordements peu communs souvent trouvés dans des systèmes de distribution. Fondées sur l'hypothèse des transformateurs monophasés reliés pour former des transformateurs triphasés, les matrices d'incidence du transformateur sont développées en suivant la même approche nodale que pour le modèle de ligne. Ainsi, la matrice $\boldsymbol{Y}_{Bus\_T}$ résultant d'un transformateur triphasé de branchement delta-étoile à la terre est montré dans l'équation (3.26), où y_t correspond à l'admittance de fuite d'unité des transformateurs monophasés et les paramètres α, β représentent la prise de tension hors nominal sur les côtés primaires et secondaires du transformateur, respectivement [39]. Par inspection de la matrice d'admittance de nœuds (3.26), le modèle du transformateur

triphasé avec ses lignes artificielles de couplage peut être facilement dérivé, et le circuit résultant est montré dans la figure 3.4.

D'autres raccordements de transformateurs, dont les modèles ont été développés dans [42], sont les transformateurs avec raccordements étoile-delta ouvert et delta ouvert-delta ouvert. Ces raccordements permettent de fournir, par exemple, un réseau biphasé avec le fil de neutre à partir d'un système triphasé dans le côté du primaire, permettant l'alimentation des charges biphasées ou monophasées à neutre, typiques dans des systèmes de distribution. Généralement les charges de distribution sont non équilibrées, impliquant le fait d'avoir des charges monophasées et triphasées présentes dans la même artère. Ainsi, les transformateurs de distribution triphasés à quatre fils avec prise milieu (« Mid-Tap ») du côté du secondaire sont très typiques dans les réseaux de distribution [44]. Ces transformateurs se composent d'un transformateur monophasé avec trois fils au secondaire, deux fils pour les phases plus un fil de neutre, ou un ou deux transformateurs monophasés avec seulement deux fils de phase. Les transformateurs de distribution triphasés à quatre fils permettent d'opérer dans des situations non équilibrées et contribuent à fournir des charges triphasées et monophasées.

C. Représentation du Générateur

Une source triphasée est représentée par son circuit équivalent de Thevenin incluant ses tensions de nœuds internes et sa matrice d'impédance équivalente de Thevenin. Pour un nœud de référence, le vecteur de tension est connu et les puissances active et réactive sont déterminées par l'écoulement de puissance du système. Pour un nœud PV, l'amplitude de la tension sur la phase a et la puissance active sont connues, et l'angle de tension et la puissance réactive sont des variables inconnues. Des sources triphasées sont typiquement représentées dans des simulateurs à séquence positive par un générateur monophasé et son impédance de source interne. Puisque les impédances internes sont couplées dans de vrais générateurs, un générateur triphasé peut être modélisé utilisant trois générateurs à séquence positive en plus d'un modèle de ligne triphasée tel que montré dans la figure 3.14. Ainsi, les impédances internes des trois générateurs Z_a, Z_b, et Z_c sont fixées à zéro et la matrice d'impédance interne est représentée avec un modèle

équivalent de ligne triphasée découplée. Dans ce cas-ci, la tension dans le noeud de référence sera la tension au terminal du noeud de la phase *a* V_a (voir figure 3.14), et la magnitude de la tension interne du générateur sera calculée itérativement. Etant donné que les tensions internes doivent être les mêmes dans chacune des trois phases du générateur, les amplitudes de tension dans les phases *b* et *c* (E_b et E_c) sont forcées à être égal à E_a à chaque itération. Les angles de phase θ_a, θ_b, et le θ_c sont placés à 0°, 120°, et -120° respectivement au nœud des sources internes. Le déphasage dû au raccordement des transformateurs mène ou traîne l'angle d'initialisation, ce qui devrait être représenté dans la valeur initiale de tous les nœuds en aval de ces transformateurs.

D. Représentation de la charge et du fil de neutre

Des modèles typiques de charge connus sous le nom d'impédance constante, courant constant, et puissance constante peuvent être modélisés avec la méthodologie proposée. Les charges à puissance constante équilibrées peuvent être facilement représentées dans un logiciel d'écoulement de puissance à séquence positive en définissant explicitement les valeurs de P et de Q comme charge équilibrée mise à une terre infinie. Cependant, dans des systèmes de distribution non équilibrés, les charges sont souvent reliées au fil de neutre ou entre phases, donc, la représentation à séquence positive ne fonctionne pas correctement.

On propose ici une méthode itérative basée sur la dépendance qu'ont les impédances sur la tension, où l'impédance de charge est une fonction de la tension appliquée. En utilisant ces représentations de charge nous pouvons modéliser toutes sortes de charges trouvées dans des systèmes de distribution. Le raccordement de charges mono, bi, et triphasées raccordées en delta ou étoile, étant équilibrées ou non équilibrées, peut être représenté avec cette méthode itérative. Les logiciels conventionnels d'écoulement de puissance à séquence positive n'incluent pas une représentation explicite ni du fil neutre ni de la résistivité à la terre. Au contraire, ils assument toujours des systèmes triphasés équilibrés avec une résistivité de terre infinie pour les charges, les transformateurs et les générateurs. Dans la méthodologie proposée, le fil de neutre et la terre peuvent être représentés de façon explicite [22]. La terre infinie, ou le nœud de tension de référence

zéro, est explicitement incluse dans la méthodologie proposée, et, à cet effet, un nœud de tension zéro doit être modélisé.

La représentation d'un nœud de référence à tension zéro, obtenue en ajoutant un nœud PV à chaque nœud qui est raccordé à la terre, s'est révélée être la méthode la plus efficace pour représenter un nœud où la tension et la puissance sont égales à zéro. En ajoutant une contrainte nulle dans un nœud de référence PV, il est possible de représenter la terre infinie dans n'importe quel système en utilisant un logiciel d'écoulement de puissance à séquence positive.

E. Conditions initiales

Une approximation d'initialisation favorable est parfois nécessaire pour une convergence réussie de grands réseaux quand la méthode de Newton-Raphson est employée. Le départ à 1.0 p.u., (« flat start ») où des grandeurs de tension sont placées égales à leurs valeurs programmées (ou valeurs nominales) et où les angles sont égaux à la tension de noeud de référence, est habituellement suffisant. Ainsi, dans un programme triphasé, les angles à chaque nœud sont équivalents à l'angle du nœud de référence et habituellement placés à 0°, -120°, et +120° pour les phases a, b et c respectivement. Il y a quelques situations pour lesquelles cette première approximation n'est pas suffisamment un bon départ. On a constaté que le départ à 1.0 p.u., suivi d'un cycle de déplacements successifs sans sur-correction, est fortement favorable. Dans une série de cas, la solution précédente est habituellement un bon début pour le prochain cas. Cependant, puisque la méthode converge rapidement d'un départ à 1.0 p.u. et que la vérification des ajustements peut avoir lieu après seulement deux itérations, il en résulte qu'il est peu intéressant d'utiliser une autre méthode d'initialisation.

La méthode d'écoulement de puissance Gauss-Seidel utilise un temps de simulation très bas pour chaque itération. Ainsi l'idée d'employer cette méthode pour établir les conditions initiales pour la méthode de Newton est très attrayante pour de grands réseaux. Cependant, la méthode d'initialisation choisie pour ce projet de recherche a été le départ à 1.0 p.u. suivi d'un cycle de déplacements successifs des tensions [12].

6 ALGORITHME D'ÉCOULEMENT DE PUISSANCE TRIPHASÉ

L'algorithme développé en Fortran-95 est composé de deux modules. Le premier module a comme fonction de modéliser et de convertir un réseau multiphasé dans une représentation équivalente de réseau monophasé découplé. En raison du processus de conversion, un fichier de sortie de données est produit dans un format monophasé approprié, qui sera lu par le solutionneur d'écoulement de puissance à séquence positive. Le deuxième module et le moteur principal correspond à un solutionneur d'écoulement de puissance à séquence positive largement utilisé dans l'industrie électrique. Une description générale de l'algorithme d'écoulement de puissance triphasé est montrée dans le diagramme de flux de la figure 4.1.

Pour l'entrée des données, un format multiphasé qui correspond à une modification du format de données standard de l'IEEE pour l'échange de données d'écoulement de puissance [46] a été développé. Le format de sortie des données inclut l'amplitude de la tension et l'angle de phase à chaque nœud du système.

7 CAS D'ÉPREUVE ET VALIDATION DE RÉSULTATS

Trois systèmes d'épreuves ont été employés pour comparer la précision, la performance, et la robustesse de la méthodologie proposée. Le premier cas d'épreuve correspond à un système de distribution non équilibré de 34 nœuds d'IEEE présenté par Ciric dans [22]. L'objectif de ce premier cas est de valider la précision des résultats des réseaux de distribution radiaux non équilibrés en les comparant avec ceux d'EMTP-RV. Le solutionneur itératif CYMDIST est inclus dans cette première épreuve de validation puisqu'une parfaite transposition de lignes a été assumée dans le système. Le deuxième cas d'épreuve présenté correspond à un système de 40 nœuds développé en vue de valider la plupart des dispositifs et les complexités trouvées dans des systèmes de transmission et de distribution réels comme les générateurs, transformateurs avec différents raccordements, réseaux radiaux et bouclés, lignes couplées et non transposées, lignes multiphasées, charges phase à neutre et entre phases et banques de condensateurs.

Puisque le logiciel CYMDIST ne peut résoudre des systèmes comprenant des lignes non transposées, cette deuxième épreuve s'est faite sans sa contribution. Le troisième cas d'épreuve correspond à un très grand réseau non équilibré, fortement bouclé et avec des lignes idéalement transposées d'environ 2,600 nœuds. Ce cas d'épreuve a été employé pour valider la robustesse et la performance de l'algorithme développé comparé à EMTP-RV et au logiciel itératif rapide CYMDIST.

A. Cas d'épreuve modifié de l'IEEE de 34 nœuds

Des tableaux 5.1 et 5.2, il peut être observé que les résultats pour l'amplitude de tension et l'angle de phase à chaque noeud sont tout à fait semblables pour tous les trois solutionneurs. La plus grande erreur de magnitude de tension trouvée est seulement de 0.28%, même si la tension dans quelques noeuds est assez basse, ce qui montre également la robustesse de convergence de la méthodologie proposée. Ce premier cas d'épreuve correspond à un système radial, non équilibré, idéalement transposé et avec des charges monophasées et triphasées à puissance constante.

B. Cas d'épreuve d'un réseau de Transmission et Distribution de 40 nœuds

Les résultats obtenus pour l'amplitude et l'angle de phase à chaque nœud sont énumérés dans les tableaux 5.3 et 5.4. Le solutionneur itératif rapide CYMDIST n'est pas inclus dans cette épreuve de validation dû à ses limitations de convergence et à sa capacité de modélisation des systèmes complexes. Les résultats obtenus avec la méthodologie proposée sont tout à fait semblables à ceux obtenus avec EMTP-RV. L'erreur maximale de l'amplitude de tension trouvée était 0.6%. Ces petites erreurs peuvent être sensiblement réduites au minimum en employant une petite tolérance de convergence, et une grande précision numérique pour les charges et les paramètres d'impédances. Seulement deux itérations sont nécessaires pour atteindre la solution avec EMTP-RV et la méthodologie proposée.

C. Cas d'épreuve d'un réseau de Distribution de 2,600 nœuds

Un troisième cas d'épreuve impliquant un grand système de plus de 2,600 nœuds a été simulé afin de comparer la performance et la robustesse de la méthodologie proposée avec EMTP-RV et CYMDIST. L'épreuve a été réalisée sur un ordinateur Pentium 4, avec

un processeur de vitesse de 2 gigahertz et une mémoire de 512 Mb. Le temps de simulation et le nombre d'itérations pour chaque solutionneur sont présentés dans le tableau 5.5. Le temps de simulation présenté inclut le temps de lecture de données, ce qui n'est pas négligeable pour de grands réseaux. Tenant compte que la méthodologie proposée n'a pas été optimisée en termes de programmation, le temps de simulation semble être assez raisonnable. Le solutionneur itératif rapide CYMDIST présente le plus bas temps de simulation, mais aussi le plus grand nombre d'itérations dû au grand nombre de boucles dans le système. EMTP-RV prend moins de temps dans la lecture des données, mais en prends plus pour le processus itératif en comparaison avec la méthodologie proposée, ce qui semble être un avantage pour cette dernière, compte tenu du fait que le processus de lecture de données peut être facilement optimisé. La robustesse d'EMTP-RV et de la méthodologie proposée sont semblables, et même supérieures à celle du solutionneur rapide, tenant compte du nombre élevé d'itérations exigées par ce dernier pour converger.

8 CONCLUSIONS

Le présent travail de recherche a consisté au développement d'une méthodologie pour résoudre des écoulements de puissance multiphasés, en utilisant un solutionneur d'écoulement de puissance à séquence positive existant basé sur la méthodologie de Newton avec un solutionneur numérique direct et un arrangement optimal des matrices. L'intégration des systèmes de transmission et de distribution dans une seule simulation, ainsi que la capacité à modéliser, de façon précise, tous les dispositifs type trouvés dans les systèmes de transmission et de distribution réels, sont les principales contributions de ce travail de recherche.

Les principaux avantages de la méthodologie proposée et de l'algorithme développé peuvent être récapitulés comme suit :

- La capacité inhérente de résoudre des systèmes multiphasés, ce qui est très attrayant pour des applications de réseaux de distribution comportant une représentation explicite du fil neutre et de la terre. Les systèmes multiphasés

incluent des sections de ligne avec n'importe quelle combinaison des conducteurs de phase et de fils neutre, tels que monophasé, monophasé avec neutre, biphasé, biphasé avec neutre, triphasé, triphasé avec neutre et ainsi de suite.

- La capacité de modéliser des circuits multiphasés parallèles avec leurs couplages électromagnétiques correspondants.
- La représentation explicite de différents types de charges telles que mono, bi ou triphasés sont acceptées.
- Des charges raccordées soit en delta ou en étoile étant équilibrées ou non équilibrées peuvent aussi être modélisées.
- Des lignes idéalement transposées et non transposées peuvent être modélisées avec cette méthodologie dû à sa capacité de représenter les couplages électromagnétiques existants entre phases d'un circuit ou entre circuits de lignes voisins.
- La capacité à simuler de grands systèmes comprenant des réseaux bouclés et radiaux dû à sa formulation matricielle et à sa robustesse de convergence.
- Toutes sortes de raccordements de transformateurs peuvent être représentés avec cette méthodologie comprenant des raccordements peu communs trouvés dans des réseaux de distribution tels que le transformateur avec raccordement en étoile ou delta ouvert, et celui avec prise milieu (« Mid-Tap »).
- De grands rapports de tension (V_{max}/V_{min}) aussi bien que de grands rapports de X/R pour les paramètres de ligne sont également soutenus.
- La possibilité de modéliser et de simuler de grands réseaux de transmission et de distribution composés, et des configurations complexes telle que les charges en phases fusionnées, qui sont des charges reliées entre les phases de conducteurs de différentes artères.

Les résultats des simulations ont montré que la méthodologie proposée est très précise. L'erreur de tension la plus élevée est inférieure à 0.2% et elle pourrait augmenter à un maximum de 0.5% pour de grands rapports de tension dans les réseaux simulés. Néanmoins, on peut éliminer cette petite erreur en considérant une plus grande précision

dans le calcul des paramètres en par unité (« per unit »), réduisant de cette façon au minimum les erreurs numériques approximatives. Le nombre d'itérations est bas et très semblable à ce qui est obtenu avec EMTP-RV, confirmant la grande robustesse de la méthodologie présentée. L'épreuve réalisée pour le cas de 2,600 nœuds a prouvé que le temps de simulation atteint par l'algorithme développé est près du temps pris par EMTP-RV. Le temps de simulation mesuré dans tous les cas d'épreuve a inclus le temps pris pour la lecture de données et le temps d'exécution.

TABLE OF CONTENTS

LIST OF TABLES

LIST OF FIGURES

1 INTRODUCTION

1.1 Power systems and load-flow

Load-flow analysis is performed for the calculation of node voltages and active and reactive line flows for a given electrical network configuration and a given load and power generation. It is mostly used in power systems planning, and control and operation analysis of transmission and distribution systems for either steady state or dynamic operation initialization.

Most load-flow analysis in transmission systems are executed for balanced networks, allowing a single-phase (or positive-sequence) representation of lines, loads and other devices. This representation is widely used for most software developers and users of load-flow applications. Positive-sequence load-flow assumptions such as perfect line transposition, balanced loads, and electromagnetically uncoupled lines have shown to be quite accurate simplifications for the performance and simulation of transmission networks. On the other hand, there are cases in which this representation is not accurate enough as is often the case with distribution systems. There are also transmission systems where non-transposed (untransposed) lines and electromagnetic coupling (mutual impedance) are present and cannot be neglected. As a result, a more accurate and full multi-phase representation of all components found in the electrical network is strongly desirable and needed to model those complex features.

Many load-flow methodologies and numerical solutions have been proposed in the past years, and some of them have been implemented in different commercial software packages. However, not many of them have been oriented to solve unusual configurations that can be often found in distribution systems involving neutral wire conductor and ground representation. This is the domain of interest and the scope of this research work.

1.2 Research objective and methodology

1.2.1 Objective

The objective of this research is to develop an algorithm that permits to solve unbalanced multi-phase load-flow for transmission and distribution systems, using an existing positive-sequence load-flow solver. The methodology utilized involves a positive-sequence representation of all multi-phase electromagnetically coupled components present in electrical networks such as generators, transmission lines, cables, transformers, shunt and series compensators, loads, and voltage-controlled devices. The motivation for choosing this particular methodology comes from an interest of developing a multi-phase load-flow algorithm using as a solver engine a positive-sequence software package readily available in the power industry.

1.2.2 Methodology

The methodology followed in this research considers several steps. First and foremost is the modeling of all four-, three-, double-, or single-phase network components in a positive-sequence representation, which involves the modeling of all electromagnetic couplings present in each of these components.

Second, once all the devices are modeled, a load-flow algorithm is implemented to solve the positive-sequence equivalent network. The algorithm is based on a conventional positive-sequence Newton-Raphson load-flow methodology that will be discussed afterwards. This solver considers an efficient handling of the Jacobian matrix to solve the node voltages in the network. The algorithm was programmed in Fortran-95 and considered a structured programming for the network devices modeling.

Finally, provided that a validation of load-flow results is required, the software EMTP-RV was chosen as the benchmark tool due to its well-known and proven performance. EMTP-RV uses its own computational method to solve unbalanced load-flow in the phase-domain [1]. In addition, the fast iterative backward-forward sweep solver CYMDIST, whose methodology is described in [2], is also used to compare the

performance against the proposed methodology for electromagnetically balanced network test cases. This validation involved the design and implementation of several test case systems in both CYMDIST and EMTP-RV graphical user interfaces (GUI).

Furthermore, format data base conversion from EMTP-RV Netlist files to a modified IEEE format was required in order to compare large systems without the necessity of building huge test cases with the EMTP-RV or CYMDIST GUI. The IEEE modified format corresponds to an extension of the known IEEE common data format, and it permits to model multi-phase devices for load-flow analysis. This benchmark analysis includes not only a comparison of the accuracy of the proposed methodology, but also other features related to robustness and performance such as number of iterations and simulation time.

1.3 Report outline

Chapter 2 presents a comprehensive description of the most important existing three-phase load-flow methodologies and numerical solutions. Scope and limitations of those techniques are also discussed. Special attention is given to the EMTP-RV and the CYMDIST load-flow solution methodologies. In chapter 3, the positive-sequence equivalent models for electromagnetic coupled devices are derived. The methodology and structure of the multi-phase load-flow algorithm is presented in chapter 4. A simple test case is presented at the end of this chapter in order to better understand functionality of the developed algorithm. Chapter 5 describes three test cases used for validation purposes. Results gathered from EMTP-RV, CYMDIST and the developed algorithm are compared and discussed. Even though the accuracy validation of the proposed methodology is the main purpose of this validation benchmark, an additional test case is included at the end of Chapter 5 to compare the performance and robustness of the methodology against the two commercial packages.

In chapter 6, the conclusion, recommendations and suggestions for further research are given.

1.4 Research contribution

The major contribution of this research is the development of a positive-sequence environment program capable of accurately modeling:

- Tens of thousands of busses of varied voltage levels to cover simultaneously generation, transmission, distribution, industrial, and residential networks.
- Swing and constant PV generators, transformer with different connections, capacitor banks, and voltage-controlled devices.
- Electromagnetic coupled and uncoupled multi-phase lines with high and low R/X ratios.
- Single-, double, three-, and four-phase lines including explicit neutral wire and ground representation.
- Heavily meshed and radial networks including both transposed and non-transposed lines.
- Delta- and wye-connected unbalanced constant power, impedance, and current loads along with phase-to-neutral, phase-to-phase and phase-merged loads.

Although voltage-controlled devices such as automatic voltage regulators or voltage-controlled capacitors were not included within the scope of this research, they can be easily incorporated by means of an iterative process, so it does not impose a limitation on the developed methodology.

Most of the convergence limitations in unbalanced backward-forward iterative load-flow solvers disappear with the methodology presented in this research, which is one of the major contributions of this work. Even though simulation time of the proposed methodology remains still high compared to fast iterative sweep methods for large systems, the ability to get accurate results is a valuable contribution specially considering the increase in computing performance such as processing time and memory capacity.

There exist in the industry several commercial packages with the capability of solving either balanced transmission systems or load unbalanced lightly meshed distribution systems with ideally-transposed lines, but few have the capability of solving

complex and compounded multi-phase transmission and distributions systems. The algorithm presented in this research is a suitable and easy to implement methodology for solving those complex systems.

Another contribution corresponds to the development of a comprehensive but not exhaustive bibliographical research about the load-flow solution methodologies for both single- and three-phase systems.

2 METHODOLOGIES AND NUMERICAL SOLUTIONS FOR POSITIVE-SEQUENCE AND THREE-PHASE LOAD-FLOW ANALYSIS

This chapter is dedicated to the description and comparison of typical load-flow methodologies and numerical solvers utilized by most of the three-phase load-flow applications. A review of the conventional positive-sequence load-flow methodologies is presented at the beginning of this chapter. Special emphasis is placed on three methodologies: backward-forward sweeps, Newton-Raphson, and Gauss-Seidel. Other methods such as Z-matrix, fast-decoupled and current injection are also presented.

Numerical solvers for matrix formulation have been widely developed and can be found in multiple publications. It is beyond the scope of this research to find a more efficient solver solution. Nevertheless, some of the most important methods are described, and their advantages and limitations discussed in this chapter.

2.1 Positive-sequence load-flow methodologies

2.1.1 Load-flow formulation

A standard positive-sequence load-flow analysis involves the calculation of voltage magnitude and phase angle at each bus in a network operating under balanced steady-state conditions. The calculation of voltages permits computing active and reactive power flows, currents and losses for each device in the network. Figure 2.1 shows all the variables associated with a bus k: voltage magnitude V_k, phase angle δ_k, net real power P_k, and reactive power Q_k. Two of these variables are generally known (input data), and the other two are the unknown variables to be computed by a load-flow algorithm.

In the following, matrices will be represented in bold uppercase characters and vectors in bold underlined characters unless otherwise is specified.

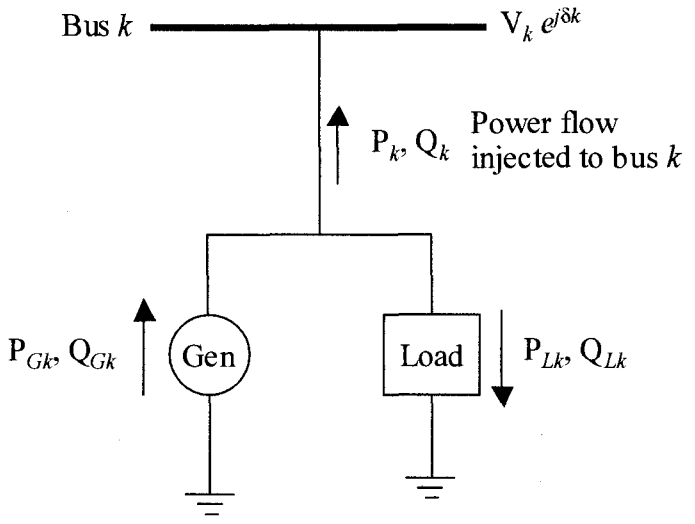

Figure 2.1 Load-flow variables associated to a bus *k*

The power delivered (injected) to bus k is separated into generation and load terms, and each bus is categorized as either swing (reference), voltage controlled, or load bus.

$$P_k = P_{Gk} - P_{Lk}$$
$$Q_k = Q_{Gk} - Q_{Lk}$$

The bus admittance matrix $\boldsymbol{Y_{Bus}}$ is assembled from lines, transformers and other devices data, and their elements are:

y_{kk} = $\sum$ (Admittances connected to bus k)

$y_{kl} = y_{lk}$ = -$\sum$ (Admittances connected between bus k and l, $k \neq n$)

The static power-flow equations for a network of n buses, considering the nx1 current vector as $\underline{\boldsymbol{I}}_{\boldsymbol{Bus}}$ and the nx1 voltage vector as $\underline{\boldsymbol{V}}_{\boldsymbol{Bus}}$, are [3]:

$$I_k = \left(\frac{S_k}{V_k}\right)^* = \frac{P_k - jQ_k}{V_k^*} \qquad \textbf{(2.1)}$$

$$I_k = \sum_{l=1}^{n} Y_{kl} V_l \qquad \textbf{(2.2)}$$

$$P_k - jQ_k = V_k^* \sum_{l=1}^{n} Y_{kl} V_l \qquad \text{with } k = 1,\ldots,n \qquad \textbf{(2.3)}$$

Replacing the bus voltage and the admittance matrix elements by their rectangular form we get:

$$V_k = e_k + jf_k$$

$$Y_{kl} = G_{kl} + jB_{kl}$$

$$P_k = e_k\left(\sum_{l=1}^{n}(G_{kl}e_l - B_{kl}f_k)\right) + f_k\left(\sum_{l=1}^{n}(G_{kl}f_l + B_{kl}e_k)\right) \quad \textbf{(2.4)}$$

$$Q_k = f_k\left(\sum_{l=1}^{n}(G_{kl}e_l - B_{kl}f_k)\right) - e_k\left(\sum_{l=1}^{n}(G_{kl}f_l + B_{kl}e_k)\right) \quad \textbf{(2.5)}$$

If the voltage polar representation is considered, the equations are:

$$V_k = |V_k|e^{j\delta_k}$$

$$Y_{kl} = |Y_{kl}|e^{j\varphi_{kl}}$$

$$P_k = |V_k|\sum_{l=1}^{n}|Y_{kl}||V_l|\cos(\delta_k - \delta_l - \varphi_{kl}) \quad \textbf{(2.6)}$$

$$Q_k = |V_k|\sum_{l=1}^{n}|Y_{kl}||V_l|\sin(\delta_k - \delta_l - \varphi_{kl}) \quad \textbf{(2.7)}$$

An alternative representation of power flow equations is the hybrid form, which is the polar voltage form mixed with the rectangular admittance elements. That is:

$$P_k = |V_k|\sum_{l=1}^{n}|Y_{kl}||V_l|[\cos(\delta_k - \delta_l)\cos\varphi_{kl} + \sin(\delta_k - \delta_l)\sin\varphi_{kl}]$$

$$Q_k = |V_k|\sum_{l=1}^{n}|Y_{kl}||V_l|[\sin(\delta_k - \delta_l)\cos\varphi_{kl} - \cos(\delta_k - \delta_l)\sin\varphi_{kl}]$$

Separating the real and imaginary parts, we obtain:

$$G_{kl} = |Y_{kl}|\cos\varphi_{kl}$$

$$B_{kl} = |Y_{kl}|\sin\varphi_{kl}$$

$$P_k = |V_k|\sum_{l=1}^{n}|V_l|[G_{kl}\cos(\delta_k - \delta_l) + B_{kl}\sin(\delta_k - \delta_l)] \quad \textbf{(2.8)}$$

$$Q_k = |V_k| \sum_{l=1}^{n} |V_l| [G_{kl} \sin(\delta_k - \delta_l) - B_{kl} \cos(\delta_k - \delta_l)] \quad \textbf{(2.9)}$$

Although the polar expressions are simpler than the Cartesian formulation, their formulations are unsuitable for computer analysis, since it would be highly inefficient to make repeated calls of implicit trigonometric functions [4]. Thus, it is very common to express the hybrid formulation equations in a more compact form by replacing the trigonometric functions by Cartesians equivalents.

2.1.2 Gauss-Seidel load-flow solution

Starting from the complex form of the equations (2.3), rearranging the terms and assuming V_1 as the reference voltage [3], we get:

$$P_k - jQ_k = V_k^* Y_{kk} V_k + V_k^* \sum_{\substack{l=1 \\ l \neq k}}^{n} Y_{kl} V_l \quad \textbf{(2.10)}$$

$$V_k = \frac{1}{Y_{kk}} \left[\frac{P_k - jQ_k}{V_k^*} - \sum_{\substack{l=1 \\ l \neq k}}^{n} Y_{kl} V_l \right] \qquad \text{with } k = 2,\ldots,n \quad \textbf{(2.11)}$$

Where n is the total number of nodes in the systems. Nodal equations $\underline{\boldsymbol{I}}_{Bus} = \boldsymbol{Y}_{Bus} \underline{\boldsymbol{V}}_{Bus}$ are a set of linear equations equivalent to $\underline{\boldsymbol{b}} = \boldsymbol{A}\underline{\boldsymbol{x}}$, which are solved by an iterative process given by:

$$V_k^{(i+1)} = \frac{1}{Y_{kk}} \left[\frac{P_k - jQ_k}{V_k^{(i)*}} - \sum_{l=1}^{k-1} Y_{kl} V_l^{(i+1)} - \sum_{l=k+1}^{n} Y_{kl} V_l^{(i)} \right] \quad \textbf{(2.12)}$$

The swing or reference voltage bus is an input data usually set to 1.0 [pu] with and angle of 0°. For a voltage-controlled bus, Q_k is unknown, and can be calculated by the equations (2.5), (2.7) or (2.9). If a given Q_k does not exceed its limits, it is used to calculate $V_k^{(i+1)}$ and $\delta_k^{(i+1)}$ which replaces the values of $V_k^{(i)}$ and $\delta_k^{(i)}$ in (2.12) for a PQ (or load) bus. In addition, only $\delta_k^{(i+1)}$ is used for voltage-controlled buses, because the voltage magnitude $V_k^{(i+1)}$ is input data. The common stopping or convergence criterion for the Gauss-Seidel method is to use the scaled difference in the voltage between one

iteration to the next, as shown in equation (2.13). When this difference is smaller than a specified convergence tolerance ε for each bus, the problem is considered solved.

$$\left|\frac{V_k^{(i+1)} - V_k^{(i)}}{V_k^{(i)}}\right| < \varepsilon \qquad \text{For all } k=1, 2, \ldots N \qquad \textbf{(2.13)}$$

To reduce the number of iterations required to reach the final solution, an acceleration factor can be added in order to project forward the calculated voltage in the direction of its trend as is shown below:

$$V_{k(acc.)}^{new} = V_k^{old} + \alpha(V_k^{new} - V_k^{old})$$

This acceleration factor α, which varies between 1.0 or 2.0, allows to reduce the number of iteration when the final voltage values are far from the initial guess.

2.1.3 Z-Matrix load-flow solution

Y-matrix methods such as the Gauss-Seidel technique described before suffer from the problem of poor convergence, or even divergence, of successive calculated voltages for ill-conditioned systems. One of the techniques that overcome some of those difficulties is the ***Z***-matrix method [4].

By inverting the $\boldsymbol{Y_{Bus}}$ matrix of the nodal equation system $\underline{\boldsymbol{I}}_{\boldsymbol{Bus}}=\boldsymbol{Y_{Bus}}\underline{\boldsymbol{V}}_{\boldsymbol{Bus}}$ we get:

$$\underline{V}_{Bus} = Z_{Bus} \times \underline{I}_{Bus} \qquad \textbf{(2.14)}$$

Where:

$$Z_{Bus} = Y_{Bus}^{-1} \qquad \textbf{(2.15)}$$

Rearranging the terms to remove the reference voltage V_1 from vector $\underline{\boldsymbol{V}}_{\boldsymbol{Bus}}$ we obtain:

$$V_k = \sum_{k=2}^{n} Z_{kj}(I_j - Y_{j1}V_1) \qquad k=2,3,\ldots,n \qquad \textbf{(2.16)}$$

$$V_k = \sum_{k=2}^{n} Z_{kj}I_j - \sum_{k=2}^{n} Z_{kj}Y_{j1}V_1 \qquad k=2,3,\ldots,n \qquad \textbf{(2.17)}$$

$$V_k = \sum_{k=2}^{n} Z_{kj}I_j - C_k \qquad k=2,3,\ldots,n \qquad \textbf{(2.18)}$$

Where:

$$C_k = \sum_{k=2}^{n} Z_{kj} Y_{j1} V_1 \qquad \textbf{(2.19)}$$

Since V_1, the reference or alack bus voltage, is fixed in magnitude and angle each C_k factor is a constant. The solution process of equation (2.18) for the block substitution of ***Z***-matrix method is as follows [4]:

1. Invert matrix $\boldsymbol{Y_{Bus}}$ and compute all the constants C_k from equation (2.19).
2. Compute all the injected currents using equation (2.1).
3. With the current obtained from the previous step, compute all the bus voltages using equation (2.18).
4. Compare the latest set of voltages with the previous ones and if the two sets are within a defined tolerance, then the process is complete. If they are not, then return to step 2.

The main advantage of the ***Z***-matrix method over the Gauss-Seidel technique is the dramatic reduction in the number of iterations required to reach the solution. Even though the inversion of the $\boldsymbol{Y_{Bus}}$ matrix is required once, its convergence performance is superior to that of the Gauss-Seidel method [4].

2.1.4 Newton-Raphson load-flow solution

The Newton-Raphson (NR) solution is a powerful and widely used methodology for solving non-linear equations. It transforms a non-linear problem into a sequence of linear problems whose solution converges to the solution of the original non-linear problem. If we consider the vector of solution $\underline{\boldsymbol{x}}^{(0)}$ for an n-dimensional equation $\underline{\boldsymbol{f(x)}}=0$, and we expand each equation in a Taylor series around an initial condition, retaining only the first derivative terms [3], we have:

$$
\begin{aligned}
& f_1(x^{(0)}) + \left(\frac{\partial f_1}{\partial x_1}\right)^{(0)} \Delta x_1 + \cdots + \left(\frac{\partial f_1}{\partial x_n}\right)^{(0)} \Delta x_n \approx 0 \\
& \vdots \\
& f_n(x^{(0)}) + \left(\frac{\partial f_n}{\partial x_1}\right)^{(0)} \Delta x_1 + \cdots + \left(\frac{\partial f_n}{\partial x_n}\right)^{(0)} \Delta x_n \approx 0
\end{aligned}
\tag{2.20}
$$

Rewriting the system of n linear equations in a matrix form:

$$
\begin{bmatrix} f_1(x^{(0)}) \\ \vdots \\ f_n(x^{(0)}) \end{bmatrix} + \begin{bmatrix} \left(\frac{\partial f_1}{\partial x_1}\right)^{(0)} & \cdots & \left(\frac{\partial f_1}{\partial x_n}\right)^{(0)} \\ \vdots & & \vdots \\ \left(\frac{\partial f_n}{\partial x_1}\right)^{(0)} & \cdots & \left(\frac{\partial f_n}{\partial x_n}\right)^{(0)} \end{bmatrix} \begin{bmatrix} \Delta x_1 \\ \vdots \\ \Delta x_n \end{bmatrix} \approx \begin{bmatrix} 0 \\ \vdots \\ 0 \end{bmatrix} \tag{2.21}
$$

$$
\underline{f}(\underline{x}^{(0)}) + J^{(0)} \Delta \underline{x}^{(0)} \approx \underline{0} \tag{2.22}
$$

Solving for the error vector $\underline{\Delta \boldsymbol{x}}^{(0)} = \underline{\boldsymbol{x}}^{(i+1)} - \underline{\boldsymbol{x}}^{(i)}$, and indicating the iterative process with the counter i, we obtain the Newton-Raphson algorithm:

$$
\underline{x}^{(i+1)} = \underline{x}^{(i)} - \left[J^{(i)}\right]^{-1} \underline{f}(\underline{x}^{(i)}) \tag{2.23}
$$

The *nxn* matrix ***J***, whose elements are the partial derivatives of the $\underline{\boldsymbol{f}}$ functions, is called the *Jacobian* matrix. For solving the linear system of (2.23) the backward and forward Gauss substitution using the ***[L\U]*** factorization is usually performed as it will be shown later in this chapter. The load-flow formulation considers the bus voltages magnitud ΔV_k and phase angles $\Delta\delta_k$ as unknown variables (state vector $\underline{\boldsymbol{x}}$), and the active ΔP_k and reactive ΔQ_k power as the mismatch error functions (vector $\underline{\boldsymbol{f}}$). Considering the swing bus variables V_1 and δ_1 as known variables, the unknown voltage-state vector and power mismatch functions are:

$$
\underline{x} = \begin{bmatrix} \Delta\underline{\delta} \\ \Delta\underline{V} \end{bmatrix} = \begin{bmatrix} \Delta\delta_2 \\ \vdots \\ \Delta\delta_n \\ \Delta V_2 \\ \vdots \\ \Delta V_n \end{bmatrix} \qquad \underline{f}(\underline{x}) = \begin{bmatrix} \Delta P_2(\underline{x}) \\ \vdots \\ \Delta P_n(\underline{x}) \\ \Delta Q_2(\underline{x}) \\ \vdots \\ \Delta Q_n(\underline{x}) \end{bmatrix} = \begin{bmatrix} \Delta P_2(\delta_2, \cdots \delta_n, V_2, \cdots V_n) \\ \vdots \\ \Delta P_n(\delta_2, \cdots \delta_n, V_2, \cdots V_n) \\ \Delta Q_2(\delta_2, \cdots \delta_n, V_2, \cdots V_n) \\ \vdots \\ \Delta Q_n(\delta_2, \cdots \delta_n, V_2, \cdots V_n) \end{bmatrix} \tag{2.24}
$$

The values of ΔP_k and ΔQ_k, expressed in the polar form, are calculated using equations (2.6) and (2.7) and the *Jacobian* matrix has the form:

$$\begin{bmatrix} \Delta\underline{\delta} \\ \Delta\underline{V} \end{bmatrix} = \begin{bmatrix} J_1(\underline{x}) & J_2(\underline{x}) \\ J_3(\underline{x}) & J_4(\underline{x}) \end{bmatrix}^{-1} \begin{bmatrix} \Delta\underline{P}(\underline{x}) \\ \Delta\underline{Q}(\underline{x}) \end{bmatrix} \tag{2.25}$$

and its elements are computed as follows [3]:

- For $k \neq l$:

$$J_{1kl} = \frac{\partial P_k}{\partial \delta_l} = |V_k||Y_{kl}||V_l| \sin(\delta_k - \delta_l - \varphi_{kl}) \tag{2.26}$$

$$J_{2kl} = \frac{\partial P_k}{\partial V_l} = |V_k||Y_{kl}| \cos(\delta_k - \delta_l - \varphi_{kl}) \tag{2.27}$$

$$J_{3kl} = \frac{\partial Q_k}{\partial \delta_l} = -|V_k||Y_{kl}||V_l| \cos(\delta_k - \delta_l - \varphi_{kl}) \tag{2.28}$$

$$J_{4kl} = \frac{\partial Q_k}{\partial V_l} = |V_k||Y_{kl}| \sin(\delta_k - \delta_l - \varphi_{kl}) \tag{2.29}$$

- For $k = l$:

$$J_{1kk} = \frac{\partial P_k}{\partial \delta_k} = -|V_k| \sum_{\substack{k=1 \\ k \neq l}}^{n} |Y_{kl}||V_l| \sin(\delta_k - \delta_l - \varphi_{kl}) \tag{2.30}$$

$$J_{2kk} = \frac{\partial P_k}{\partial V_k} = -|V_k||Y_{kk}| \cos(\varphi_{kk}) + \sum_{k=1}^{n} |Y_{kl}||V_l| \cos(\delta_k - \delta_l - \varphi_{kl}) \tag{2.31}$$

$$J_{3kk} = \frac{\partial Q_k}{\partial \delta_k} = |V_k| \sum_{\substack{k=1 \\ k \neq l}}^{n} |Y_{kl}||V_l| \cos(\delta_k - \delta_l - \varphi_{kl}) \tag{2.32}$$

$$J_{4kk} = \frac{\partial Q_k}{\partial V_k} = -|V_k||Y_{kk}| \sin(\varphi_{kk}) + \sum_{k=1}^{n} |Y_{kl}||V_l| \sin(\delta_k - \delta_l - \varphi_{kl}) \tag{2.33}$$

Finally, the voltage-state vector at each iteration is computed as follows:

$$\begin{bmatrix} \underline{\delta}^{(i+1)} \\ \underline{V}^{(i+1)} \end{bmatrix} = \begin{bmatrix} \underline{\delta}^{(i)} \\ \underline{V}^{(i)} \end{bmatrix} + \begin{bmatrix} \Delta\underline{\delta}^{(i)} \\ \Delta\underline{V}^{(i)} \end{bmatrix} \tag{2.34}$$

In this methodology, the convergence is reached once the active and reactive power mismatches are smaller than a given tolerance or when the maximum number of iterations is exceeded.

2.1.5 Fast-decoupled load-flow solution

The fast-decoupled load-flow algorithm corresponds to a modified version of Newton's methodology. This algorithm developed by Stott [5] takes advantage of the weak coupling between active and reactive power, neglecting sub-matrices $\boldsymbol{J_2}$ and $\boldsymbol{J_3}$ in (2.25), and using the two constant sub-matrices $\boldsymbol{J_1}$ and $\boldsymbol{J_4}$ for representing the decoupled *Jacobian* admittance matrix. The derivation of the basic algorithm using Cartesian coordinates is summarized below:

$$\begin{bmatrix} J_1(\underline{x}) & 0 \\ 0 & J_4(\underline{x}) \end{bmatrix} \times \begin{bmatrix} \Delta\underline{\delta} \\ \Delta\underline{V} \end{bmatrix} = \begin{bmatrix} \Delta\underline{P}(\underline{x}) \\ \Delta\underline{Q}(\underline{x}) \end{bmatrix} \tag{2.35}$$

$$\begin{bmatrix} \Delta\underline{P}(\underline{x}) \\ \Delta\underline{Q}(\underline{x}) \end{bmatrix} = \begin{bmatrix} J_1(\underline{x})\Delta\underline{\delta} \\ J_4(\underline{x})\Delta\underline{V} \end{bmatrix} \tag{2.36}$$

Where:

$$J_{1kl} = J_{4kl} = |V_k||V_l|(G_{kl}\sin(\delta_k - \delta_l) - B_{kl}\cos(\delta_k - \delta_l))$$

$$J_{1kk} = -B_{kk}V_k^2 - Q_k$$

$$J_{4kk} = -B_{kk}V_k^2 + Q_k$$

Let us make the following assumptions, which are almost always valid:

$$\cos(\delta_k - \delta_l) \approx 1$$

$$G_{kl}\sin(\delta_k - \delta_l) << B_{kl}$$

$$Q_k << B_{kk}V_k^2$$

Thus, setting all the values of V_l to 1.0 and dividing by V_k, the equations in (2.36) become:

$$\frac{\Delta P_k}{|V_k|} = \sum_{l=2}^{n} -B_{kl}\Delta\delta_l \tag{2.37}$$

$$\frac{\Delta Q_k}{|V_k|} = \sum_{l=2}^{n} -B_{kl}\frac{\Delta|V_k|}{|V_k|} \tag{2.38}$$

In matrix formulation we obtain:

$$\begin{bmatrix} \Delta \underline{P} \\ \Delta \underline{Q} \end{bmatrix} = \begin{bmatrix} B' \Delta \underline{\delta} \\ B'' \Delta \underline{V} \end{bmatrix} \tag{2.39}$$

Where ***B'*** and ***B"*** are real sparse matrices and have the same structure of J_1 and J_4 respectively.

The fast-decoupled load-flow methodology uses the same convergence criterion as that of the full Newton's formulation. It is widely used for load-flow simulations of very large balanced systems when a large number of simulations are required in a short period of time such as contingency analysis and real-time simulations.

2.1.6 Second order load-flow solution

The equation (2.3) corresponds to a second order complex equation in $\underline{V}$ and so are equations (2.4) and (2.5) in a Cartesian coordinate system. Expanding these two equations in a second order Taylor series we have:

$$\Delta P_k = \frac{\partial P_k}{\partial f^T}\Delta f + \frac{\partial P_k}{\partial e^T}\Delta e + \frac{1}{2}\left[\Delta f^T \frac{\partial^2 P_k}{\partial f \partial f^T}\Delta f + \Delta f^T \frac{\partial^2 P_k}{\partial f \partial e^T}\Delta e + \Delta e^T \frac{\partial^2 P_k}{\partial e \partial e^T}\Delta e + \Delta e^T \frac{\partial^2 P_k}{\partial e \partial f^T}\Delta f\right] \tag{2.40}$$

$$\Delta Q_k = \frac{\partial Q_k}{\partial f^T}\Delta f + \frac{\partial Q_k}{\partial e^T}\Delta e + \frac{1}{2}\left[\Delta f^T \frac{\partial^2 Q_k}{\partial f \partial f^T}\Delta f + \Delta f^T \frac{\partial^2 Q_k}{\partial f \partial e^T}\Delta e + \Delta e^T \frac{\partial^2 Q_k}{\partial e \partial e^T}\Delta e + \Delta e^T \frac{\partial^2 Q_k}{\partial e \partial f^T}\Delta f\right] \tag{2.41}$$

Expressed in a matrix form:

$$\begin{bmatrix} \Delta \underline{P} \\ \Delta \underline{Q} \end{bmatrix} = J \begin{bmatrix} \Delta \underline{f} \\ \Delta \underline{e} \end{bmatrix} + [\Delta \underline{S}]$$

$$J = \begin{bmatrix} \frac{\partial P_k}{\partial f^T} & \frac{\partial P_k}{\partial e^T} \\ \frac{\partial Q_k}{\partial f^T} & \frac{\partial Q_k}{\partial e^T} \end{bmatrix}$$

Where $\underline{\Delta S}$ the second order term vector and J the *Jacobian* matrix whose elements are defined in [6] along with the solution algorithm.

This methodology is practically useless since it present a lower performance in comparison with the Newton method in terms of computing memory and CPU-time requirement.

2.1.7 Backward-forward sweep load-flow solution

The load-flow solution of a single network is achieved iteratively using a few sets of equations and applying a backward and forward directions recursive solution methodology. In the single-phase π line model of figure 2.2, where i is a branch connected between nodes k and m, R_i+jX_i, and y_i are the series impedance and shunt admittance, the active P_i' and reactive Q_i' power flow through the branch i can be calculated as [7]:

$$P_i' = P_{mL} + P_{mF} - P_{ml} \tag{2.42}$$

$$Q_i' = Q_{mL} + Q_{mF} - Q_{ml} - V_k^2 \frac{y_i}{2} \tag{2.43}$$

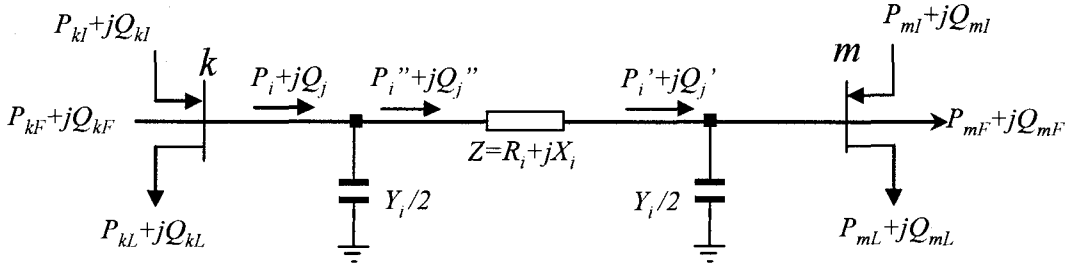

Figure 2.2 Branch π-circuit model

The subscripts L, F and l in P and Q represent the load, flow and injection respectively. P_{mF} and Q_{mF}, are the sum of the power flow through all the downstream branches that are connected to bus m.

In the following, we will assume a radial branch, the procedure of finding the injections P_{ml} and P_{ml} for loop break points is described in detail in [7]. Thus, neglecting loops, we can assume that:

$$P_i' = P_{mL} + P_{mF} \tag{2.44}$$

$$Q_i' = Q_{mL} + Q_{mF} - V_k^2 \frac{y_i}{2} \tag{2.45}$$

and that the expressions for the power flow at node *k* are:

$$P_i = P_i' + R_i \frac{P_i'^2 + Q_i'^2}{V_m^2} \tag{2.46}$$

$$Q_i = Q_i' + X_i \frac{P_i'^2 + Q_i'^2}{V_m^2} - V_k^2 \frac{y_i}{2} \tag{2.47}$$

Equations (2.46) and (2.47) are used recursively in a backward direction in order to find the power flowing in each branch of the network. In the backward sweep the equations are first applied to the last branch and then proceed in reverse direction until the first branch in reached. Once the power flow is known in all branches, the node voltage at each bus is calculated in a recursive forward sweep from the following equation. If we consider that the angle of voltage at bus *k* is zero, the complex voltage at bus *m* V_m in figure 2.2, is computed as follows:

$$V_m = V_k - I_i Z_i = V_k - \left(\frac{S_i''}{V_k}\right)^* (R_i + jX_i)$$

$$V_m = V_k - \left(\frac{P_i'' - jQ_i''}{V_k}\right)(R_i + jX_i)$$

$$V_m = \left[V_k - \left(\frac{P_i'' R_i + Q_i'' X_i}{V_k}\right)\right] - j\left(\frac{P_i'' X_i - Q_i'' R_i}{V_k}\right)$$

$$V_m = \sqrt{V_k^2 - 2(P_i'' R_i + Q_i'' X_i) + (P_i''^2 + Q_i''^2)\left(\frac{R_i^2 + X_i^2}{V_k^2}\right)} \tag{2.48}$$

Where $S_i'' = P_i'' + Q_i''$, $P_i'' = P'_i$, $Q_i'' = Q_i - V_k^2 \frac{y_i}{2}$, and the angle δ_m is:

$$\delta_m = -\tan^{-1}\left(\frac{P_i'' X_i - Q_i'' R_i}{V_k^2 - P_i'' R_i + Q_i'' X_i}\right) \tag{2.49}$$

If the voltage angle at bus k δ_k is other than zero, then the angle δ_m will be:

$$\delta_m = \delta_k - \tan^{-1}\left(\frac{P_i'' X_i - Q_i'' R_i}{V_k^2 - P_i'' R_i + Q_i'' X_i}\right) \quad \textbf{(2.50)}$$

The equations (2.48) and (2.50), can be used recursively in a forward sweep to find the voltage and phase angle for all the nodes in the network. When the voltage difference between two consecutive iterations is lower than a defined tolerance for each bus, the convergence is reached and the problem is solved.

The backward-forward sweep method, also known as the ladder methodology, used by the iterative software CYMDIST [2] computes the branch currents instead of the power flow. Thus, assuming a known initial nominal voltage for all the end nodes (node m in figure 2.2), the load and shunt branch currents can be calculated. Adding these currents and applying Kirchhoff's voltage law, the upstream node voltage (node k) is computed. This forward sweep is performed from all the end nodes towards the first reference node where the calculated voltage is compared with the specified voltage. As the difference is higher than the tolerance, the backward sweep starts using the new voltage and branch currents obtained from the forward sweep, in order to compute the new downstream voltages [2].

A compensation based technique proposed by Shirmohammadi in [8] allows performing unbalanced load-flow for weakly meshed networks using the backward and forward methodology. In this methodology, all the loops are opened before running the load-flow simulation, and replaced by current sources whose injected currents are determined iteratively using a compensation methodology.

To better understand the backward-forward sweep methodology a simple radial example is illustrated herein. Let us consider the system in figure 2.3:

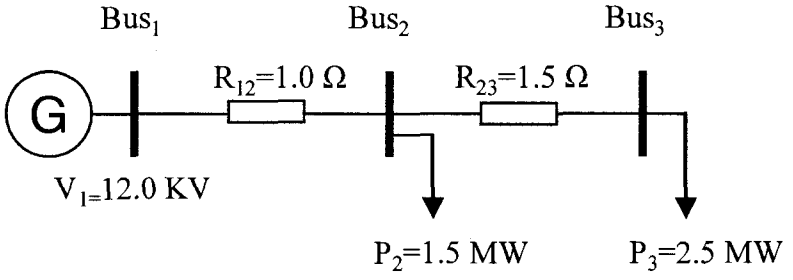

Figure 2.3 Backward-forward method illustrative case

The forward sweep begins assuming the phase-to-phase voltage at node 3 to be 12.0/0 kV. Thus the load current at node 3 which is the same current flowing from bus 2 to 3 is:

$$I_3 = I_{23} = \left(\frac{2.5e6}{\sqrt{3} \times 12e3} \right) = 120.28 \text{ [A]}$$

The phase to ground and phase-to-phase voltages at node 2 are:

$$V_{2\_LG} = V_3 + Z_{23} I_{23} = \frac{12e3}{\sqrt{3}} + 1.5 \times 120.28 = 7{,}108.6 \text{ [V]}$$

$$V_{2\_LL} = 12{,}312.5 \text{ [V]}$$

The load current at node 2 is:

$$I_2 = \left(\frac{1.5e6}{\sqrt{3} \times 12.3125e3} \right) = 70.34 \text{ [A]}$$

The current flowing from node 1 to 2 is:

$$I_{12} = I_{23} + I_2 = 120.28 + 70.34 = 190.62 \text{ [A]}$$

The computed phase to ground and phase-to-phase voltages at the source node 1 are:

$$V_{1\_LG} = V_2 + Z_{12} I_{12} = \frac{12.3125e3}{\sqrt{3}} + 1.0 \times 190.62 = 7{,}299.2 \text{ [V]}$$

$$V_{1\_LL} = 12{,}642.7 \text{ [V]}$$

At this point the magnitude of the computed voltage at node 1 is compared to the magnitude of the specified source voltage of 12.0 kV and if the error is less than the specified tolerance, the solution is reached.

$$Error = \left| |V_S| - |V_1| \right| = 7{,}200.0 - 7299.2 = 99.2 \text{ [V]}$$

If the error is grater than the tolerance as in this example, the backward sweep begins by setting the voltage at node 1 to the specified voltage of 12.0/0 kV. Now the voltage at node 2 is computed using the values of the node 1 voltage and the computed line current obtained from the forward sweep.

$$V_{2\_LG} = V_1 - Z_{12} I_{12} = \frac{12e3}{\sqrt{3}} - 1.0 \times 190.62 = 6{,}737.6 \text{ [V]}$$

The backward seep continues by computing the next downstream voltage using the branch current obtained from the forward sweep process.

$$V_{3\_LG} = V_2 - Z_{23} I_{23} = 6{,}737.6 - 1.5 \times 120.28 = 6.557.2 \text{ [V]}$$

This completes the first iteration. At this point the forward sweep will be repeated starting with the new voltage at node 3 rather than the initially assumed voltage.

2.1.8 Load-flow methods performance comparison

The methods briefly described before are part of the most widely known algorithms for single-phase or positive-sequence load-flow solutions [9]. In the following, we will briefly compare some computing performance features for the first four methodologies [6], which present similar solving features and sparse matrix solver requirements. On the other hand, due to the fact that the backward and forward sweep solution method does not need to solve matrix inversion, it shall be excluded from this comparison. Nonetheless, some performance features of this load-flow methodology, extracted form [10], will be depicted at the end of this section.

- Memory requirements

  Considering the sparsity storage scheme for the admittance and *Jacobian* matrices mentioned in [6] and presented later in this chapter, the resulting memory requirements are listed in table 2.1, for a power system of over 1,000

buses. It can be concluded that the memory requirements increase from methods (a) to (d).

Table 2.1 Memory requirements (Bytes)

(a) Gauss-Seidel	*(b) N-R Fast Decoupled*	*(c) Newton-Raphson*	*(d) Second order LF*
96*N+48*L	144*N+96xL	240*N+256*L	256xN+256xL

N = Number of buses, L = Number of lines

Even tough the memory requirements depend on the programming techniques, the results will not be far from the ones listed above. The Gauss-Seidel method presents the better performance in terms of memory requirements.

- CPU-time requirements

The CPU time processing is higher for Newton–Raphson method in comparison to the Fast decoupled and Gauss-Seidel methods. Even though most of these algorithms show fast performance in time simulation due to the fast processing time of current personal computers, Fast decoupled Newton method remains the fastest solver, followed by Gauss-Seidel.

- Iteration requirements and convergence characteristics

The Newton-Raphson and the second order load-flow methods usually take between two to five iterations to solve a fully loaded system if the initial node voltage guess are close enough of the solution. On the other hand, Gauss-Seidel takes from 10 to 50 iterations for similar systems and does not guarantee the convergence for very large systems. Fast decoupled load-flow method needs more iterations than full Newton-Raphson method. Although full Newton–Raphson method reaches a solution with a smaller number of iterations, it takes more computer processing time [6].

- Ill-conditioned systems with high R/X ratios

  If the condition number of either the $\boldsymbol{Y_{Bus}}$ or *Jacobian* matrices is large then such a matrix is said to be ill-conditioned. That matrix is almost singular and the computation of its inverse, or solution of a linear system of equations, is prone to large numerical errors. Depending on the number of lines with high R/X ratios those matrices can become ill-conditioned increasing the number of iterations to get the solution. As is shown in [6], the number of iterations for Gauss-Seidel and fast decoupled load-flow methods are increased between 2 to 5 iterations, while the full Newton and second order methods remain with almost the same number of iterations, being the two latter practically unaffected by the ill-conditioned feature.

- Initial voltage profiles or guess

  From Gauss-Seidel algorithm convergence characteristics, it has been observed that the mismatch decreases quickly at the early iterations. These Gauss-Seidel iterations take, in turn, very low processing time as mentioned before, so the idea of using the Gauss-Seidel method to set up initial guess for the full Newton or second order load-flow solution is very attractive. In [6] it has been shown that a solution with few iterations using Gauss-Seidel method gives a good starting voltage for others methods with longer simulation time. A full Newton solution using a flat-start voltage profile could diverge if the solution is too far from the initial guess.

The ***backward and forward sweep*** load-flow solution method presents the highest performance in terms of simulation time especially for large and radial systems, even though the number of iterations required is higher in comparison with the full Newton and second order methodologies. However, for heavily meshed networks compensation methods have to be incorporated reducing the performance of this iterative methodology. Convergence problems are also found in iterative methods for some critical meshed cases with high R/X ratio [10].

2.2 Numerical load-flow solvers

Load-flow methodologies involving iterative Newton's solution methods solve large either $\boldsymbol{Y_{Bus}}$ or *Jacobian* matrices. The typical matrix equations to be solved has the form $\boldsymbol{A}\underline{\boldsymbol{x}}=\underline{\boldsymbol{b}}$, were $\boldsymbol{A}$ must be non-singular. Depending on the methodology and system modeling, $\boldsymbol{A}$ can be a symmetric or a non-symmetric sparse matrix. The solution for finding the vector $\underline{\boldsymbol{x}}$ involves the numerical solution of the system of linear equations $\boldsymbol{A}\underline{\boldsymbol{x}}=\underline{\boldsymbol{b}}$. Direct and iterative methods, which are the most known linear system solvers, are described below.

2.2.1 Matrix sparsity techniques

Before starting with the description of matrix numerical methodologies, a quick review of matrix sparsity techniques is presented. A typical power system has on average three or fewer lines connected to each bus, which means that each row of both the $\boldsymbol{Y_{Bus}}$ and also the Jacobian matrices have on average fewer than four nonzero elements. Such matrices with few nonzero elements are called *sparse matrices.* A typical sparse matrix density plot, where the non-zero elements are shown in black, is presented in figure 2.4.

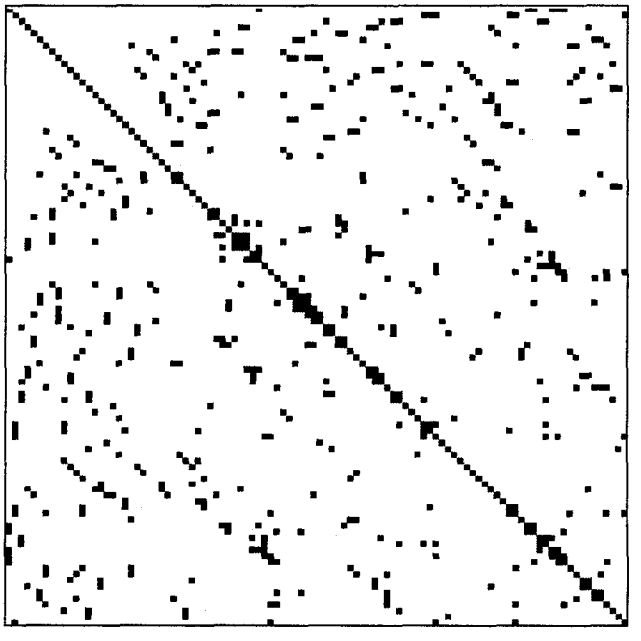

Figure 2.4 Sample density plot of a sparse matrix

The computational process can profit from the matrix sparsity exhibited in large power systems. The matrix sparsity factor S according to [11] can be calculated as:

$$S = \frac{z}{n^2}$$

Where z is the number of zero elements, and n the size of the square matrix. This factor varies between 50% for small systems to 98% for very large systems.

As an illustration let us define the following theoretical Y_{BUS} matrix of a small 5-bus system:

$$Y_{BUS} = \begin{bmatrix} 3.8 & -2.1 & 0 & -1.1 & 0 \\ -2.1 & 3.5 & 0 & 0 & 0 \\ 0 & 0 & 5.5 & 0 & 0 \\ -1.1 & 0 & 0 & 3.3 & -2.2 \\ 0 & 0 & 0 & -2.2 & 4.2 \end{bmatrix}$$

$$S = \frac{z}{n^2} = \frac{14}{5^2} = 0.56 pu = 56\%$$

Let us define now the diagonal vector $\underline{\boldsymbol{Z}}_{Diag}$, and off-diagonal vector $\underline{\boldsymbol{Z}}_{Off}$:

$$Z_{Diag} = [3.8 \quad 3.5 \quad 5.5 \quad 3.3 \quad 4.2]$$

$$Z_{Off} = [-2.1 \quad -1.1 \quad -2.1 \quad -1.1 \quad -2.2 \quad -2.2]$$

To position the elements of the $\underline{\boldsymbol{Z}}_{Off}$ vector in their proper place in $\boldsymbol{Y}_{Bus}$, two other vectors have to be defined:

$$I_{row} = [2 \quad 1 \quad 0 \quad 2 \quad 1]$$

$$I_{col} = [2 \quad 4 \quad 1 \quad 1 \quad 5 \quad 4]$$

Where $\underline{\boldsymbol{I}}_{row}$ indicates the number of off-diagonal elements in each row of $\boldsymbol{Y}_{Bus}$ and $\underline{\boldsymbol{I}}_{col}$ identify the column position of each off-elements in $\boldsymbol{Y}_{Bus}$. The vector $\underline{\boldsymbol{Z}}_{Diag}$ and $\underline{\boldsymbol{I}}_{row}$ contain n elements each, and the vector $\underline{\boldsymbol{Z}}_{Off}$ and $\underline{\boldsymbol{I}}_{col}$, n^2-n-Z elements each, thus the total number of elements E_t is [11]:

$$E_t = 2n + 2(n^2 - n - z) = 2n^2(1 - S) \qquad \textbf{(2.51)}$$

$$E_t = 2 \times 5^2 (1 - 0.56) = 22$$

The memory saving is not important for small systems (matrices). In the above example the number of elements to store is 22 compared to 25 in the original matrix. Nevertheless, for a matrix of 500 buses and sparsity of 98% E_t is 10,000 which is much lower than 125,250, the required memory size without packing obtained from the equation $\left(\frac{n(n+1)}{2}\right)$.

2.2.2 Direct methods for sparse linear systems

Optimally ordered triangular factorization of sparse matrices is one of the most efficient and widely used techniques for solving load-flow by Newton's method [12]. It presents important computational advantages to find the solution of a set of linear equations in the form $\boldsymbol{A}\underline{\boldsymbol{x}}=\underline{\boldsymbol{b}}$. Higher speed, lower computer memory requirements, and reduction of round-off errors are some of the main advantages of this direct method which is computed from sparse matrix factors [13].

The direct method consists of two parts: first the recording of the operations of triangular decomposition of the matrix $\boldsymbol{A}$ so that repeated direct solutions of $\boldsymbol{A}\underline{\boldsymbol{x}}=\underline{\boldsymbol{b}}$ can be obtained without repeating the factorizing process, and second the ordering of the operations to keep the sparsity of the original system. While the first part is applicable to any matrix, the second is limited to sparse matrices whose nonzero pattern is symmetrical. Factored direct solution and sparse matrix ordering methods are briefly described below.

A. Triangular decomposition

Triangular decomposition using Gaussian elimination is widely described in many matrix analysis books, and publications [13]. This consists in the elimination of elements below the main diagonal in successive columns, although in terms of computer programming for a sparse matrix, it is usually more efficient to do the elimination by successive rows. The development is based on the equation $\boldsymbol{A}\underline{\boldsymbol{x}}=\underline{\boldsymbol{b}}$, where $\boldsymbol{A}$ is a non-singular matrix, $\underline{\boldsymbol{x}}$ is a column vector of unknowns, and $\underline{\boldsymbol{b}}$ is a

known vector with at least one non-zero element. In the computer algorithm the *nxn* A matrix is augmented by the vector $\underline{b}$ as in (2.52):

$$\begin{bmatrix} a_{11} & a_{12} & \cdots & a_{1n} & b_1 \\ a_{21} & a_{22} & \cdots & a_{2n} & b_2 \\ a_{31} & a_{32} & \cdots & a_{3n} & b_3 \\ \vdots & \vdots & \cdots & \vdots & \vdots \\ a_{n1} & a_{n2} & \cdots & a_{nn} & b_n \end{bmatrix} \tag{2.52}$$

The first step is to divide the elements of the first row by a_{11} as indicated in (2.53):

$$a_{1j}^{(1)} = (\frac{1}{a_{11}})a_{1j} \qquad j=2,\ldots,n \tag{2.53}$$

$$b_{1j}^{(1)} = (\frac{1}{a_{11}})b_1 \tag{2.54}$$

The subscripts indicate the order of the derived system. The next step is to eliminate a_{21} from the second row by linear combinations with the derived first row, and then to divide the remaining derived elements on the second row by its new derived diagonal element.

$$\begin{bmatrix} 1 & a_{12}^{(1)} & a_{13}^{(1)} \cdots & a_{1n}^{(1)} & b_1^{(1)} \\ & 1 & a_{23}^{(2)} \cdots & a_{2n}^{(2)} & b_2^{(2)} \\ & & & & \\ \vdots & \vdots & & \vdots & \vdots \\ a_{n1} & a_{n2} & a_{n3} \cdots & a_{nn} & b_n \end{bmatrix}$$

$$a_{2j}^{(1)} = a_{2j} - a_{21}a_{1j}^{(1)} \qquad j=2,\ldots,n \tag{2.55}$$

$$b_2^{(1)} = b_2 - a_{21}b_1^{(1)}$$

$$a_{2j}^{(2)} = (1/a_{22}^{(2)})a_{2j}^{(1)} \qquad j=3,\ldots,n \tag{2.56}$$

$$b_2^{(2)} = (1/a_{22}^{(1)})b_2^{(1)}$$

The next step is to eliminate elements to the left of the diagonal of the third row, and to divide the remaining derived elements of the row by the derived diagonal element. Following this procedure the final system is:

$$\begin{bmatrix} 1 & a_{12}^{(1)} & \cdots & a_{1n}^{(1)} & b_1^{(1)} \\ & 1 & \cdots & a_{2n}^{(2)} & b_2^{(2)} \\ & & & \vdots & \vdots \\ & & & \vdots & \vdots \\ & & & 1 & b_n^{(n)} \end{bmatrix}$$

Now the solution of the linear system equations is obtained by backwards substitution:

$$x_n = b_n^{(n)}$$

$$x_{n-1} = b_{n-1}^{(n-1)} - a_{n-1,n}^{(n-1)} x_n$$

$$x_i = b_i^{(i)} - \sum_{j=i+1}^{n} a_{ij}^{(i)} x_j \qquad \textbf{(2.57)}$$

The backwards substitution can be developed by columns instead of by rows, having the same number of operations.

B. Operations Recording

The recording of vector $\underline{\boldsymbol{b}}$ and the upper triangle for the back substitution permits us to solve $\boldsymbol{A}\underline{\boldsymbol{x}}=\underline{\boldsymbol{b}}$ for any vector $\underline{\boldsymbol{b}}$ without repeating the triangularization. On the other hand, the recording of each forward operation is defined by the row and column coordinates and the value of a single element $a_{ij}^{(j-1)}$ $(i \geq j)$ that occurs in the process [13]. The rules for recording the forward operations of the triangularization are: first, when $1/a_{ij}^{(j-1)}$ is computed, it must be stored in location *ii*, and second, every derived term $a_{ij}^{(j-1)}$ $(i \geq j)$, must be stored in the lower $\boldsymbol{L}$ triangle.

Since forward and backward substitution operations are recorded in this scheme, it is no longer necessary to include the vector $\underline{\boldsymbol{b}}$. The final result of the triangularization of $\boldsymbol{A}$ and recording the forward operations is shown in (2.62):

$$\begin{matrix} d_{11} & u_{12} & u_{13} & \cdots & u_{1n} \\ l_{21} & d_{22} & u_{23} & \cdots & u_{2n} \\ l_{31} & l_{32} & d_{33} & \cdots & u_{3n} \\ \vdots & \vdots & \cdots & \cdots & \vdots \\ l_{n1} & l_{n2} & l_{n3} & \cdots & d_{nn} \end{matrix} \tag{2.58}$$

$$d_{ii} = 1 / a_{ii}^{(i-1)} \tag{2.59}$$

$$u_{ij} = a_{ij}^{(i)} \qquad i < j \tag{2.60}$$

$$l_{ij} = a_{ij}^{(j-1)} \qquad j < i. \tag{2.61}$$

The ordering (2.58) is not a matrix, but also a scheme of recording usually referred to as the *table of factors.* The scheme in (2.58) is usually shown as a factoring of the inverse matrix $\boldsymbol{A}$ into the product of an upper $\boldsymbol{U}$ and a lower $\boldsymbol{L}$ triangular matrix which is typically known as *[L\U]* factorization [13].

C. *Computing direct solutions*

It is useful to represent (2.58) as a set of non-singular matrices defined as follows:

$$D_i = Row_i = (0,0,...0,d_{ii},0,...0,0)$$

$$L_i = Col_i = (0,0,...0,1,-l_{i+1,i},-l_{i+2,i},...-l_{n-1,i},-l_{n,i})^T$$

$$L_i^* = Col_i = (-l_{i,1},-l_{i,2},...-l_{i,j-1},1,0,...0,0)$$

$$U_i = Row_i = (0,0,...0,1,-u_{i,i+1},-u_{i,i+2},...-u_{i,n-1},-u_{i,n,})^T$$

$$U_i^* = Col_i = (-u_{1,i},-u_{2,i},...-u_{i-1,i},1,0,...0,0)$$

The inverse of D_i implies the reciprocal of each element d_{ii}, and the inverse of the matrices L_i and U_i involves just a reversal of sign of all off-diagonal elements. Thus, the inverse $\boldsymbol{A}^{-1}$ can be expressed as a pre-multiplication of matrices D_i, L_i, and U_i, and the solution $\underline{\boldsymbol{x}}=\boldsymbol{A}^{-1}\underline{\boldsymbol{b}}$ is computed as follows [13]:

$$U_1U_2 \ldots U_{n-2}U_{n-1}D_nL_{n-1}D_{n-1}L_{n-2} \cdots L_2D_2L_1D_1b = A^{-1}b = x$$

$$U_1U_2\ldots U_{n-2}U_{n-1}D_nL_n^*D_{n-1}L_{n-1}^*\cdots L_3^*D_2L_2^*D_1b = A^{-1}b = x$$

$$U_2^*U_3^*\ldots U_{n-1}^*U_n^*D_nL_{n-1}D_{n-1}L_{n-2}\cdots L_2D_2L_1D_1b = A^{-1}b = x$$

$$U_2^*U_3^*\ldots U_{n-1}^*U_n^*D_nL_n^*D_{n-1}L_{n-1}^*\cdots L_3^*D_2L_2^*D_1b = A^{-1}b = x$$

Each of these four equations is equivalent to pre-multiply $\boldsymbol{A}^{-1}$ by $\underline{\boldsymbol{b}}$. For an nth order system the number of multiplication-additions is n^2. The convenience of using one equation over another is related to the programming techniques. When $\boldsymbol{A}$ is symmetric, only the factors d_{ii} and u_{ij} are needed and this also permits to save almost half of the triangularization operations because it is unnecessary to perform any operation on the left side of the diagonal to obtain the derived element $a_{ij}^{(j-1)}$ $(i \geq j)$. The $[\boldsymbol{L}\backslash\boldsymbol{U}]$ (or $[\boldsymbol{LDU}]$) factorization, with $\boldsymbol{L}$ lower and $\boldsymbol{U}$ upper triangular matrices, is closely related to the row reduction algorithm, which is also known as the Gaussian elimination, since in a real sense the factorization is a record of the steps taken in the elimination. There are other factorization algorithms such as the orthogonal matrix triangularization or *Q-R* decomposition, which guarantees numerical stability by minimizing errors caused by machine round-offs, and the *Cholesky* decomposition, which decompose $\boldsymbol{A}$ as $\boldsymbol{A}=\boldsymbol{LL}^T$, where $\boldsymbol{L}$ is a lower triangular matrix, called the *Cholesky triangle*, with positive diagonal elements.

D. Near-optimal ordering

Node ordering schemes are important in minimizing the number of multiplications and divisions required for both triangularization and the Gauss substitution process. In sparse matrices, the number of nonzero elements in the resulting upper triangle matrix depends on the order in which the rows are processed. Great savings in operations and computer memory can be achieved by keeping the table of factors as sparse as possible. The optimal ordering of elimination is reached when the table of factors has the minimum number of terms. Even though the absolute optimal ordering method does not exist, several near-optimal schemes have been developed. The inspection algorithms for near-

optimal ordering described here is applicable to sparse matrices that are symmetrical in pattern of nonzero off-diagonal terms, which are matrices mostly found in power systems networks. This ordering algorithm should be applied before the triangularization, and the eliminations are performed in ascending sequence of the renumbering by inspection. Three schemes of renumbering near-optimal ordering are described below [13]:

1. Number the rows according to the number of nonzero off-diagonal or fewest connected branches terms before elimination. Here rows with one off-diagonal term are numbered first, those with two terms second, etc., and those with the most terms, last. This scheme does not take into account any of the subsequence effects of the elimination process. The only information needed is a list of the number of nonzero terms in each row of the original matrix. This method is the simplest to program and the fastest to execute.
2. Number the rows so that at each step of the process the next row to be operated upon is the one with the fewest nonzero terms or fewest connected branches. This scheme requires a simulation of the effects on the accumulation of nonzero terms of the elimination process. The input information required is a list by rows of the column numbers of the nonzero off-diagonal terms.
3. Number the rows so that at each step of the process the next row to be operated upon is the one that will introduce the fewest new nonzero terms. This involves a trial simulation of every feasible alternative of the elimination process at each step. The input information is the same as for the scheme 2.

Experience indicates that the second method, known in the literature as Tinney-2, presents the best performance for nodal equations of power networks [13] and this is the ordering method utilized by the positive-sequence used in this research.

The minimum degree ordering algorithm (MDO) used by EMTP-RV, and originally known as the Tinney-2 scheme described above [14], produces factors with low fill-in on a large range of matrices. This graphical version of Tinney's method performs its pivot selection by choosing from a graph a node of minimum degree (fewest connected branches or nonzero elements). Later implementations have widely improved the computational time requirements of Tinney and Walker original method, maintaining the basic idea of selecting a node or a set of nodes of minimum degree. All these improvements have reduced the complexity in the handling of the memory so that the algorithm can operate within the storage capacity of the original matrix, and have also reduced the work needed to keep track of the degrees of nodes in the graph, which is the most computationally consuming part of the algorithm. Reference [15] shows a detailed description of the modern MDO algorithm using graph theory.

2.2.3 Iterative methods for sparse linear systems

The main disadvantage when using direct solvers in Newton's power-flow method is that the *Jacobian* matrix has to be factorized at each iteration. As the size of a matrix increase, even being sparse, the $[L\backslash U]$ factorization can become extremely time consuming [16]. Iterative solvers work very well for systems with small condition number. For large condition number ($>10^3$) the incorporation of preconditioners is usually necessary to guarantee convergence and to improve the overall efficiency of the iterative solver.

The idea of preconditioner is to pre-multiply the system of equations by a good approximation of the matrix inverse. If we ideally pre-multiply a matrix by its inverse the solution would be obtained directly, but this is impractical. A typical pre-conditioner used in power systems is the $[L\backslash U]$ and the incomplete $[L\backslash U]$ factorization of the matrix.

Continuous research in mathematics has resulted in the development of very efficient iterative solvers for linear systems [17], being Krylov subspace and its varieties among the most efficient for large sparse linear systems. For symmetrical systems, we

find the conjugate gradient (CG), minimal residues (MINRES), and Chebyshev iterative algorithms within the Matlab library. For non-symmetrical systems, the generalized minimal residues (GMRES), bi-conjugate gradient (BiCG), bi-conjugate gradient stabilized (BiCGSTAB), conjugate gradient squared (CGS), and quasi-minimal residual (QMR) methods are at the foreground and are also available in the Matlab library.

Even though for most systems $[\boldsymbol{L}\backslash\boldsymbol{U}]$ direct solvers present a better performance than iterative solvers, in very large systems (over 3,000 buses) and implementing optimal stopping strategies, the latter reach faster responses as shown in [16].

2.3 Three-phase load-flow methodologies

Positive-sequence load-flow algorithms assume a balanced operation of power systems, however, most of the systems include non-transposed transmission lines and unbalanced load which cannot be ignored. In addition, it is important that the load-flow be solved as efficiently as possible since most of planning and operational network applications require fast and repetitive simulations. Multi-phase load-flow algorithms, and in particular three-phase load-flow algorithms, are used to deal with these complexities.

Several three-phase load-flow methodologies have been proposed in the past, many of them were derived from known methods such as Newton's, Gauss-Seidel, and back and forward sweep already discussed before. This section describes in some detail the most known existing three-phase methodologies along with other less conventional ones. Special emphasis will be put on the augmented nodal matrix method used by the EMTP-RV load-flow algorithm, which is the software utilized as the validation tool in the present research work.

2.3.1 Full and fast-decoupled Newton methods

The full three-phase Newton method is derived from the conventional positive-sequence load-flow algorithm described in section 2.1.4. Firstly proposed by Birt in [18], Smith and Arrillaga in [19], and later modified by Nguyen [20] to its complex form,

Newton's method remain one of the most used methodologies for solving accurate unbalanced three-phase load-flows in both transmission and distribution systems. The three-phase load-flow equations for a bus k and phase p are [21]:

$$\Delta P_k^p = (P_k^p)^{spec} - P_k^p = 0 \qquad k=1,...,nb$$

$$\Delta Q_k^p = (Q_k^p)^{spec} - Q_k^p = 0 \qquad k=1,...,nb$$

$$P_k^p = |V_k^p| \sum_{l=1}^{nb} \sum_{m\in(a,b,c)} |V_l^m| \left[G_{kl}^{pm} \cos(\delta_{kl}^{pm}) + B_{kl}^{pm} \sin(\delta_{kl}^{pm}) \right] \tag{2.62}$$

$$Q_k^p = |V_k^p| \sum_{l=1}^{nb} \sum_{m\in(a,b,c)} |V_l^m| \left[G_{kl}^{pm} \sin(\delta_{kl}^{pm}) - B_{kl}^{pm} \cos(\delta_{kl}^{pm}) \right] \tag{2.63}$$

Where nb is the total number of buses, and p and m represent the phases (a, b, or c), and k and l represent busbars indices. G, and B are the real and imaginary parts of the admittance matrix $\boldsymbol{Y_{Bus}}$, which includes all couplings existing in the network. The angle δ_{kl} represents the angle difference between the voltages at nodes k and l. Applying the standard Newton method to the previous equations (2.62) and (2.63), we get for phase p:

$$\begin{bmatrix} \Delta P \\ \Delta Q \end{bmatrix} = \begin{bmatrix} A & I \\ C & K \end{bmatrix} \begin{bmatrix} \Delta \delta \\ \Delta V \end{bmatrix} \tag{2.64}$$

Where $\boldsymbol{A_p}$, $\boldsymbol{I_p}$, $\boldsymbol{C_p}$, and $\boldsymbol{K_p}$ are the Jacobian sub-matrices which are computed as follows:

$$\begin{bmatrix} A & I \\ C & K \end{bmatrix} = \begin{bmatrix} \left[\frac{\partial P_k^p}{\partial \delta_l^m}\right] & \left[\frac{\partial P_k^p}{\partial V_l^m}\right] \\ \left[\frac{\partial Q_k^p}{\partial \delta_l^m}\right] & \left[\frac{\partial Q_k^p}{\partial V_l^m}\right] \end{bmatrix} \tag{2.65}$$

In the iterative solution process the Jacobian matrix has to be repeated for each phase of the system, thus the equations system will have $3(2n)$x$3(2n)$ or $36n^2$ entries for a three-phase system.

The algorithm is similar to the positive-sequence method, but here the phase voltage initialization matrix $\boldsymbol{\Psi^{ini}}$ has to consider a 120 degree-difference between phase angles.

$$\Psi_{kl}^{ini} = \begin{bmatrix} 0 & 2\pi/3 & -2\pi/3 \\ -2\pi/3 & 0 & 2\pi/3 \\ 2\pi/3 & -2\pi/3 & 0 \end{bmatrix}$$

In the complex form, the voltages are expressed as $V_k = e_k + jf_k$. Thus, variations in complex power due to changes in complex voltages become:

$$\Delta S_k = \sum_{i=1}^{n} \Delta V_k Y_{ki}^* V_i^* + \sum_{i=1}^{n} V_k Y_{ki}^* \Delta V_i^* \qquad \textbf{(2.66)}$$

The system equations relating the changes in complex power to the changes in bus complex voltages through the *Jacobian* matrix is [20]:

$$\Delta \underline{S}^{abc} = diag(\Delta \underline{V}^{abc}) Y^{abc*} \underline{V}^{abc*} + diag(\underline{V}^{abc}) Y^{abc*} \Delta \underline{V}^{abc*} \qquad \textbf{(2.67)}$$

$$\text{or} \qquad \Delta \underline{S}^{abc} = J \Delta \underline{V}^{abc*} \qquad \textbf{(2.68)}$$

Where $\underline{\boldsymbol{S}}^{abc}$ is the three-phase bus complex power vector, $diag(\underline{\boldsymbol{V}}^{abc})$ is a diagonal three-phase bus voltage matrix, and $\boldsymbol{Y}^{abc}$ is the three-phase bus admittance matrix of the system including all the electromagnetically couplings.

Fast-decoupled three-phase load-flow method considers the same simplifications made in the positive-sequence formulation. Since this approach is not attractive for distribution systems with high *R/X* ratio, an alternative method proposed by Garcia in [21] is depicted below. Let us define the following matrix system:

$$\begin{bmatrix} \Delta \underline{P} \\ \Delta \underline{Q}^m \end{bmatrix} = \begin{bmatrix} J_1 & J_2 \\ 0 & J_4^m \end{bmatrix} \begin{bmatrix} \Delta \underline{\delta} \\ \Delta \underline{V} \end{bmatrix} \qquad \textbf{(2.69)}$$

Where $J_4^m = J_4 - J_3 J_1^{-1} J_2$, and $\Delta \underline{Q}^m = \Delta \underline{Q} - J_3 J_1^{-1} \Delta \underline{P}$.

By neglecting the sub-matrix $\boldsymbol{J_2}$ in (2.69), the vector angle deviation $\Delta \underline{\boldsymbol{\delta}}$ and the new angle vector $\underline{\boldsymbol{\delta}}$ can be obtained.

$$\begin{aligned} \Delta \underline{P} &\approx \Delta J_1 \Delta \underline{\delta} \\ \underline{\delta}^{new} &= \underline{\delta}^{old} + \Delta \underline{\delta} \end{aligned} \qquad \textbf{(2.70)}$$

Thus, the $\Delta \underline{\boldsymbol{Q}}^{mod}$ vector can be approximated as:

$$\Delta \underline{Q}^{m} \approx \Delta \underline{Q}(\underline{V}, \underline{\delta}^{new}) = \underline{Q}^{spec} - \underline{Q}(\underline{V}, \underline{\delta}^{new}) \tag{2.71}$$

2.3.2 Current injection Newton's method

Three-phase load-flow using the Newton's current injection method was early developed by da Costa [24] and Garcia [25]. Penido, in latter research added the neutral wire to this methodology [26], and Monfared in [27] reduced the convergence time by drastically reducing the number of iterations. This formulation has shown to be very robust and it also allows the representation of both radial and meshed networks.

The method is based on the current injected at every node of the power system. Since the complete formulation is detailed in [25], only the basic equations are presented here. The current mismatch for a given bus k and phase s are:

$$\Delta I_k^s = \frac{(P_k^{spec})^s - j(Q_k^{spec})^s}{V_k^{s*}} - \sum_{i \in \Omega_k} \sum_{t \in \alpha_p} V_i^t Y_{ki}^{st} \tag{2.72}$$

Where:

$s, t \in \alpha_p = (a, b, c)$

Ω_k : Set of buses directly connected to bus k.

Equation (2.72) can be expressed in terms of its real (r) and imaginary (m) parts as follows:

$$\Delta I_{k\,r}^s = \frac{(P_k^{spec})^s V_{k\,r}^s + (Q_k^{spec})^s V_{k\,m}^s}{(V_{k\,r}^s)^2 + (V_{k\,m}^s)^2} - \sum_{i \in \Omega_k} \sum_{t \in \alpha_p} (G_{ki}^{st} V_{i\,r}^t - B_{ki}^{st} V_{i\,m}^t) \tag{2.73}$$

$$\Delta I_{k\,m}^s = \frac{(P_k^{spec})^s V_{k\,m}^s - (Q_k^{spec})^s V_{k\,r}^s}{(V_{k\,r}^s)^2 + (V_{k\,m}^s)^2} - \sum_{i \in \Omega_k} \sum_{t \in \alpha_p} (G_{ki}^{st} V_{i\,m}^t - B_{ki}^{st} V_{i\,r}^t) \tag{2.74}$$

Equations (2.73) and (2.74) in terms of specified and calculated valued are:

$$\Delta I_{k\,r}^s = (I_k^{spec})_r^s - (I_k^{calc})_r^s \tag{2.75}$$

$$\Delta I_{k\,m}^s = (I_k^{spec})_m^s - (I_k^{calc})_m^s \tag{2.76}$$

Applying Newton's method to equations (2.73) and (2.74), the following set of linear equations for an n-bus system is obtained:

$$\begin{bmatrix} \Delta I_{1_m}^{abc} \\ \Delta I_{1_r}^{abc} \\ \hline \Delta I_{2_m}^{abc} \\ \Delta I_{2_r}^{abc} \\ \hline \vdots \\ \hline \Delta I_{n_m}^{abc} \\ \Delta I_{n_r}^{abc} \end{bmatrix}_{6xn} = \begin{bmatrix} J_{11}^{abc} & J_{12}^{abc} & \cdots & J_{1n}^{abc} \\ \hline J_{21}^{abc} & J_{22}^{abc} & \cdots & J_{2n}^{abc} \\ \hline \vdots & \vdots & \vdots & \vdots \\ \hline J_{n1}^{abc} & J_{n2}^{abc} & \cdots & J_{nn}^{abc} \end{bmatrix}_{6nx6n} \times \begin{bmatrix} \Delta V_{1_r}^{abc} \\ \Delta V_{1_m}^{abc} \\ \hline \Delta V_{2_r}^{abc} \\ \Delta V_{2_m}^{abc} \\ \hline \vdots \\ \hline \Delta V_{n_r}^{abc} \\ \Delta V_{n_m}^{abc} \end{bmatrix}_{nx6} \tag{2.77}$$

The off-diagonal sub-matrices $\boldsymbol{J_{ki}}$ of the Jacobian matrix in (2.77) are the elements of the system admittance matrix $\boldsymbol{Y_{Bus}}$ and remain constant during the iterative Newton's solution process. These sub-matrices have the form:

$$J_{ki}^{abc} = \begin{bmatrix} B_{ki}^{aa} & B_{ki}^{ab} & B_{ki}^{ac} & G_{ki}^{aa} & G_{ki}^{ab} & G_{ki}^{ac} \\ B_{ki}^{ba} & B_{ki}^{bb} & B_{ki}^{bc} & G_{ki}^{ba} & G_{ki}^{bb} & G_{ki}^{bc} \\ B_{ki}^{ba} & B_{ki}^{cb} & B_{ki}^{cc} & G_{ki}^{ca} & G_{ki}^{cb} & G_{ki}^{cc} \\ G_{ki}^{aa} & G_{ki}^{ab} & G_{ki}^{ac} & -B_{ki}^{aa} & -B_{ki}^{ab} & -B_{ki}^{ac} \\ G_{ki}^{ba} & G_{ki}^{bb} & G_{ki}^{bc} & -B_{ki}^{ba} & -B_{ki}^{bb} & -B_{ki}^{bc} \\ G_{ki}^{ca} & G_{ki}^{cb} & G_{ki}^{cc} & -B_{ki}^{ca} & -B_{ki}^{cb} & -B_{ki}^{cc} \end{bmatrix} \tag{2.78}$$

The diagonal sub-matrices $\boldsymbol{J_{kk}}$ of the Jacobian depend on the load model and they are computed in the same way as in (2.78) but adding a sub-matrix which the load [25].

$$J_{kk}^{abc} = \left[J_{kk}^{abc}\right]_{Y_{Bus}} + \left[L_{kk}^{abc}\right]_{Load} \tag{2.79}$$

The active and reactive power mismatches for phase *s* are given by:

$$\Delta P_k^s = (P_k^{spec})^s - (P_k^{calc})_r^s \tag{2.80}$$

$$\Delta Q_k^s = (Q_k^{spec})^s - (Q_k^{calc})_r^s \tag{2.81}$$

Where:

$$(P_k^{calc})^s = V_{k\,r}^s (I_k^{calc})_r^s + V_{k\,m}^s (I_k^{calc})_m^s \tag{2.82}$$

$$(Q_k^{calc})^s = V_{k\,r}^s (I_k^{calc})_m^s - V_{k\,r}^s (I_k^{calc})_m^s \tag{2.83}$$

The updated voltages at each iteration *h* are given by:

$$(V_k^{abc})_{rm}^{h+1} = (V_k^{abc})_{rm}^h + (\Delta V_k^{abc})_{rm}^h \tag{2.84}$$

Where the voltage vector $(V_k^{abc})_{rm}$ is defined as follows:

$$(V_k^{abc})_{rm} = \begin{bmatrix} V_{k\,r}^{a} \\ V_{k\,r}^{b} \\ V_{k\,r}^{c} \\ V_{k\,m}^{a} \\ V_{k\,m}^{b} \\ V_{k\,m}^{c} \end{bmatrix} \quad \textbf{(2.85}$$

2.3.3 Z_{Bus} Matrix Iterative Gauss-Seidel Method

Within the three-phase load-flow iterative methodologies, the implicit $\boldsymbol{Z_{Bus}}$ is the most commonly used method for radial distribution systems [28,29]. It works on the principle of superposition applied to the system bus voltages. According to this principle, only one type of source voltage is considered at time for the calculation of bus voltages. Initially, all the bus voltage magnitudes are assumed equal to the swing bus voltage (generally 1.0 p.u.), and the phase angles and current injections at load buses are set to zero. In the next step, the current injections and voltages are calculated iteratively. The simplified algorithm is as follows [28]:

- First, bus voltages are assumed to have some initial value, and the $\boldsymbol{Y_{Bus}}$ matrix is formed.
- Then, the current injections are computed using (2.86), and the initial voltage values.

$$I_k^{(i)} = \left(\frac{P_k^{spec} - jQ_k^{spec}}{V_k^{(i)*}} \right) \quad \textbf{(2.86)}$$

- The voltage deviation $\underline{\Delta V}$ due to current injections is calculated by the factorization of $\boldsymbol{Y_{Bus}}$ in (2.87).

$$\underline{I}^{(i)} = [Y_{Bus}][\underline{\Delta V}]^{(i)} \quad \textbf{(2.87)}$$

The factorization of $\boldsymbol{Y_{Bus}}$ gives the $\boldsymbol{Z_{Bus}}$ matrix, thus the system to solve in (2.77) is equivalent to:

$$[\underline{\Delta V}]^{(i)} = [Z_{Bus}]\underline{I}^{(i)}$$

- The voltage deviations calculated before, are superimposed on the no load bus voltage $\underline{V}_{NL}$, then the bus voltages are updated in (2.88), and the convergence is checked.

$$\underline{V}^{(i+1)} = \underline{V}_{NL} + [\underline{\Delta V}]^{(i)} \quad \textbf{(2.88)}$$

The implicit $\boldsymbol{Z_{Bus}}$ method described above requires the factorization of $\boldsymbol{Y_{Bus}}$ matrix, negatively affecting the performance in terms of speed. For this reason, a new method was proposed by Teng in [30], which uses the $\boldsymbol{Z_{Bus}}$ and Gauss-Seidel methods to improve the computational efficiency. The bus voltage in Gauss-Seidel method is computed according to equation (2.12), where the right hand side of this equation, for a *n*x*n* system, can be written in the matrix form as follows [28]:

$$\begin{bmatrix} Y_{11} & \cdots & Y_{1k} & \cdots & Y_{1n} \\ \vdots & & \vdots & & \vdots \\ Y_{k1} & \cdots & Y_{kk} & \cdots & Y_{kn} \\ \vdots & & \vdots & & \vdots \\ Y_{n1} & \cdots & Y_{nk} & \cdots & Y_{nn} \end{bmatrix} \begin{bmatrix} V_1^{(i)} \\ \vdots \\ V_k^{(i-1)} \\ \vdots \\ V_n^{(i-1)} \end{bmatrix} = \begin{bmatrix} I_1 \\ \vdots \\ I_k \\ \vdots \\ I_n \end{bmatrix} \quad \textbf{(2.89)}$$

Each element of $\boldsymbol{Y_{Bus}}$ corresponds to a 3x3 matrix:

$$Y_{kk} = \begin{bmatrix} Y_{kk-aa} & Y_{kk-ab} & Y_{kk-ac} \\ Y_{kk-ba} & Y_{kk-bb} & Y_{kk-bc} \\ Y_{kk-ca} & Y_{kk-cb} & Y_{kk-cc} \end{bmatrix} \quad \textbf{(2.90)}$$

Accordingly, the matrix $\boldsymbol{Y_{Bus}}$ can be arranged as:

$$Y_{Bus} = \begin{bmatrix} Y_{AA} & Y_{AB} & Y_{AC} \\ Y_{BA} & Y_{BB} & Y_{BC} \\ Y_{CA} & Y_{CB} & Y_{CC} \end{bmatrix} \quad \textbf{(2.91)}$$

Where each element is a *n*x*n* sub-matrix. Thus, equation (2.87) can be written as:

$$\begin{bmatrix} \underline{I}_A \\ \underline{I}_B \\ \underline{I}_C \end{bmatrix} = \begin{bmatrix} Y_{AA} & Y_{AB} & Y_{AC} \\ Y_{BA} & Y_{BB} & Y_{BC} \\ Y_{CA} & Y_{CB} & Y_{CC} \end{bmatrix} \begin{bmatrix} \Delta\underline{V}_A \\ \Delta\underline{V}_B \\ \Delta\underline{V}_C \end{bmatrix} \quad \textbf{(2.92)}$$

Where A, B, and C are the three phases of the system. Rearranging the set of linear equations (2.92), we get:

$$\Delta \underline{V}_A^{(i)} = Y_{AA}^{-1}(\underline{I}_A - Y_{AB}\underline{V}_B^{(i-1)} - Y_{AC}\underline{V}_C^{(i-1)}) \quad \textbf{(2.93)}$$

$$\underline{V}_A^{(i)} = \underline{V}_{A,NL} + \Delta \underline{V}_A^{(i)}$$

$$\Delta \underline{V}_B^{(i)} = Y_{BB}^{-1}(\underline{I}_B - Y_{BA}\underline{V}_A^{(i)} - Y_{BC}\underline{V}_C^{(i-1)}) \quad \textbf{(2.94)}$$

$$\underline{V}_B^{(i)} = \underline{V}_{B,NL} + \Delta \underline{V}_B^{(i)}$$

$$\Delta \underline{V}_C^{(i)} = Y_{CC}^{-1}(\underline{I}_C - Y_{CA}\underline{V}_A^{(i)} - Y_{CB}\underline{V}_B^{(i)}) \quad \textbf{(2.95)}$$

$$\underline{V}_C^{(i)} = \underline{V}_{C,NL} + \Delta \underline{V}_C^{(i)}$$

The values of voltages used in the modified Gauss-Seidel method are the most recently computed values, whereas the voltages used in the implicit $\boldsymbol{Z_{Bus}}$ methods are the values obtained in the previous iteration [28].

2.3.4 $\mathbf{Y_{Bus}}$ matrix iterative Gauss-Seidel method

The $\boldsymbol{Y_{Bus}}$ matrix method is based on the iterative solution of the linear equation $\underline{\boldsymbol{I}}_{\boldsymbol{Bus}} = \boldsymbol{Y_{Bus}}\underline{\boldsymbol{V}}_{\boldsymbol{Bus}}$ for the bus voltages using the relaxation algorithm described in [17]. The principle is the same used for positive-sequence systems described in section 2.1.2. The bus voltage at each node k is computed iteratively as follows [28]:

$$V_k^{(i+1)} = \frac{1}{Y_{kk}}\left[\frac{P_k - jQ_k}{V_k^{(i)*}} - \sum_{l=1}^{k-1} Y_{kl}V_l^{(i+1)} - \sum_{l=k+1}^{n} Y_{kl}V_l^{(i)}\right] \quad \textbf{(2.96)}$$

The $\boldsymbol{Y_{Bus}}$ matrix now is formed as in (2.89) including all the couplings present in three-phase systems and the voltage $\underline{V}$ vector has the dimension 3(2n)x1 owing to the three phase representation in real and imaginary part at each node. Due to iterative methods converge slowly, acceleration techniques are used to speed up the convergence. The most popular acceleration method is the successive over-relaxation (SOR) which can be explained using equation (2.97) where a fixed empirical factor α is applied to each voltage change.

$$\Delta V_k = \alpha \frac{\Delta S_k^*}{V_k^* Y_{kk}} \tag{2.97}$$

A good choice of α can significantly improve the convergence, and some divergent cases can sometimes converge.

2.3.5 Back and forward method

This methodology was developed by Ciric in [22] for four-wire unbalanced radial distribution systems. The algorithm is described in detail below for a single line l placed between nodes i and j. Let us define the impedance matrix for a section l with neutral wire and ground representation as:

$$Z_l = \begin{bmatrix} Z_{aa} & Z_{ab} & Z_{ac} & Z_{an} & Z_{ag} \\ Z_{ba} & Z_{bb} & Z_{bc} & Z_{bn} & Z_{bg} \\ Z_{ca} & Z_{cb} & Z_{cc} & Z_{cn} & Z_{cg} \\ Z_{na} & Z_{nb} & Z_{nc} & Z_{nn} & Z_{ng} \\ Z_{ga} & Z_{gb} & Z_{gc} & Z_{gn} & Z_{gg} \end{bmatrix} \tag{2.98}$$

Neglecting the shunt capacitances and assuming the same numbering scheme as in [23], the backward and forward proposed method consists of three steps. First, assuming a slack node with known voltage, the nodal current calculation at each iteration h is obtained from:

$$\begin{bmatrix} I_{ia} \\ I_{ib} \\ I_{ic} \\ I_{in} \\ I_{ig} \end{bmatrix}^{(h)} = \begin{bmatrix} (\frac{S_{ia}}{V_{ia}})^{(h-1)*} \\ (\frac{S_{ib}}{V_{ib}})^{(h-1)*} \\ (\frac{S_{ic}}{V_{ic}})^{(h-1)*} \\ -\frac{Z_{gi}}{Z_{nni}+Z_{gi}}(I_{ia}^h + I_{ib}^h + I_{ic}^h) \\ -\frac{Z_{nni}}{Z_{nni}+Z_{gi}}(I_{ia}^h + I_{ib}^h + I_{ic}^h) \end{bmatrix} - \begin{bmatrix} Y_{ia} & & & & \\ & Y_{ib} & & & \\ & & Y_{ic} & & \\ & & & Y_{in} & \\ & & & & 0 \end{bmatrix} \begin{bmatrix} V_{ia} \\ V_{ib} \\ V_{ic} \\ V_{in} \\ V_{ig} \end{bmatrix}^{(h-1)} \tag{2.99}$$

Where for each phase (a, b, c, n, and g), I_i is the current injection at node i, S_i the scheduled power injection at node i, V_i the voltage at node i, and Y_i the admittance of all

shunt elements at node *i*. Z_{gi} is the sum of the ground impedance and ground resistivity. The second step is the backwards sweep, where section currents are calculated starting from the last layer and moving backwards the root or slack node. The section currents are computed by:

$$\begin{bmatrix} J_{La} \\ J_{Lb} \\ J_{Lc} \\ J_{Ln} \\ J_{Lg} \end{bmatrix}^{(h)} = -\begin{bmatrix} I_{ja} \\ I_{jb} \\ I_{jc} \\ I_{jn} \\ I_{jg} \end{bmatrix}^{(h)} + \sum_{m \in M} \begin{bmatrix} J_{Ma} \\ J_{Mb} \\ J_{Mc} \\ J_{Mn} \\ J_{Mg} \end{bmatrix}^{(h)} \tag{2.100}$$

Where J_L and J_M are the currents in sections l and m respectively, and M corresponds to the set of sections connected downstream to node j. The third step is the forward sweep, where bus voltages are computed starting for the root bus and moving forwards the last layer. The voltage at node j is:

$$\begin{bmatrix} V_{ja} \\ V_{jb} \\ V_{jc} \\ V_{jn} \\ V_{jg} \end{bmatrix}^{(h)} = \begin{bmatrix} V_{ia} \\ V_{ib} \\ V_{ic} \\ V_{in} \\ V_{ig} \end{bmatrix}^{(h)} - \begin{bmatrix} Z_{aa} & Z_{ab} & Z_{ac} & Z_{an} & Z_{ag} \\ Z_{ba} & Z_{bb} & Z_{bc} & Z_{bn} & Z_{bg} \\ Z_{ca} & Z_{cb} & Z_{cc} & Z_{cn} & Z_{cg} \\ Z_{na} & Z_{nb} & Z_{nc} & Z_{nn} & Z_{ng} \\ Z_{ga} & Z_{gb} & Z_{gc} & Z_{gn} & Z_{gg} \end{bmatrix} \begin{bmatrix} J_{La} \\ J_{Lb} \\ J_{Lc} \\ J_{Ln} \\ J_{Lg} \end{bmatrix}^{(h)} \tag{2.101}$$

The voltage in the grounded nodes has to be corrected with the following expression:

$$V_{in}^{(h)} = Z_{grl} J_{lg}^{(h)}, \; i \in \{\text{grounded nodes}\} \tag{2.102}$$

The convergence criteria is computed from the power at each node for all phases, neutral and ground. As example, for phase *a*, we have:

$$\Delta \underline{S}_{an}^{(h)} = \underline{V}_{ia}^{(h)} \underline{I}_{ia}^{(h)*} - Y_{ia}^{*} \left| \underline{V}_{ia}^{(h)} \right|^2 - \underline{S}_{ia} \tag{2.103}$$

Similarly to previous methods, the initial voltage for all the nodes is defined as:

$$\begin{bmatrix} V_{ia} \\ V_{ib} \\ V_{ic} \\ V_{in} \\ V_{ig} \end{bmatrix} = \begin{bmatrix} V_{ref} \\ a^2 V_{ref} \\ aV_{ref} \\ 0 \\ 0 \end{bmatrix} \qquad a = e^{j2\pi/3} \tag{2.104}$$

When uniform grounded earth is found in a system, Carson's equations allow us to reduce the 5x5 matrix to a 4x4 impedance matrix with ground implicit in the four conductors. Kron's reduction can also be applied in order to reduce further the matrix eliminating the neutral conductor and getting a 3x3 phase matrix size with both ground and neutral wire implicit [22]. Using Carson and Kron's approximations, any three-phase load-flow method can be applied to the impedance matrix defined in (2.98).

2.3.6 Modified Augmented Nodal Matrix (EMTP-RV)

The EMTP-RV algorithm is included in this section since this tool is utilized for the purpose of validating the present research work. EMTP-RV is a powerful tool for analyzing electromagnetic transient phenomena in power systems, and for solving multi-phase unbalanced load-flow systems. Its load-flow solution is also essential for initializing time-domain system simulations. The EMTP-RV load-flow methodology developed by Mahseredjian in [32] is based on a multi-phase Newton formulation of the admittance matrix described in section 2.1.4, and is known as the modified-augmented nodal matrix. The general system of equations, including all the load-flow constraints, is given by:

$$\begin{bmatrix} Y_n & V_c & D_c & S_c & A_{IL} & A_{IG} & 0 \\ V_r & 0 & 0 & 0 & 0 & 0 & 0 \\ D_r & 0 & 0 & 0 & 0 & 0 & 0 \\ S_r & 0 & 0 & S_d & 0 & 0 & 0 \\ C_{LPQ} & 0 & 0 & 0 & D_{LPQ} & 0 & 0 \\ Y_{GI} & 0 & 0 & 0 & 0 & B_{GI} & Y_{GE} \\ C_{GPQ} & 0 & 0 & 0 & 0 & D_{GPQ} & 0 \\ H_{PV} & 0 & 0 & 0 & 0 & 0 & 0 \\ H_{sl} & 0 & 0 & 0 & 0 & 0 & 0 \end{bmatrix} \times \begin{bmatrix} \Delta V_n \\ \Delta I_V \\ \Delta I_D \\ \Delta I_S \\ \Delta I_L \\ \Delta I_G \\ \Delta E_{GA} \end{bmatrix} = -\begin{bmatrix} f_n \\ f_V \\ f_D \\ f_S \\ f_{LPQ} \\ f_{GI} \\ f_{GPQ} \\ f_{GPV} \\ f_{sl} \end{bmatrix} \tag{2.105}$$

If the load currents are represented by subscript $_L$ and machine currents by subscript $_G$, the network equations at each iteration k can be written as follows:

$$Y_n V_n + V_c I_V + D_c I_D + S_c I_S + A_{IL} I_L + A_{IG} I_G - In = f_n = 0 \qquad \textbf{(2.106)}$$

This formulation accounts for an arbitrary network that might include any EMTP-RV devices. The matrices $\boldsymbol{A_{IL}}$ and $\boldsymbol{A_{IG}}$ are adjacency matrices, vector $\underline{\boldsymbol{I_D}}$ holds dependent branch currents (ideal transformers, for example), $\underline{\boldsymbol{I_S}}$ holds switch currents, $\underline{\boldsymbol{I_L}}$ load currents, $\underline{\boldsymbol{I_G}}$ machine generator currents, and $\underline{\mathbf{I}}_\mathbf{n}$ independent source injections. The Jacobian terms at the iteration k are found from the following system of equations:

$$f_n^{(k)} + Y_n \Delta V_n + V_c \Delta I_V + D_c \Delta I_D + S_c \Delta I_S + A_{IL} \Delta I_L + A_{IG} \Delta I_G = 0 \qquad \textbf{(2.107)}$$

The equations to find the Jacobian terms are described as follows:

- Independent voltage sources between nodes k and m, where m is usually ground.

$$V_k - V_m - V_b = f_V = 0$$

$$f_V^{(h)} - \Delta V_k - \Delta V_m = 0 \qquad \textbf{(2.108)}$$

- Ideal transformers between pair of nodes mk and ij

$$V_k - V_m - gV_i + gV_j = f_D = 0$$

$$f_D^{(h)} + \Delta V_k - \Delta V_m - g\Delta V_i + g\Delta V_j = 0 \qquad \textbf{(2.109)}$$

- Ideal switches between nodes k and m

$$V_k - V_m = f_S = 0$$

$$f_S^{(h)} - \Delta V_k - \Delta V_m = 0 \qquad \textbf{(2.110)}$$

$\Delta I_S = 0$, when a switch is open.

- Load (single–phase branch)

$P = 3\,\mathrm{Re}\{V_L I_L^*\}$, and $Q = 3\,\mathrm{Im}\{V_L I_L^*\}$

$V_L = e_r + je_i$, and $I_L = i_r + ji_i$

$$P' - e_r i_r + e_i i_i = f_{LP} = 0$$

$$Q' - e_i i_r + e_r i_i = f_{LQ} = 0$$

$$f_{LP}^{(h)} - \Delta e_r i_r - \Delta e_i i_i - e_r \Delta i_r - e_i \Delta i_i = 0 \quad \textbf{(2.111)}$$

$$f_{LQ}^{(h)} - \Delta e_i i_r + \Delta e_r i_i - e_i \Delta i_r + e_r \Delta i_i = 0 \quad \textbf{(2.112)}$$

It contributes into the matrices $\boldsymbol{C_{LPQ}}$ and $\boldsymbol{D_{LPQ}}$ of the system (2.105).

- Machine current constraint (between k and m)

$$f_{GI}^{(h)} - Y_{GI}(\Delta V_k - \Delta V_m - \Delta E_G) - \Delta I_G = 0 \quad \textbf{(2.113)}$$

$$\Delta E_G = \begin{bmatrix} 1 \\ a^2 \\ a \end{bmatrix} \Delta E_{GA} \quad , \ \Delta E_{GA} : \text{Internal machine voltage (phase } a\text{).}$$

The above equations contribute into the matrices $\boldsymbol{Y_{GI}}$, $\boldsymbol{B_{GI}}$, and $\boldsymbol{Y_{GE}}$ with:

$$Y_{GE} = \begin{bmatrix} 1 \\ a^2 \\ a \end{bmatrix} Y_{GI}$$

- PV Machine with constraint on the magnitude of one phase p:

$$f_{GPV}^{(h)} - \frac{(e_r^p \Delta e_r^p + e_i^p \Delta e_i^p)}{\sqrt{(e_r^p)^2 + (e_i^p)^2}} = 0 \quad \textbf{(2.114)}$$

The above equation contributes into the matrix H_{PV}.

- Slack machine

$$f_{slr}^{(h)} - \frac{1}{3}\Delta e_{ra} + \frac{1}{6}\Delta e_{rb} + \frac{\sqrt{3}}{6}\Delta e_{ib} + \frac{1}{6}\Delta e_{rc} - \frac{\sqrt{3}}{6}\Delta e_{ic} = 0 \quad \textbf{(2.115)}$$

$$f_{sli}^{(h)} - \frac{1}{3}\Delta e_{ia} + \frac{1}{6}\Delta e_{ib} - \frac{\sqrt{3}}{6}\Delta e_{rb} + \frac{1}{6}\Delta e_{ic} + \frac{\sqrt{3}}{6}\Delta e_{rc} = 0 \quad \textbf{(2.116)}$$

The above equation contributes into the matrix H_{sl}.

The complete set of equations required to form the Jacobian matrix can be found in reference [32].

The linearized system equations presented in (2.105) is solved with an iterative method starting with an initial voltage and current vectors. Each complex quantity is converted to a two-by-two block in the nodal matrix and each vector of unknowns includes real and imaginary parts. The numerical solver considers a "Minimum-degree

Ordering" (MDO) in the elimination process of the augmented nodal matrix at each iteration.

The initialization in EMTP-RV starts from a steady-state phasor solution by replacing all the loads by equivalent shunt branches and by eliminating all other load-flow constraints. This approach forces the system to become linear and allows finding the unknown vectors $\underline{V}_n$, $\underline{I}_V$, $\underline{I}_D$, and $\underline{I}_S$. The amplitude and phase of the voltage and current sources are those provided by the user. In cases where this information is not available from practical data or previous load-flow studies of the given network, the user can always enter perfectly balanced sources with phase-*a* set at zero degrees. Such situations might not be realistic for power transmissions constrain, but it is still expected to achieve convergence using the above steady-state phase solution guess.

3 POSITIVE-SEQUENCE EQUIVALENT MODELS OF MUTUALLY-COUPLED MULTI-PHASE DEVICES

The equivalent circuits of mutually-coupled multi-phase networks presented here were originally proposed by Alvarado [35] and Smolleck [37], and afterwards generalized by Chen [29,36]. The method produces a positive-sequence representation of all electromagnetically coupled and uncoupled components in electrical systems including multi-phase transmission lines, cables, transformers, loads, generators, voltage-controlled regulators, and compensation devices. The procedure, which can be applied to the analysis of any unbalanced transmission or distribution network with or without transposition, produces no additional buses of a multi-phase system maintaining the same structure of the original system.

This positive-sequence representation can be easily derived and understood in terms of elementary graph theory. Once this has been done, the branch elements can be determined by inspection for the majority of cases. The resulting elements can be easily added in the admittance matrix of the network, independently of the size of the system, after applying the inversion of a small and symmetric primitive impedance matrix. This method is theoretically exact and numerically stable. It has proven to be computationally robust for real and artificially complex transmission and distribution systems [34].

Most common devices are presented in this research work. The exceptions are the voltage-controlled devices, which are out of the scope of the present work. However, they could be included in the future by using the same iterative method implemented for representing constant power loads discussed at the end of this chapter.

3.1 Representation of transmission lines and cables

The most general line representation, neglecting capacitive coupling, corresponds to a three-phase four-wire multi-grounded line configuration as shown in figure 3.1. There, the neutral conductor and the ground are explicitly represented as it is found in real distribution systems. In the same figure, the coupled impedances for the phase *a* are shown.

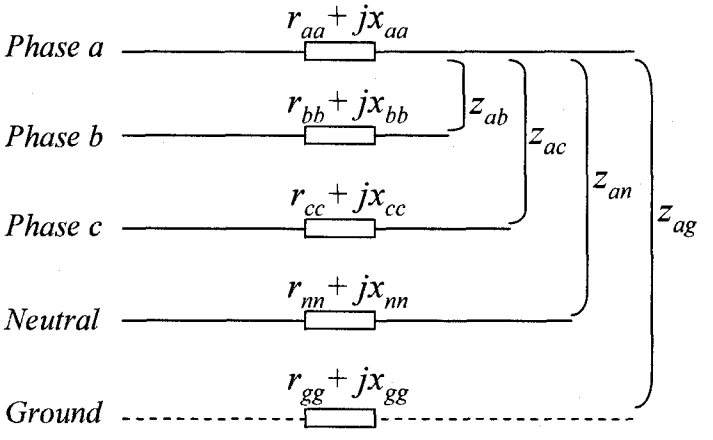

Figure 3.1 General four-wire line and ground representation

The primitive impedance matrix $\boldsymbol{Z_{prim}}$ of the line section in figure 3.1 is given by:

$$Z_{prim} = \begin{bmatrix} Z_{aa} & Z_{ab} & Z_{ac} & Z_{an} & Z_{ag} \\ Z_{ba} & Z_{bb} & Z_{bc} & Z_{bn} & Z_{bg} \\ Z_{ca} & Z_{cb} & Z_{cc} & Z_{cn} & Z_{cg} \\ Z_{na} & Z_{nb} & Z_{nc} & Z_{nn} & Z_{ng} \\ Z_{ga} & Z_{gb} & Z_{gc} & Z_{gn} & Z_{gg} \end{bmatrix} \quad \textbf{(3.1)}$$

Before developing this general case, let us first make some simplifications in order reduce this configuration to a three-phase three-wire line representation by applying the Carson's equations and Kron reduction [2,38].

3.1.1 Carson's equations and Kron reduction

Carson's equations permit to represent implicitly the ground coupling effect over the line wires [38]. Thus, for a four-wire line segment, the series impedance matrix elements, considering a uniform ground resistivity of 100 [Ω-m] and a frequency of 60 Hz, are given by:

$$z_{ii} = r_i + 0.0953 + j0.12134 \times \left[\ln\left(\frac{1}{GMR_i}\right) + 7.934 \right] \quad [\Omega/mi] \tag{3.2}$$

$$z_{ij} = 0.0953 + j0.12134 \times \left[\ln\left(\frac{1}{D_{ij}}\right) + 7.934 \right] \quad [\Omega/mi] \tag{3.3}$$

Where r_i is the conductor resistance, GMR_i the conductor geometric means radius, and D_{ij} the spacing between conductors i and j with $i, j \in (a,b,c,n)$. Thus, the impedance matrix $\boldsymbol{Z}^c_{prim}$ shown in (3.1) becomes:

$$Z^c_{prim} = \begin{bmatrix} z_{aa} & z_{ab} & z_{ac} & z_{an} \\ z_{ba} & z_{bb} & z_{bc} & z_{bn} \\ z_{ca} & z_{cb} & z_{cc} & z_{cn} \\ z_{na} & z_{nb} & z_{nc} & z_{nn} \end{bmatrix} \quad [\Omega/mi] \tag{3.4}$$

In addition, matrix (3.4) can be reduced to a 3x3 size matrix by using the Kron reduction. By doing this, the elements of the derived matrix are given by:

$$z^r_{ii} = z_{ij} - z_{in}\frac{z_{nj}}{z_{nn}} \quad [\Omega/mi] \qquad , \qquad i,j \in (a,b,c) \tag{3.5}$$

Thus, the reduced primitive impedance matrix for a three-phase line is given by:

$$Z^r_{abc} = \begin{bmatrix} z^r_{aa} & z^r_{ab} & z^r_{ac} \\ z^r_{ba} & z^r_{bb} & z^r_{bc} \\ z^r_{ca} & z^r_{cb} & z^r_{cc} \end{bmatrix} [\Omega/mi] \tag{3.6}$$

To complete the three-phase line model we need to know the reduced admittance matrix $\boldsymbol{B^r_{abc}}$, which includes all the capacitive coupled elements [38]:

$$B^r_{abc} = \begin{bmatrix} b^r_{aa} & b^r_{ab} & b^r_{ac} \\ b^r_{ba} & b^r_{bb} & b^r_{bc} \\ b^r_{ca} & b^r_{cb} & b^r_{cc} \end{bmatrix} [\mu S / mi] \tag{3.7}$$

The elements of $\boldsymbol{B^r_{abc}}$ are given by:

$$B^r_{abc} = 2\pi \times f \times \left[C^r_{abc}\right] \ [\mu S / mi] \tag{3.8}$$

Where,

$$\left[C^r_{abc}\right] = \left[P^r_{abc}\right]^{-1} = \begin{bmatrix} p^r_{aa} & p^r_{ab} & p^r_{ac} \\ p^r_{ba} & p^r_{bb} & p^r_{bc} \\ p^r_{ca} & p^r_{cb} & p^r_{cc} \end{bmatrix}^{-1} [\mu S / mi] \tag{3.9}$$

The elements of $\boldsymbol{P_{abc}}$ before Kron reduction are given by:

$$p_{ii} = 11.17689 \ln\left(\frac{S_{ii}}{RD_i}\right) [mi / \mu F] \tag{3.10}$$

$$p_{ij} = 11.17689 \ln\left(\frac{S_{ij}}{RD_{ij}}\right) [mi / \mu F] \tag{3.11}$$

Where RD_i is the radius of the conductor i, and S_{ij} the spacing between conductors i and j with $i,j \in (a,b,c,n)$. To get the matrix (3.9), the Kron reduction shown in (3.12) is previously required.

$$P^r_{abc} = \left[P_{ij}\right] - \left[P_{in}\right]\left[P_{nn}\right]^{-1}\left[P_{nj}\right] \tag{3.12}$$

3.1.2 Three-phase mutually-coupled line model

In positive-sequence load-flow solvers, a balanced three-phase line is typically represented by only its positive-sequence series impedance and two shunt admittances (π model). In the proposed methodology, a three-phase line section *k-m* is represented by 21 lines as shown in figure 3.2. There are 15 lines that represent the impedance matrix, and 6 lines represent the capacitive mutual couplings. The 6 mutual capacitances can be paralleled with the 6 fictitious mutual inductances in order to reduce the number of lines to 15. The 6 shunt capacitances can be entered as shunt admittances in the single-phase π line model connecting same phase buses (k_a-m_a, k_b-m_b, and k_c-m_c). These artificial lines do not have a physical meaning [36,37].

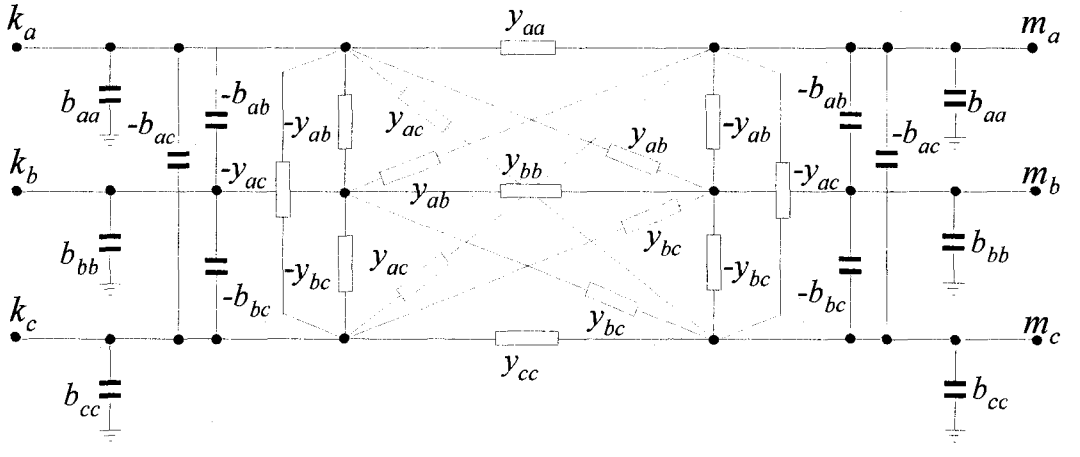

Figure 3.2 Positive-sequence equivalent circuit of a three-phase mutually coupled line section

The bus admittance matrix $\boldsymbol{Y_{Bus\_L}}$ of the line section circuit in figure 3.2 is obtained by multiplying the inverse of the primitive impedance matrix $\boldsymbol{Z_{abc}}$ and the branch-bus incidence matrix $\boldsymbol{N}$ [37] as is shown in (3.13).

$$Y_{Bus\_L} = N^T \times Z_{abc}^{-1} \times N \qquad \textbf{(3.13)}$$

Where:

$$Z_{abc}^{-1} = Y_{abc} = \begin{bmatrix} z_{aa} & z_{ab} & z_{ac} \\ z_{ba} & z_{bb} & z_{bc} \\ z_{ca} & z_{cb} & z_{cc} \end{bmatrix}^{-1} = \begin{bmatrix} y_{aa} & y_{ab} & y_{ac} \\ y_{ba} & y_{bb} & y_{bc} \\ y_{ca} & y_{cb} & y_{cc} \end{bmatrix} \tag{3.14}$$

$$N = \begin{bmatrix} 1 & 0 & 0 & -1 & 0 & 0 \\ 0 & 1 & 0 & 0 & -1 & 0 \\ 0 & 0 & 1 & 0 & 0 & -1 \end{bmatrix}$$

Thus, the equivalent three-phase $\boldsymbol{Y_{Bus\_L}}$ matrix of the circuit in figure 3.2, including the capacitive elements, is computed as follows:

$$Y_{Bus\_L} = \begin{bmatrix} y_{aa} & y_{ab} & y_{ac} & -y_{aa} & -y_{ab} & -y_{ac} \\ y_{ba} & y_{bb} & y_{bc} & -y_{ba} & -y_{bb} & -y_{bc} \\ y_{ca} & y_{cb} & y_{cc} & -y_{ca} & -y_{cb} & -y_{cc} \\ -y_{aa} & -y_{ab} & -y_{ac} & y_{aa} & y_{ab} & y_{ac} \\ -y_{ba} & -y_{bb} & -y_{bc} & y_{ba} & y_{bb} & y_{bc} \\ -y_{ca} & -y_{cb} & -y_{cc} & y_{ca} & y_{cb} & y_{cc} \end{bmatrix} + \begin{bmatrix} b_{aa} & b_{ab} & b_{ac} & 0 & 0 & 0 \\ b_{ba} & b_{bb} & b_{bc} & 0 & 0 & 0 \\ b_{ca} & b_{cb} & b_{cc} & 0 & 0 & 0 \\ 0 & 0 & 0 & b_{aa} & b_{ab} & b_{ac} \\ 0 & 0 & 0 & b_{ba} & b_{bb} & b_{bc} \\ 0 & 0 & 0 & b_{ca} & b_{cb} & b_{cc} \end{bmatrix} \tag{3.15}$$

This matrix is equivalent to the admittance matrix proposed by Alvarado in [35] for a three-phase coupled line between nodes *k* and *m*, and which derived from the nodal formulation as follows:

$$I_{km}^{abc} = Y_{Bus\_L} \times V_{km}^{abc} \tag{3.16}$$

$$Y_{Bus\_L} = \begin{bmatrix} Y_{km}^{abc} + B_{kk}^{abc} & -Y_{km}^{abc} \\ -Y_{mk}^{abc} & Y_{km}^{abc} + B_{mm}^{abc} \end{bmatrix} \tag{3.17}$$

For an electromagnetically unbalanced three-phase transmission line, the admittance matrix is symmetric and it has a maximum of six different values, which are: y_{aa}, y_{bb}, y_{cc}, y_{ab}, y_{bc}, and y_{ac}. As it was shown in chapter 2, the admittance elements of the system matrix $\boldsymbol{Y_{Bus}}$ are computed as follows:

y_{kk} = $\sum$ (Admittances connected to bus *k*)

y_{kl} = y_{lk} = -$\sum$ (Admittances connected between bus *k* and *l*, $k \neq l$)

Thus, the values of the line impedance matrix elements of the equivalent three-phase representation, which will be added to the complete system matrix $\boldsymbol{Y_{Bus}}$, are given by:

$$z_{ij} = -z_{ij'} = z_{i'j'} = -\frac{1}{y_{ij}} \tag{3.18}$$

$$z_{ii'} = \frac{1}{y_{ii}} \tag{3.19}$$

with $i, j, i', j' \in (a, b, c)$.

The mutual capacitive effects of the circuit in figure 3.2, are represented by the reduced matrix (3.7). Thus, six additional artificial lines have to be entered into the system matrix $\boldsymbol{Y_{Bus}}$, having the following impedances values:

$$z_{ij}^{c} = z_{i'j'}^{c} = -j\frac{2}{b_{ij}} \tag{3.20}$$

As it was explained before, the impedances derived from (3.20) can be paralleled to those derived from (3.18) in order to reduce the number of artificial lines. Finally, the mutual-susceptances b_{ab}, b_{bc}, and b_{ca} should not add up to the sum of the diagonal elements. Therefore, the difference has to be added in a capacitor to ground whose phase value is given by:

$$b_{gi} = b_{ii} - \sum_{j \neq i} b_{ij} \qquad i, j \in (a,b,c) \tag{3.21}$$

These shunt impedances need to be entered in both sides of the transmission lines connecting buses k_a-m_a, k_b-m_b, and k_c-m_c, divided by to two in order to get the definitive π model.

The three-wire line model derived before can represent a three-phase line, a two-phase plus explicit neutral conductor, or even a single-phase plus explicit neutral conductor and ground representation. The number of artificial lines of the derived model, neglecting the capacitive couplings, can be computed with the equation $Np(Np\text{-}1)/2$,

being *Np* two times the number of phases (or wires) *n* of the line section. For a three-phase line *Np* is 6, which implies a number of artificial lines equal to 6x(6-1)/2=15.

For a four-wire three-phase line, which can represent a three-phase line plus neutral conductor, a three-phase line plus explicit ground or a two-phase line plus neutral conductor and ground, the number of artificial lines is 8x(8-1)/2=28. Due to the complexity of the four-wire line model, the drawing of its circuit is not included in this report. However this model, which is derived in the same way as for the three-phase line model, is included within the developed algorithm and test cases in the validation benchmark. Even though the ground representation can be easily added in the line model, the difficulty of getting the ground resistivity data will usually lead us to represent the ground in an implicit way using Carson's equations.

3.1.3 Two-phase mutually-coupled line model

The two-wire representation can model a two-phase line or a single-phase plus neutral (or ground), which is extremely useful for distribution networks analysis. Its representation is similar to the three-wire line case, but the number of artificial lines is 4x(4-1)/2=6. A two-phase line section *k-m* is represented by the circuit shown in figure 3.3.

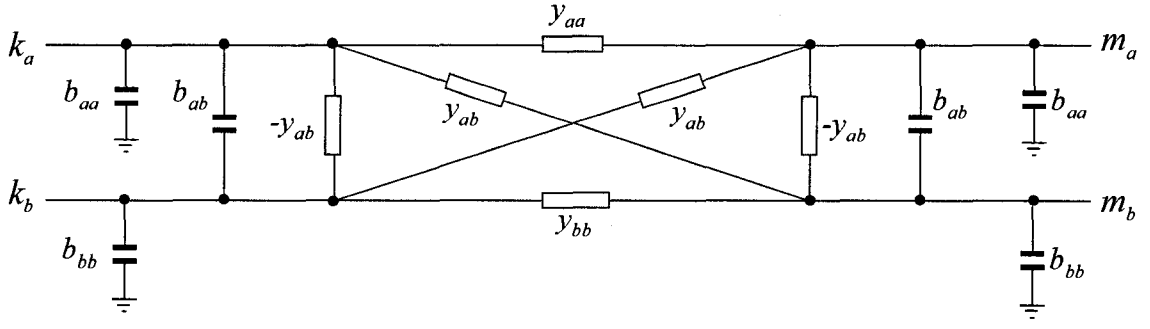

Figure 3.3 Positive-sequence equivalent circuit of a two-phase mutually coupled line section

The bus admittance matrix $\boldsymbol{Y}_{Bus\_L}$ of the circuit of figure 3.3 is formed by multiplying the inverse of the primitive impedance $\boldsymbol{Z}_{ab}$ matrix and the branch-bus incidence matrix $\boldsymbol{N}$ as in (3.22).

$$Y_{Bus\_L} = N^T \times Z_{ab}^{-1} \times N \tag{3.22}$$

Where,

$$Z_{ab}^{-1} = Y_{ab} = \begin{bmatrix} z_{aa} & z_{ab} \\ z_{ba} & z_{bb} \end{bmatrix}^{-1} = \begin{bmatrix} y_{aa} & y_{ab} \\ y_{ba} & y_{bb} \end{bmatrix}$$

$$N = \begin{bmatrix} 1 & 0 & -1 & 0 \\ 0 & 1 & 0 & -1 \end{bmatrix}$$

Thus, the equivalent two-phase line $\boldsymbol{Y_{Bus\_L}}$ matrix is given by:

$$Y_{Bus\_L} = \begin{bmatrix} y_{aa} & y_{ab} & -y_{aa} & -y_{ab} \\ y_{ba} & y_{bb} & -y_{ba} & -y_{bb} \\ -y_{aa} & -y_{ab} & y_{aa} & y_{ab} \\ -y_{ba} & -y_{bb} & y_{ba} & y_{bb} \end{bmatrix} \tag{3.23}$$

The values of the line impedance matrix elements of the equivalent two-phase representation, which will be added to the complete system matrix $\boldsymbol{Y_{Bus\_L}}$, are given by:

$$z_{ij} = -z_{ij'} = z_{i'j'} = -\frac{1}{y_{ij}} \tag{3.24}$$

$$z_{ii'} = \frac{1}{y_{ii}} \tag{3.25}$$

With $i, j, i', j' \in (a, b)$.

Matrix $\boldsymbol{B_{ab}}$ represents the mutual capacitive effect of the circuit in figure 3.3, and its elements are computed as in equation (3.8).

3.2 Transformer representation

The proposed transformers modeling method was first developed by Chen in [39,40,41], and it basically computes the admittance matrix formed by the connection of single-phase transformers units. Only the transformer leakage impedance is considered, which means that core losses are neglected. Most typical transformer connections models are derived in this section, including some unusual connections mostly used in distribution systems.

3.2.1 Three-phase transformer models

Based on the assumption of single-phase transformers connected to form three-phase transformers, the transformer admittance matrices are developed following the same approach as in the line model. Thus, performing the same nodal analysis, and determining the incidence matrix N, a three-phase delta-grounded wye transformer the admittance matrix $\boldsymbol{Y}_{Bus\_T}$ is computed as [39]:

$$Y_{Bus\_T} = \begin{bmatrix} \frac{2y_t}{3\alpha^2} & \frac{-y_t}{3\alpha^2} & \frac{-y_t}{3\alpha^2} & \frac{-y_t}{\sqrt{3}\alpha\beta} & 0 & \frac{y_t}{\sqrt{3}\alpha\beta} \\ \frac{-y_t}{3\alpha^2} & \frac{2y_t}{3\alpha^2} & \frac{-y_t}{3\alpha^2} & \frac{y_t}{\sqrt{3}\alpha\beta} & \frac{-y_t}{\sqrt{3}\alpha\beta} & 0 \\ \frac{-y_t}{3\alpha^2} & \frac{-y_t}{3\alpha^2} & \frac{2y_t}{3\alpha^2} & 0 & \frac{y_t}{\sqrt{3}\alpha\beta} & \frac{-y_t}{\sqrt{3}\alpha\beta} \\ \frac{-y_t}{\sqrt{3}\alpha\beta} & \frac{y_t}{\sqrt{3}\alpha\beta} & 0 & \frac{y_t}{\beta^2} & 0 & 0 \\ 0 & \frac{-y_t}{\sqrt{3}\alpha\beta} & \frac{y_t}{\sqrt{3}\alpha\beta} & 0 & \frac{y_t}{\beta^2} & 0 \\ \frac{y_t}{\sqrt{3}\alpha\beta} & 0 & \frac{-y_t}{\sqrt{3}\alpha\beta} & 0 & 0 & \frac{y_t}{\beta^2} \end{bmatrix} \quad \textbf{(3.26)}$$

Where y_t is the per unit leakage admittance of the single-phase transformer. For the sake of simplicity, the leakage admittances of each phase are assumed to be identical. The parameters α and β represent the off-nominal tap at the primary and secondary sides of the transformer. Therefore, the ratio α/β corresponds to the transformer ratio. The three-phase transformer model with the artificial coupled lines can be derived by inspection of the admittance matrix (3.26). The resulting circuit is shown in figure 3.4.

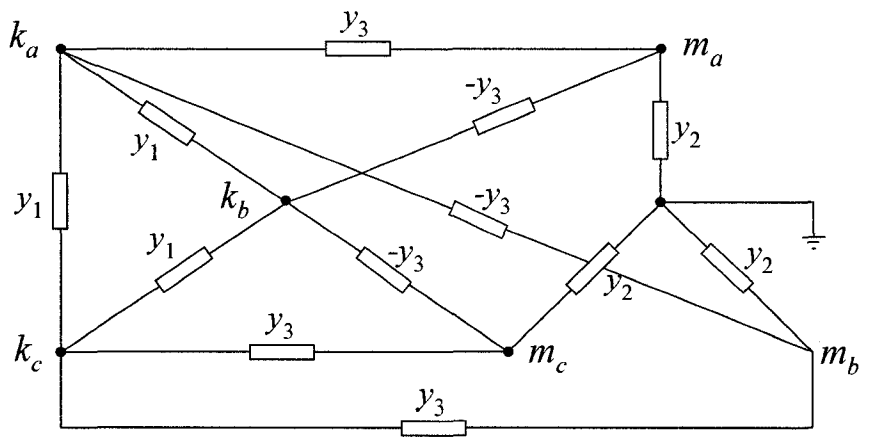

Figure 3.4 Positive-sequence equivalent circuit of a three–phase delta-grounded wye transformer

Where y_1, y_2, and y_3 are computed as follows:

$$y_1 = \frac{y_t}{3\alpha^2} \qquad y_2 = \frac{y_t}{\beta^2} \qquad y_3 = \frac{y_t}{\sqrt{3}\alpha\beta} \tag{3.27}$$

Let us define the following sub-matrices:

$$Y_I = \begin{bmatrix} y_t & 0 & 0 \\ 0 & y_t & 0 \\ 0 & 0 & y_t \end{bmatrix},\ Y_{II} = \frac{1}{3}\begin{bmatrix} 2y_t & -y_t & -y_t \\ -y_t & 2y_t & -y_t \\ -y_t & -y_t & 2y_t \end{bmatrix},\ \text{and}\ \ Y_{III} = \frac{1}{\sqrt{3}}\begin{bmatrix} -y_t & y_t & 0 \\ 0 & -y_t & 0 \\ y_t & 0 & -y_t \end{bmatrix}$$

Thus, the delta-grounded wye transformer the admittance matrix $\boldsymbol{Y_{Bus\_T}}$ can be expressed as:

$$Y_{Bus\_T} = \begin{bmatrix} Y_{pp} & Y_{ps} \\ Y_{sp} & Y_{ss} \end{bmatrix} = \begin{bmatrix} Y_{II} & Y_{III}^T \\ Y_{III} & Y_I \end{bmatrix}$$

Where p and s indicate the primary and secondary sides of the transformer. The admittance sub-matrices used in forming the three-phase transformer admittance matrix $\boldsymbol{Y_{Bus\_T}}$ for the most typical connections are given in table 3.1.

Table 3.1 Sub-matrices for typical three-phase transformer connections

Primary	Secondary	Y_{pp}	Y_{ss}	Y_{ps}	Y_{sp}
Y_g	Y_g	Y_I	Y_I	$-Y_I$	$-Y_I$
Y_g	Y	Y_{II}	Y_{II}	$-Y_{II}$	$-Y_{II}$
Y_g	Δ	Y_I	Y_{II}	Y_{III}	Y_{III}^T
Y	Y_g	Y_{II}	Y_{II}	$-Y_{II}$	$-Y_{II}$
Y	Y	Y_{II}	Y_{II}	$-Y_{II}$	$-Y_{II}$
Y	Δ	Y_{II}	Y_{II}	Y_{III}	Y_{III}^T
Δ	Y_g	Y_{II}	Y_I	Y_{III}^T	Y_{III}
Δ	Y	Y_{II}	Y_{II}	Y_{III}^T	Y_{III}
Δ	Δ	Y_{II}	Y_{II}	$-Y_{II}$	$-Y_{II}$

This three-phase transformer modeling is described in detail by Chen in [39], and Xiao in [41].

3.2.2 Open delta-open delta and open wye-open delta transformers

The open delta-open delta and open wye-open delta transformer models for three-phase distribution analysis are developed in [42] and [43]. Following the same approach as before, let us consider the circuit for the open delta-open delta transformer shown in figure 3.5.

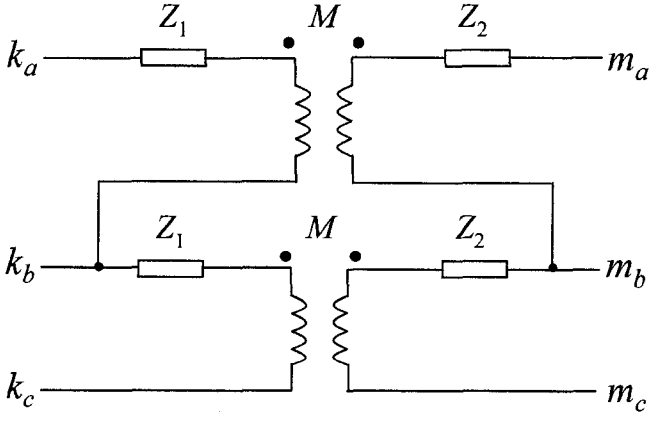

Figure 3.5 Two single-phase transformers for an open delta-open delta connection

The circuit in figure 3.5, corresponds to two identical single-phase transformers with leakage impedances given by:

$$\begin{aligned} z_1 &= R_1 + j\omega L_1 \\ z_2 &= R_2 + j\omega L_2 \\ z_m &= j\omega M \end{aligned} \tag{3.28}$$

Then, applying the nodal analysis over the circuit and multiplying by the incidence matrix ***N***, the resulting admittance matrix $\boldsymbol{Y_{Bus\_T}}$ for the open delta-open delta transformer connection is given by:

$$Y_{Bus\_T} = \frac{1}{z_1 z_2 - z_m^2} \begin{bmatrix} z_2 & -z_2 & 0 & -z_m & z_m & 0 \\ -z_2 & 2z_2 & -z_2 & z_m & -2z_m & z_m \\ 0 & -z_2 & z_2 & 0 & z_m & -z_m \\ -z_m & z_m & 0 & z_1 & -z_1 & 0 \\ z_m & -2z_m & z_m & -z_1 & 2z_1 & -z_1 \\ 0 & z_m & -z_m & 0 & -z_1 & z_1 \end{bmatrix} \tag{3.29}$$

The ratio n_1/n_2 corresponds to the single-phase transformer ratio. Assuming the coupling coefficient equal to unity, we get:

$$M \approx \frac{n_1}{n_2} \times L_2 \approx \frac{n_2}{n_1} \times L_1 \tag{3.30}$$

and,

$$\frac{z_m}{z_1 z_2 - z_m^2} \approx \frac{n_1}{n_2} \times \frac{z_2}{z_1 z_2 - z_m^2} \approx \frac{n_2}{n_1} \times \frac{z_1}{z_1 z_2 - z_m^2} \tag{3.31}$$

Now, being y_t the short-circuit admittance of a single-phase transformer, defined as:

$$y_t = \frac{z_2}{z_1 z_2 - z_m^2} \tag{3.32}$$

And the parameters α, and β equal to the off-nominal tap at the primary and the secondary sides of the transformer, the admittance matrix $\boldsymbol{Y_{Bus\_T}}$ is computed as [43]:

$$Y_{Bus\_T} = \begin{bmatrix} \frac{y_t}{\alpha^2} & -\frac{y_t}{\alpha^2} & 0 & -\frac{y_t}{\alpha\beta} & \frac{y_t}{\alpha\beta} & 0 \\ -\frac{y_t}{\alpha^2} & 2\frac{y_t}{\alpha^2} & -\frac{y_t}{\alpha^2} & \frac{y_t}{\alpha\beta} & -2\frac{y_t}{\alpha\beta} & \frac{y_t}{\alpha\beta} \\ 0 & -\frac{y_t}{\alpha^2} & \frac{y_t}{\alpha^2} & 0 & \frac{y_t}{\alpha\beta} & -\frac{y_t}{\alpha\beta} \\ -\frac{y_t}{\alpha\beta} & \frac{y_t}{\alpha\beta} & 0 & \frac{y_t}{\beta^2} & -\frac{y_t}{\beta^2} & 0 \\ \frac{y_t}{\alpha\beta} & -2\frac{y_t}{\alpha\beta} & \frac{y_t}{\alpha\beta} & -\frac{y_t}{\beta^2} & 2\frac{y_t}{\beta^2} & -\frac{y_t}{\beta^2} \\ 0 & \frac{y_t}{\alpha\beta} & -\frac{y_t}{\alpha\beta} & 0 & -\frac{y_t}{\beta^2} & \frac{y_t}{\beta^2} \end{bmatrix} \quad \textbf{(3.33)}$$

By inspection of the admittance matrix (3.33), the transformer model circuit with the artificial lines is shown in the figure 3.6.

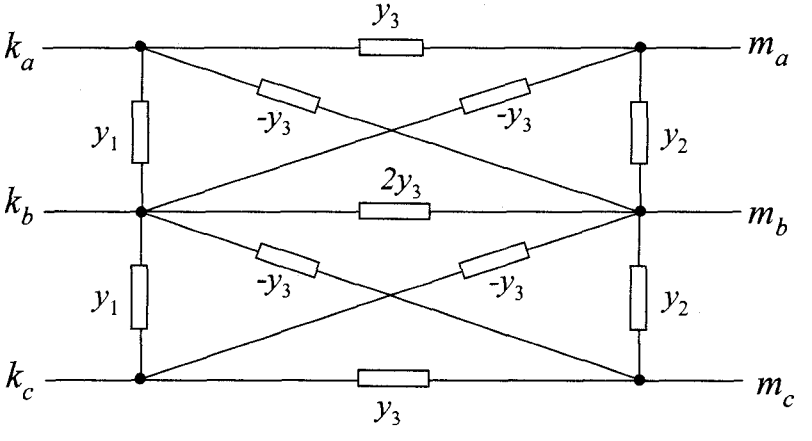

Figure 3.6 Positive-sequence equivalent circuit of an open delta-open delta transformer

Where y_1, y_2, and y_3 are computed as follows:

$$y_1 = \frac{y_t}{\alpha^2} \qquad y_2 = \frac{y_t}{\beta^2} \qquad y_3 = \frac{y_t}{\alpha\beta} \quad \textbf{(3.34)}$$

Another transformer connection, usually found in distribution networks, is the open wye-open delta connection [42], whose model is derived from the circuit shown in figure 3.7.

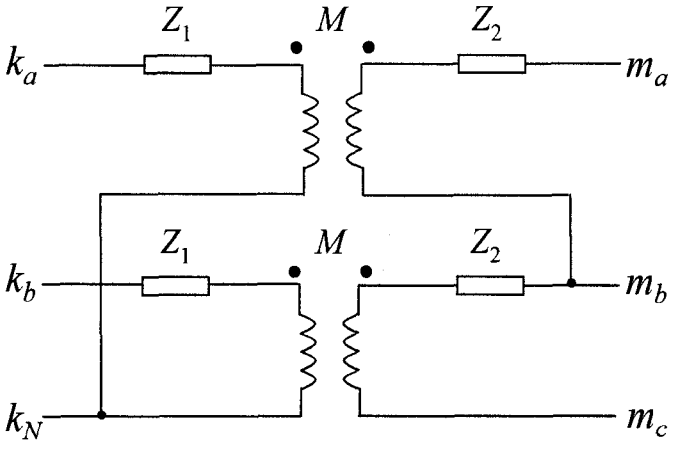

Figure 3.7 Two single-phase transformer for an open wye-open delta connection

This connection permits to supply, for instance, a two single-phase plus neutral wire network from a three-phase system in the primary side, allowing feeding two-phase or single-phase to neutral loads. Following the same approach as before, the nodal admittance matrix $\boldsymbol{Y_{Bus\_T}}$ for an open wye-open delta transformer connection is computed as follows [42]:

$$Y_{Bus\_T} = \begin{bmatrix} \frac{y_t}{\alpha^2} & 0 & \frac{-y_t}{\sqrt{3}\alpha\beta} & \frac{y_t}{\sqrt{3}\alpha\beta} & 0 \\ 0 & \frac{y_t}{\alpha^2} & 0 & \frac{-y_t}{\sqrt{3}\alpha\beta} & \frac{y_t}{\sqrt{3}\alpha\beta} \\ \frac{-y_t}{\sqrt{3}\alpha\beta} & 0 & \frac{y_t}{3\beta^2} & \frac{-y_t}{3\beta^2} & 0 \\ \frac{y_t}{\sqrt{3}\alpha\beta} & \frac{-y_t}{\sqrt{3}\alpha\beta} & \frac{-y_t}{3\beta^2} & \frac{2y_t}{3\beta^2} & \frac{-y_t}{3\beta^2} \\ 0 & \frac{y_t}{\sqrt{3}\alpha\beta} & 0 & \frac{-y_t}{3\beta^2} & \frac{y_t}{3\beta^2} \end{bmatrix} \quad \textbf{(3.35)}$$

By inspection of the admittance matrix (3.35), the transformer model circuit with the artificial lines is shown in the figure 3.8.

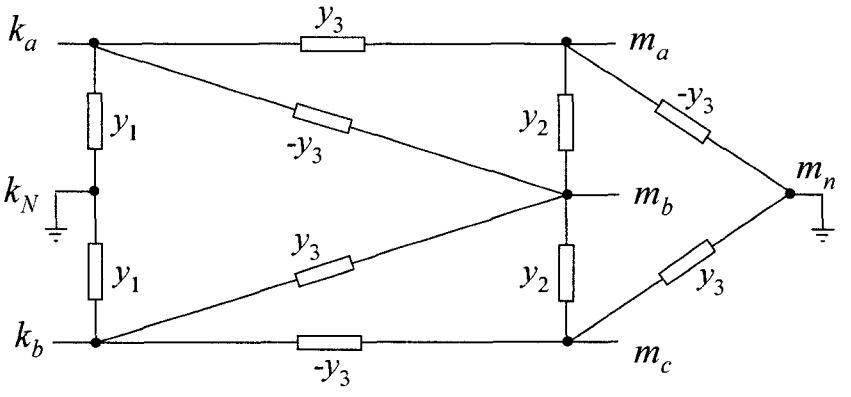

Figure 3.8 Positive-sequence equivalent circuit of an open wye-open delta transformer

Where y_1, y_2, and y_3 are computed as follows:

$$y_1 = \frac{y_t}{\alpha^2} \qquad y_2 = \frac{y_t}{3\beta^2} \qquad y_3 = \frac{y_t}{\sqrt{3}\alpha\beta} \tag{3.36}$$

3.2.3 Mid-tap transformers

In general distribution loads are unbalanced involving single-phase and three-phase loads merged in the same feeder. Thus, three-phase four-wire distribution transformers with grounded mid-tap on the secondary side are widespread in distribution networks [44]. These transformers are composed of either one single-phase transformer with three secondary wires, two phase-wires and one neutral wire, or one or two single-phase transformers with only two phase-wires. Three-phase four-wire distribution transformers allow operating in unbalanced situations and contributing to both single-phase and three-phase loads. Even though all mid-tap transformers can be modeled with the methodology presented in this research, only the three-phase grounded wye-delta and delta-delta mid-tap transformer models are developed in this section.

The winding connection of a grounded wye-delta transformer with mid-tap on the secondary side is presented in the figure 3.9.

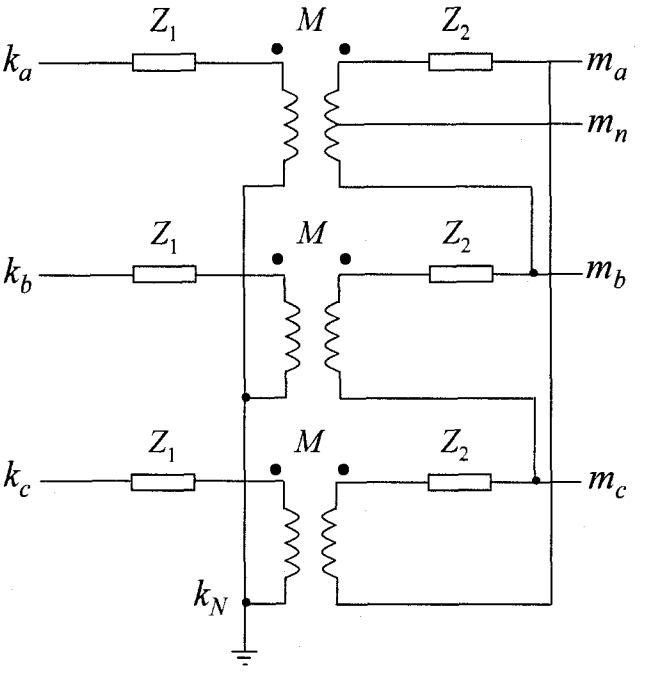

Figure 3.9 Winding connection of a grounded wye-delta transformer with mid-tap on the secondary side

Considering the effects of off-nominal tap ratio and the winding connections of primary and secondary sides, the nodal admittance matrix $\boldsymbol{Y}_{Bus\_T}$ of the grounded wye-delta mid-tap transformer is given by [44]:

$$Y_{Bus\_T} = \begin{bmatrix} \frac{y_t}{\alpha^2} & 0 & 0 & \frac{-y_t}{\sqrt{3}\alpha\beta} & \frac{y_t}{\sqrt{3}\alpha\beta} & 0 & 0 \\ 0 & \frac{y_t}{\alpha^2} & 0 & 0 & \frac{-y_t}{\sqrt{3}\alpha\beta} & \frac{y_t}{\sqrt{3}\alpha\beta} & 0 \\ 0 & 0 & \frac{y_t}{\alpha^2} & \frac{y_t}{\sqrt{3}\alpha\beta} & 0 & \frac{-y_t}{\sqrt{3}\alpha\beta} & 0 \\ \frac{-y_t}{\sqrt{3}\alpha\beta} & 0 & \frac{y_t}{\sqrt{3}\alpha\beta} & \frac{y_t}{\beta^2} & 0 & \frac{-y_t}{3\beta^2} & \frac{-2y_t}{3\beta^2} \\ \frac{y_t}{\sqrt{3}\alpha\beta} & \frac{-y_t}{\sqrt{3}\alpha\beta} & 0 & 0 & \frac{y_t}{\beta^2} & \frac{-y_t}{\beta^2} & \frac{-2y_t}{3\beta^2} \\ 0 & \frac{y_t}{\sqrt{3}\alpha\beta} & \frac{-y_t}{\sqrt{3}\alpha\beta} & \frac{-y_t}{3\beta^2} & \frac{-y_t}{3\beta^2} & \frac{2y_t}{3\beta^2} & 0 \\ 0 & 0 & 0 & \frac{-2y_t}{3\beta^2} & \frac{-2y_t}{3\beta^2} & 0 & \frac{4y_t}{3\beta^2} \end{bmatrix} \quad \textbf{(3.37)}$$

The coupling-free circuit with the artificial lines of a grounded wye-delta three-phase transformer with mid-tap on the secondary side is shown in figure 3.10.

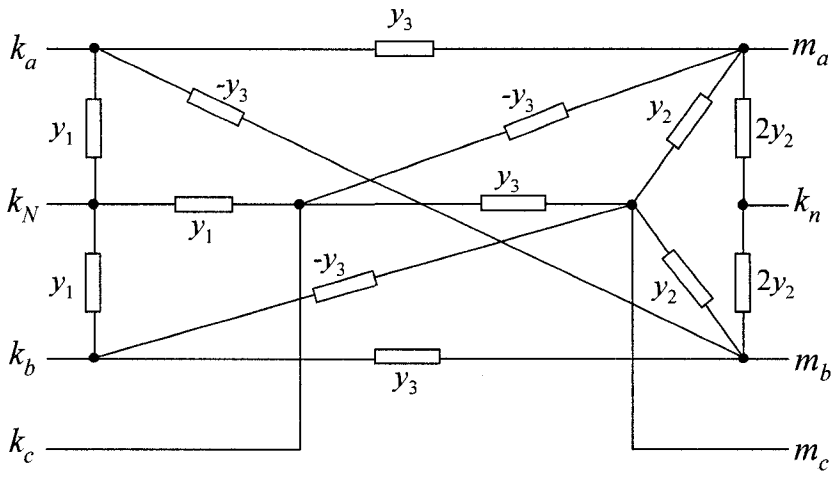

Figure 3.10 Positive-sequence circuit of a grounded Wye-delta three-phase transformer with mid-tap on the secondary side

Where y_1, y_2, and y_3 are computed as follows:

$$y_1 = \frac{y_t}{\alpha^2} \qquad y_2 = \frac{y_t}{3\beta^2} \qquad y_3 = \frac{y_t}{\sqrt{3}\alpha\beta} \tag{3.38}$$

The winding connection of a delta-delta transformer with mid-tap on the secondary side is presented in the figure 3.11.

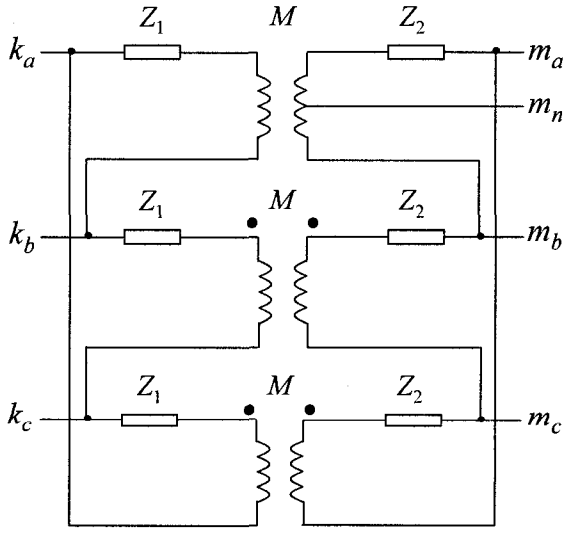

Figure 3.11 Winding connection of a delta-delta transformer with mid-tap on the secondary side

Considering the effects of off-nominal tap ratio and the winding connections of primary and secondary sides, the nodal admittance matrix $\boldsymbol{Y_{Bus\_T}}$ of the delta-delta mid-tap transformer is given by [44]:

$$Y_{Bus} = \begin{bmatrix} \frac{2y_t}{\alpha^2} & \frac{-y_t}{\alpha^2} & \frac{-y_t}{\alpha^2} & \frac{-2y_t}{\alpha\beta} & \frac{y_t}{\alpha\beta} & \frac{y_t}{\alpha\beta} & 0 \\ \frac{-y_t}{\alpha^2} & \frac{2y_t}{\alpha^2} & \frac{-y_t}{\alpha^2} & \frac{y_t}{\alpha\beta} & \frac{-2y_t}{\alpha\beta} & \frac{y_t}{\alpha\beta} & 0 \\ \frac{-y_t}{\alpha^2} & \frac{-y_t}{\alpha^2} & \frac{2y_t}{\alpha^2} & \frac{y_t}{\alpha\beta} & \frac{y_t}{\alpha\beta} & \frac{-2y_t}{\alpha\beta} & 0 \\ \frac{-2y_t}{\alpha\beta} & \frac{y_t}{\alpha\beta} & \frac{y_t}{\alpha\beta} & \frac{3y_t}{\beta^2} & 0 & \frac{-y_t}{\beta^2} & \frac{-2y_t}{\beta^2} \\ \frac{y_t}{\sqrt{3}\alpha\beta} & \frac{-2y_t}{\alpha\beta} & \frac{y_t}{\alpha\beta} & 0 & \frac{3y_t}{\beta^2} & \frac{-y_t}{\beta^2} & \frac{-2y_t}{\beta^2} \\ \frac{y_t}{\alpha\beta} & \frac{y_t}{\alpha\beta} & \frac{-2y_t}{\alpha\beta} & \frac{-y_t}{\beta^2} & \frac{-y_t}{\beta^2} & \frac{2y_t}{3\beta^2} & 0 \\ 0 & 0 & 0 & \frac{-2y_t}{\beta^2} & \frac{-2y_t}{\beta^2} & 0 & \frac{4y_t}{3\beta^2} \end{bmatrix} \quad \textbf{(3.39)}$$

The electromagnetic coupling-free model with the artificial lines of a delta-delta three-phase transformer with mid-tap on the secondary side is shown in figure 3.12.

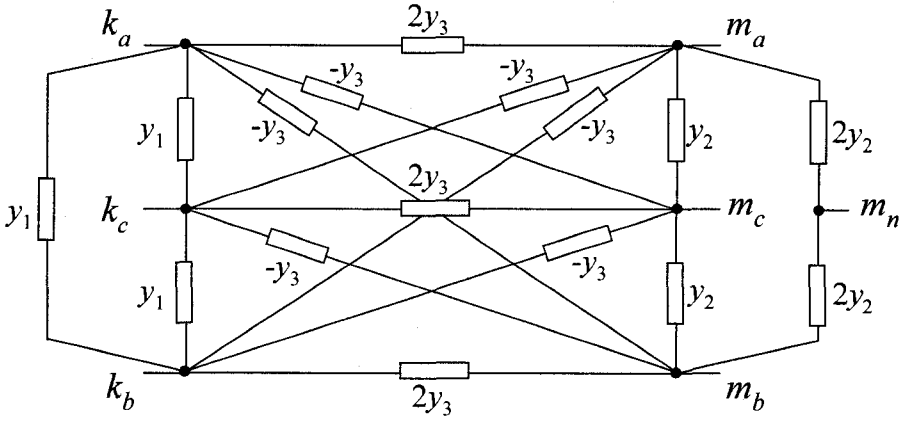

Figure 3.12 Positive-sequence circuit of a delta-delta three-phase transformer with mid-tap on the secondary side

Where y_1, y_2, and y_3 are computed as follows:

$$y_1 = \frac{y_t}{\alpha^2} \qquad y_2 = \frac{y_t}{\beta^2} \qquad y_3 = \frac{y_t}{\alpha\beta} \quad \textbf{(3.40)}$$

3.3 Generator representation

A three-phase source is represented by its equivalent unbalanced Thevenin circuit [45] shown in the figure 3.13.

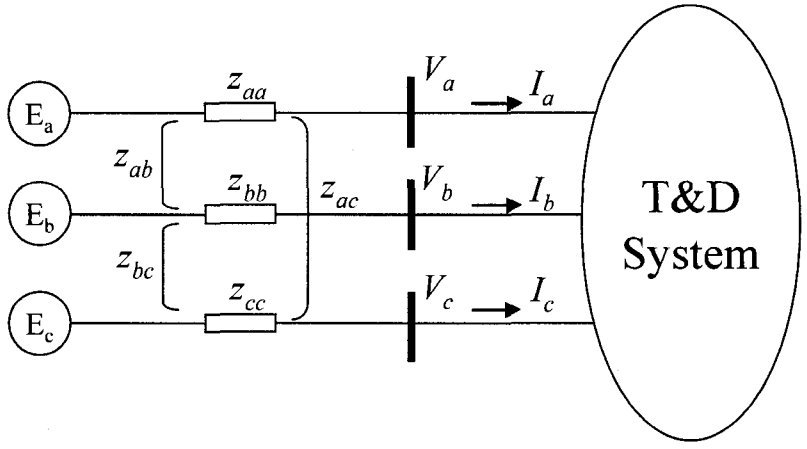

Figure 3.13 Three-phase source equivalent circuit for unbalanced systems

The Thevenin impedance matrix and the node voltages and currents are computed as follows:

$$Z_{Th\_abc} = \begin{bmatrix} z_{aa} & z_{ab} & z_{ac} \\ z_{ba} & z_{bb} & z_{bc} \\ z_{ca} & z_{cb} & z_{cc} \end{bmatrix} \tag{3.41}$$

$$E_{Th\_abc} - Z_{Th\_abc} \times I_{abc} = V_{abc} \tag{3.42}$$

$$I_{abc} = \left(\frac{S_{abc}}{V_{abc}} \right)^* \tag{3.43}$$

The values of vectors $\underline{V}_{abc}$ and $\underline{I}_{abc}$ are dependent on the bus type, which can be a swing bus, a PV bus, or a PQ bus. For a swing or slack bus, the voltage vector is known and the active and reactive power are determined by the system load-flow. For a PV bus, the voltage magnitude at the phase *a* and the active power are known, and the voltage angle and reactive power are the unknown variables.

Three-phase sources are typically represented in positive-sequence simulators by one single-phase generator plus its internal impedance. Since the internal impedances are

coupled in real generators, a three-phase generator is modeled here by using three positive-sequence generators whose internal impedances Z_a, Z_b, and Z_c are set up to zero and the real coupled internal impedance matrix is represented by the unbalanced and non-symmetric matrix $\boldsymbol{Y}_{BUSgen}$ as shown in figure 3.14. The $\boldsymbol{Y}_{BUSgen}$ matrix is the inverse of matrix $\boldsymbol{Z}_{Th\_abc}$, which is formed from the sequence impedances of the three-phase generator.

The reference node voltage will be the voltage at the terminal node of the phase *a* V_a, and the internal voltage magnitude E_a will be computed iteratively. Due to the internal voltages must be balanced, the internal voltage magnitudes for phases *b* and *c* (E_b and E_c) at each iteration are forced to be equal to E_a with the angles -120° and +120° shifted respectively. The voltage initialization is set up to one for the magnitudes, and the phase angles θ_a, θ_b, and θ_c are set to 0°, 120°, and –120° respectively.

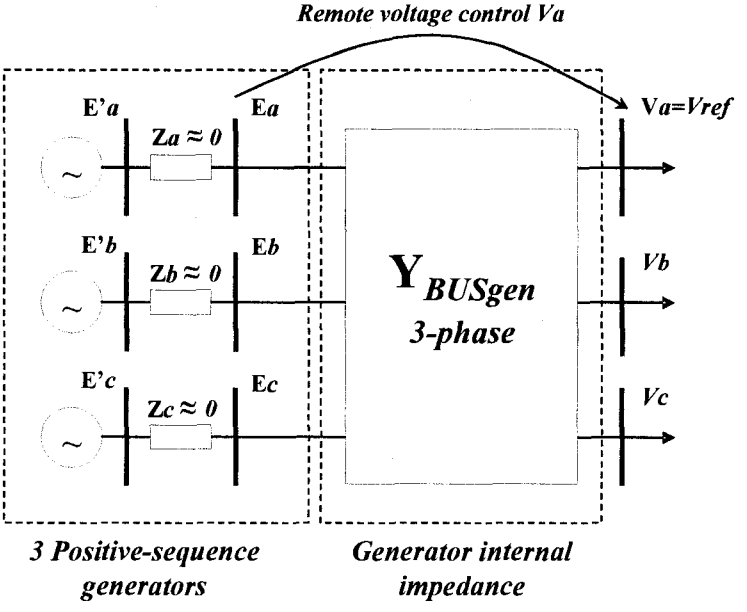

Figure 3.14 Positive-sequence equivalent model of a three-phase generator

Since positive-sequence load-flow simulators consider a single-phase representation, the three-phase power generation is divided by three. Therefore, the three-phase power generation needs to be multiplied by three before being entered in our

algorithm in order to compensate the single-phase modeling assumption of the positive-sequence solver.

Phase-shift due to transformers connection leads or lags the initialization angle, which has to be represented in the initial values of all the buses downstream of these transformers. Usually a phase angle by voltage level is defined depending on the type of transformer connections in the network.

3.4 Loads and shunt capacitors representation

Typical load model known as constant current, constant impedance, and constant power are presented in this section. These load models generally found in transmission and distribution systems are included in the proposed three-phase load-flow methodology.

The easier representation corresponds to the constant impedance load model, since a simple impedance is modeled and its power varies depending on the applied voltage. The equivalent circuit is presented in figure 3.15.

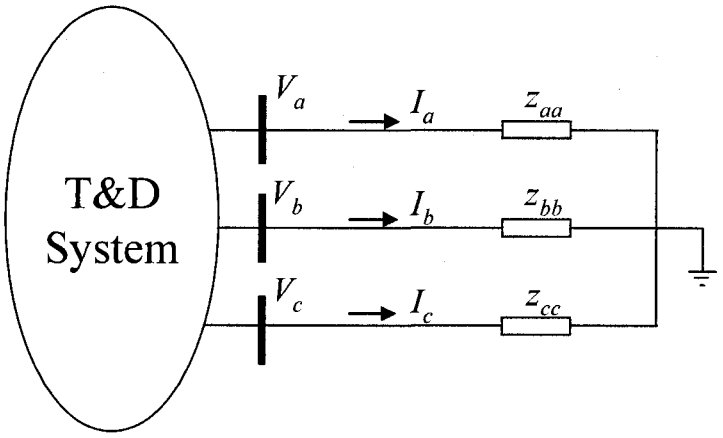

Figure 3.15 Three-phase constant impedance load equivalent circuit

The power vector for a constant impedance load is computed as follows:

$$S_{abc} = V_{abc} \times I^*_{abc} = V_{abc} \times \left[Y_{abc} \times V_{abc}\right]^* \quad \textbf{(3.44)}$$

$$S_{abc} = V_{abc} \times \left[Z^{-1}_{abc} \times V_{abc}\right]^* \quad \textbf{(3.45)}$$

Shunt capacitor banks are also represented as shunt capacitive impedances, thus they can be modeled by simple adding a single- or three-phase shunt branch whose initial constant reactance is calculated from the equation (3.45) considering both the nominal reactive power and voltage. The constant current and power models are determined with the same equation (3.45), but using in those cases an iterative methodology.

Constant power loads can be easily represented in a positive sequence load-flow analysis by defining explicitly the values of P and Q as a balanced load connected to an infinite ground. However, in distribution systems, loads are often found connected to neutral or between phases. Thus, the positive-sequence representation does not work properly. An iterative voltage-dependent impedance based method is proposed here, where the load impedance is a function of the applied voltage. Let us define S_S, V_S, I_S and Z_S as the specified nominal complex power, voltage, current and impedance. Thus, we get:

$$S_S = \frac{|V_S|^2}{Z_S} = P_S + jQ_S \tag{3.46}$$

$$Z_S = \left(\frac{P_S - jQ_S}{P_S^2 + Q_S^2} \right) |V_S|^2 = \alpha |V_S|^2 \tag{3.47}$$

$$\Delta Z_S = 2\alpha |V_S| \Delta V_S \tag{3.48}$$

$$\alpha = \frac{P_S - jQ_S}{P_S^2 + Q_S^2}$$

The voltage V_S can be approximated to a 1.0 in per unit in equation (2.48). Thus, the constant power impedance in each iteration is given by:

$$Z_{n+1} = Z_n + \Delta Z_{n+1} \tag{3.49}$$

$$Z_{n+1} = \alpha V_n^2 + 2\alpha V_{n+1} \Delta V_{n+1} \tag{3.50}$$

$$Z_{n+1} \approx \alpha (V_n^2 + 2\Delta V_{n+1}) \tag{3.51}$$

An acceleration factor λ_{CP} shown in (3.52), whose value is generally set between one and two, can be added in order to reach faster the final impedance, which corresponds to the specified constant power defined at the beginning of the process.

$$Z_{n+1} \approx \alpha(V_n^2 + 2\lambda_{CP}\Delta V_{n+1}) \tag{3.52}$$

The same approach is applied for constant current loads. In this case, the impedance dependence is linear regarding its applied voltage:

$$Z_{n+1} = Z_n + \Delta Z_{n+1} \tag{3.53}$$

$$Z_n = \beta V_n \tag{3.53}$$

$$\Delta Z_{n+1} = \beta \Delta V_{n+1} \tag{3.54}$$

With,

$$\beta = \frac{1}{I_S} = \left[\frac{V_S}{P_S + jQ_S}\right]^*$$

Including the acceleration factor λ_{CC}, the final impedance model for constant current loads is given by:

$$Z_{n+1} = \beta(V_n + \lambda_{CC}\Delta V_{n+1}) \tag{3.55}$$

Using these load representations we are able to model all kinds of loads found in distribution systems. Delta- or wye-connected, single-, two-, and three-phase loads being either balanced or unbalanced can be represented with this iterative method. Similar to power generation, the three-phase loads have to be multiplied by three before being entered in the developed algorithm.

3.5 Neutral wire and ground representation

Conventional positive-sequence load-flow software's do not include an explicit representation of neither neutral wire nor ground resistivity. On the contrary, they always assume balanced three-phase systems with a perfect infinite ground for loads, transformers and generators. In the proposed methodology, both neutral wire and ground are represented as explicit lines [22].

The infinite ground or zero reference voltage is also explicitly included, and for that purpose a zero-voltage bus has to be modeled. In distribution systems, zero-voltage reference or ground is mainly found in single-phase to neutral loads, and grounded wye-connected transformers and generators. The most effective zero voltage reference bus representation is obtained by adding a PV bus at each required ground node, with voltage and power set to zero. Figure 3.16 shows a positive-sequence representation of a load connected to ground.

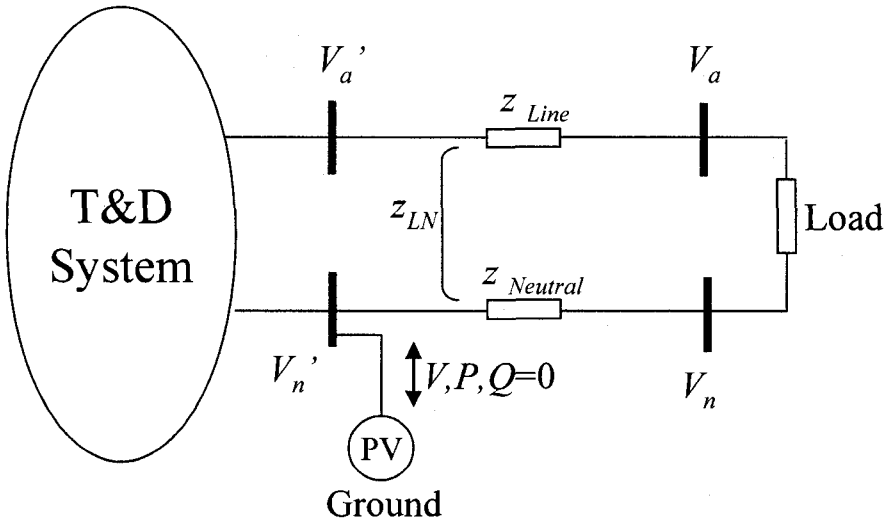

Figure 3.16 Explicit zero-voltage reference bus in a positive-sequence load-flow representation

By adding a zero value PV generator bus it is possible to represent the infinite ground in any system using a positive-sequence load-flow software. There are other ways of representing a zero-reference voltage such as by setting a zero nominal voltage bus, but in those cases it is not always possible to keep a zero voltage level in the selected bus.

3.6 Initial Conditions

A favorable starting approximation is sometimes necessary for successful convergence of large systems when Newton's method is used. The flat voltage start, where voltage magnitudes are set equal to their scheduled (or nominal) values and angles

equal to the slack node voltage angle, is usually sufficient. Thus, for a three-phase program the angles at each node is set equal to the angle of the slack reference bus which is usually 0°, -120°, and –120° for phases *a*, *b* and *c* respectively.

There are some situations for which this initial guess is not a sufficiently good start. It has been found that the flat start followed by one cycle of successive displacements without overcorrection is consistently favorable. As would be expected, a more accurate initial approximation reduces the number of iterations required for solution. In a series of related problems the previous solution is usually a good start for the next problem. However, since the method converges rapidly from a flat start and checking for adjustments can take place after only two iterations, it is hardly worthwhile using any other starting method. Using the voltages of a related case would save only one iteration.

As it was mentioned in section 2.1.8, Gauss-Seidel load-flow iterations take very low processing time, thus the idea of using the Gauss-Seidel method to set up initial conditions for the Newton's method is very attractive for very large systems. However, the starting method chosen for the purpose of this research was the flat start followed by one cycle of successive displacements [12].

4 UNBALANCED MULTI-PHASE LOAD-FLOW PROGRAM

The algorithm developed is composed of two modules. The first and main module corresponds to an optimized balanced positive-sequence load-flow solver widely utilized in the power systems industry. The second module, developed in Fortran-95, has the function of modeling and converting multi-phase systems to positive-sequence equivalent system that will be solved by the positive-sequence load-flow solver. The main advantage of the proposed methodology is its capability to simulate a multi-phase load-flow network with any existing positive-sequence solver readily available in the power system industry.

4.1 Flowchart of the multi-phase load-flow algorithm

Since the positive-sequence load-flow algorithm used in this research project is a registered commercial product, its code will not be shown. A general description of the multi-phase algorithm is depicted in the flowchart of figure 4.1.

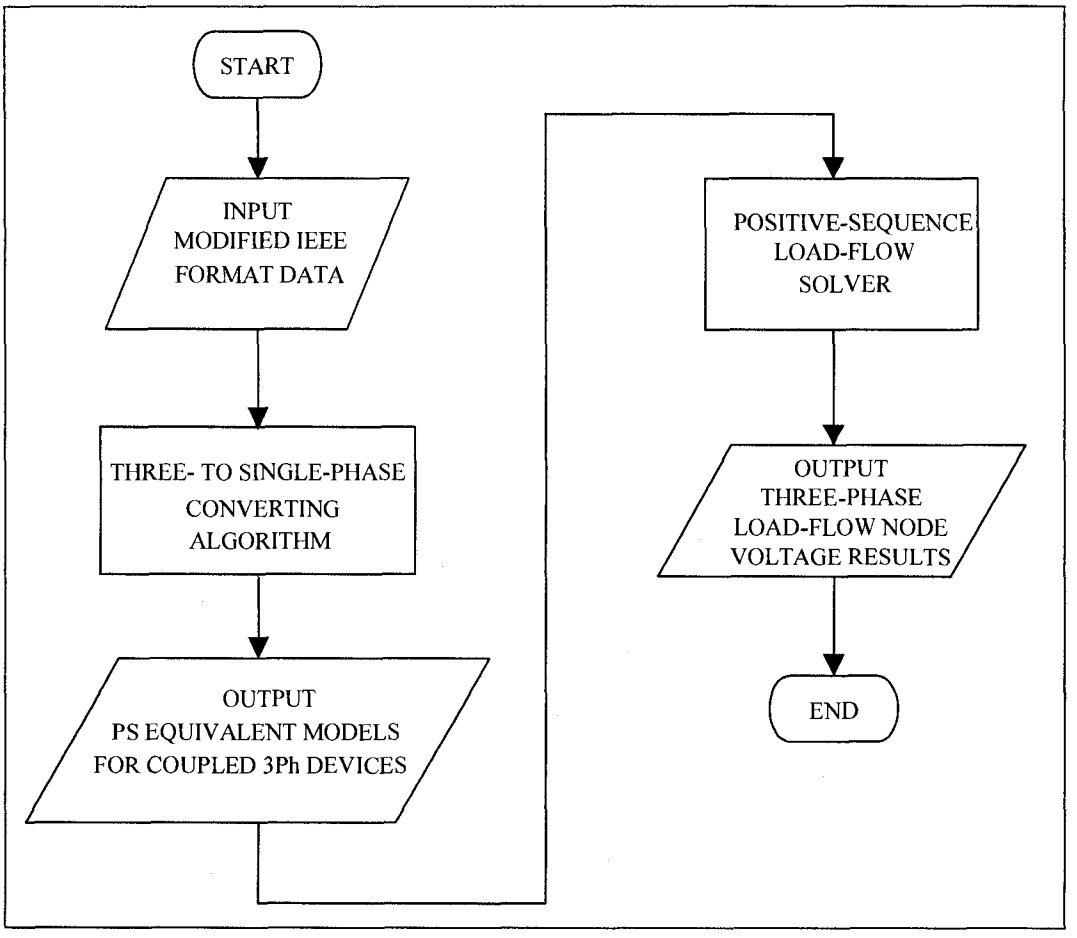

Figure 4.1 Multi-phase load-flow program flowchart

4.2 Input-output data

A special multi-phase load-flow input data format was developed as a part of this research, which corresponds to a modification of the standard IEEE common data for the exchange of solved load-flow data, whose complete description can be found in reference [46]. This IEEE multi-phase input format, partially shown in figure 4.2, is composed of different device modules such as bus data, branch data, transformer data, and so on.

The output data format includes the magnitude and phase angle of the voltage at each node of the system. The node voltage data will be used to validate the proposed methodology against the results obtained from the EMTP-RV load-flow package.

****NEW TEST CASE FROM EMTP.NET FILE****

BUS DATA FOLLOWS — N° ITEMS

N°	Bus mane	Phase	Status	Number of phases	Bus Type	Voltage	Voltage pu	Initial angle	Load	Generation	Shunt Compensation
1	BUS_xx	A,B,C	On/Off	1,2,3...n	PV,PQ,Slack, ground	kV	1.0000	0°, 120°, 120°	Constant P,Q	Constant P,Q	Rated Reactive power Q

-999

BRANCH DATA FOLLOWS — N° ITEMS

From bus	To bus	Line name	Phases	Status	Number of phases	Capacity	Impedance matrices for n wires		
Bus_xx	Bus_yy	Line_xx	ABC	On/Off	1,2,3...n	MVA	[Rn;1]	[Rn2]	.....[Rnn]
							[Xn1]	[Xn2]	.....[Xnn]
							[Bn1]	[Bn2]	.....[Bnn]

-999

TRANSFORMER DATA FOLLOWS — N° ITEMS

From bus	To bus	Tr. name	Phases	Connection	Status	Number of phases	Capacity	Primiry/Secondary Voltage	Zpu	X/R ratio	Prim/Sec tap-off
Bus_xx	Bus_yy	Transf_xx	ABC	YgYg, DYg....	On/Off	1,2,3	MVA	kV / kV	%Pbase	times	1.00/1.00

-999

END OF DATA

Figure 4.2 IEEE Multi-phase load-flow input data format

4.3 Multi- to single-phase converting algorithm

Multi-phase to single-phase (or positive-sequence) converting algorithm is the most important contribution of this research work. Its purpose is to convert a multi-phase system into an equivalent positive-sequence system. The input of this program is the modified IEEE multi-phase format shown in figure 4.2 and, as a result of the conversion process, an output data file is generated in a suitable single-phase format which will be read by the positive-sequence optimized load-flow solver. The basic structure of the conversion algorithm is described as follows:

- Network device sample structure

  The networks devices are characterized as objects or structures called *Type*. Each structure is composed by the relevant parameters associated with the correspondent device. In the case of the object *Bus* the relevant attributes are: number, name, phase, state (on/off), number of phases, type of bus, voltage, angle, load, generation, and shunt compensation as can be seen in the code below.

```
Type Bus
  Integer::Num
  Character(10)::Name
  Character(1)::Phase
  Integer::State,NumPhase,BType
  Real::KV,VM,VPh
  Real::P,Q,GP,GQ
End Type Bus
```

- Type structure definition

  The *Type* structure is defined as an object with an allocatable dimension, which means that the size of any *Type* vector is defined by the system automatically, giving flexibility and optimizing the processing memory utilization.

```
Type(Bus),Dimension(:),Allocatable::BusArray
Type(Branch),Dimension(:),Allocatable::BranchArray
Type(ImpededanceLoad),Dimension(:),Allocatable::ImpLoadArray
Type(Transformer),Dimension(:),Allocatable::TransfoArray
```

- Four-wire line sample model

  The code below shows the positive-sequence equivalent representation structure for a four-wire line. Once the primitive impedance and shunt admittance matrix data is allocated, the $\boldsymbol{Z_{prim}}$ matrix inversion routine is called and then the new impedance matrix is formed including all the coupling lines. Then the information is converted to a per unit base system and prepared to be entered into the new positive-sequence $\boldsymbol{Y_{Bus}}$ system matrix.

```
Do k=1,NumBranches
    m=BranchArray(k)%NumCond
    n=BranchArray(k)%NumCond
    If ((m==4).and.(BranchArray(k)%State==1)) then
        Allocate(RL_inv(m,n),XL_inv(m,n),GL(m,n),BL(m,n))
        Allocate(ZL(2*m,2*n),ZL_inv(2*m,2*n))
        Allocate(B(m,n),Ybus(m,n))
        !Build ZL for matrix inversion
        Do i=1,m
            Do j=1,n
                B(i,j)=cmplx(0,BranchArray(k)%B(i,j))
                ZL(i,j)=BranchArray(k)%R(i,j)
                ZL(i,j+n)=BranchArray(k)%X(i,j)
                ZL(i+m,j)=-BranchArray(k)%X(i,j)
                ZL(i+m,j+n)=BranchArray(k)%R(i,j)
            End do
        End do
        !Call Subroutine for matrix inversion
        Call matrix_inverse(2*m,2*n,ZL,ZL_inv,ierror)
```

```
!Store values of G and B
Do i=1,m
    Do j=1,n
        GL(i,j)=ZL_inv(i,j)
        BL(i,j)=ZL_inv(i,j+n)
    End do
End do
!Generate Ybus
!Search line base voltage
Do i=1,NumNodes
    If (BusArray(i)%Name==BranchArray(k)%NodeFrom) then
        LineKVBase=BusArray(i)%KV
        Exit
    Endif
End Do
NewKV=(Vbase/LineKVBase)**2
Do i=1,m
    Do j=1,m
        Ybus(i,j)=cmplx(GL(i,j),BL(i,j))/NewKV
        B(i,j)=B(i,j)/NewKV
        BranchArray(k)%B(i,j)=BranchArray(k)%B(i,j)/NewKV
    End Do
End Do
```

- Grounded wye-delta transformer sample model

  A similar approach is implemented for the transformer modeling, but in this case it is not needed to perform any matrix inversion and the positive-sequence representation is more direct as is shown below for a three-phase grounded wye-delta transformer connection.

```
!Yg-D transformer model
Else If ((TransfoArray(k)%Connection(3:)=='YgD').and.
    (TransfoArray(k)%State==1)) Then
    Zbt=Vbase**2/TransfoArray(k)%Pnom
    rt=TransfoArray(k)%Z/sqrt(TransfoArray(k)%X_R**2+1)
    xt=TransfoArray(k)%Z/sqrt(1+(1/TransfoArray(k)%X_R)**2)
    Ztpu=cmplx(rt,xt)
    Zt=Ztpu*Zbt              !System base
    Yt=1/Zt
    alpha=TransfoArray(k)%TapP
    beta=TransfoArray(k)%TapS
    Y1=Yt/(alpha**2)
    Y2=Yt/(3*(beta**2))
    Y3=Yt/(sqrt(3.0)*alpha*beta)
    !Shunt impedance calcul
    Psh1=Vbase**2*Real(Y1)
    Qsh1=Vbase**2*Imag(Y1)
    Psh1=TransfoArray(k)%VP**2*Real(Y1)
    Qsh1=TransfoArray(k)%VP**2*Imag(Y1)
```

These are some examples of how the converting algorithm works and how the different multi-phase devices are represented in an positive-sequence environment.

4.4 Positive-sequence load-flow solver

A simplified flowchart of the positive-sequence load-flow algorithm, extracted from [4], is shown in figure 4.3. This solver uses the Newton methodology and the optimal sparse matrices ordering proposed by Tinney in [12] and [13]. The Newton methodology and the numerical solution method presented in this section have been described in chapter 2.

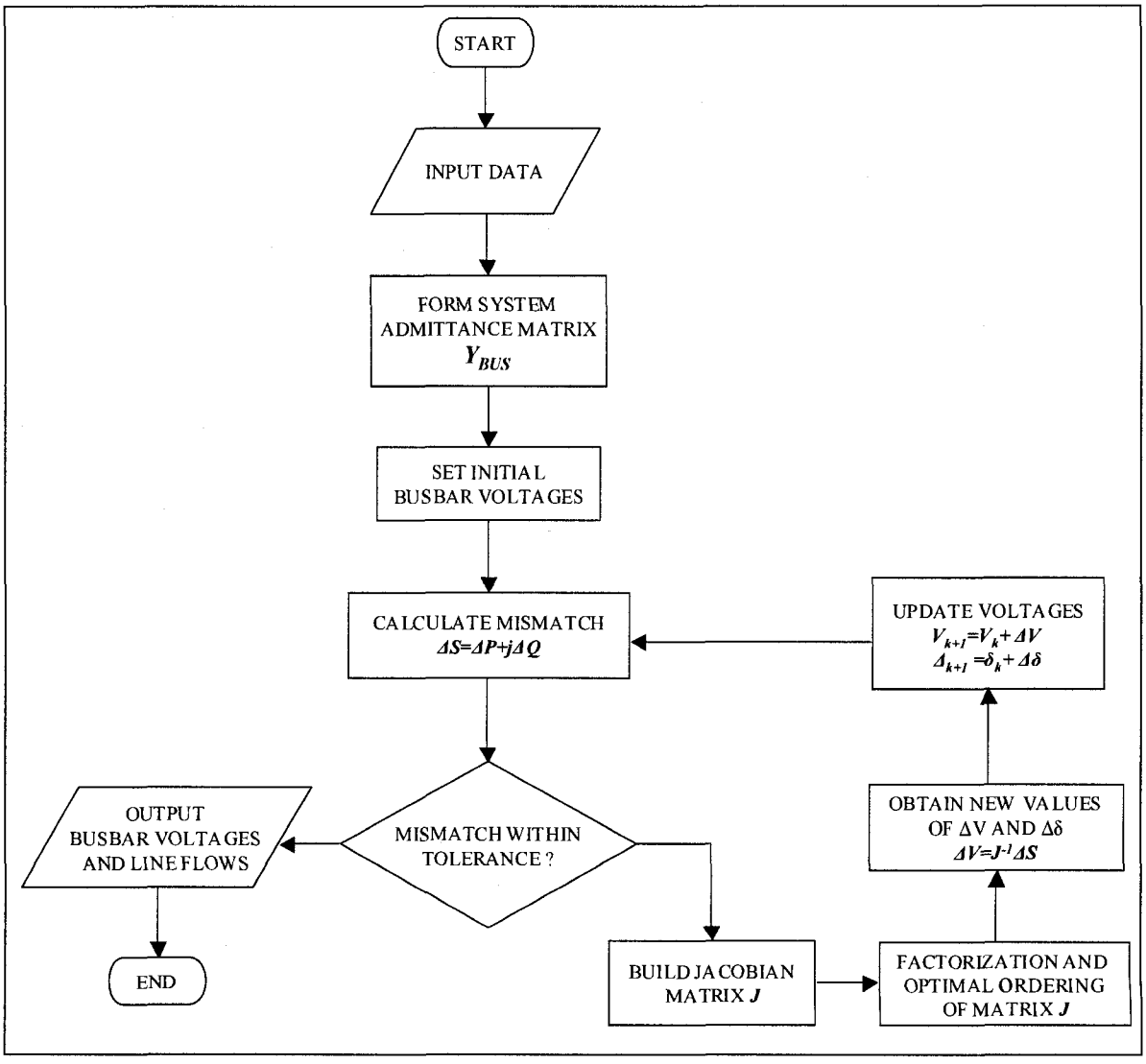

Figure 4.3 Positive-sequence load-flow algorithm flowchart

4.5 Data format converting algorithm

This algorithm has the function of converting either EMTP-RV Nestlist data format to multi-phase IEEE load-flow input data format, or inversely IEEE input data format to EMTP-RV Nest-list data format. The code was written in Python, a language widely used to handle different text formats and data files. This program was developed for result-validation purposes. EMTP-RV has a function that permits to run load-flow simulations directly from editable text files, without having to draw the network in its graphical user interface (GUI). This function allows the running of large systems with thousands of buses and the testing of computer simulation time. Some devices samples of the EMTP-RV Nestlist format are listed below.

- Three-phase π-line model format

```
_PI;PI1a;6;2;BUS_xxA,BUS_yyA,
3ph,1,0,1H,0,1F,0,1,1,1,1,
_PI;PI1b;6;2; BUS_xxB,BUS_yyB,
_PI;PI1c;6;2; BUS_xxC,BUS_yyC,
Raa Rab Rac
Rba Rbb Rbc
Rca Rcb Rcc
Xaa Xab Xac
Xba Xbb Xbc
Xca Xcb Xcc
Baa Bab Bac
Bba Bbb Bbc
Bca Bcb Bcc
```

- Single-phase constant PQ load

```
_PQload;Load_xxA;1;1;BUS_xxA,
kVRMSLL,PkW,QkVAR,0,frec,1,0,
```

- Three-phase slack source

```
_Slack;BUS_xxA;3ph;1;BUS_yyA,
frec,kVRMSLL,0,1,1,1Ohm,1,,
_Slack; BUS_xxB;3ph;1;BUS_yyB,
_Slack; BUS_xxC;3ph;1;BUS_yyC,
Internal impedance
```

4.6 Illustrative test case

To better understand the methodology developed, a simple illustrative case is included in this section. The case is composed by a three-phase 13.8 kV slack generator, one non-transposed three-phase transmission line, one 13.8/6 kV 2.0 MVA delta-grounded wye connected transformer (Z_T=6.0%), and an unbalanced constant power load at the secondary side of the transformer as is shown in figure 4.4.

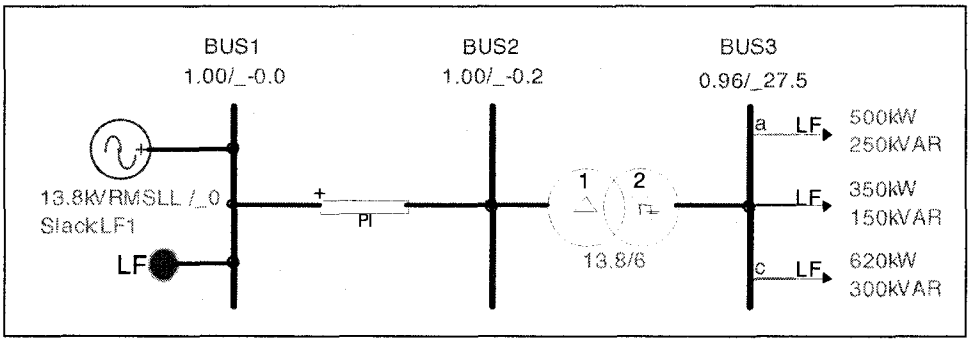

Figure 4.4 3-Bus illustrative case EMTP-RV diagram

Since this case has been initially drawn on the EMTP-RV GUI, the first step is to generate the EMTP-RV Nestlist file, and then convert it to the modified IEEE multi-phase data file format. The complete data files for this case are shown in Appendix A. The second step is to run the algorithm, which converts the three-phase network in an positive-sequence equivalent network representation, and then to generate the *LFNetfile* file shown in appendix A. The latter file uses a special load-flow data format that is required for the positive-sequence load-flow solver. After reading the file, the positive-sequence solver runs the load-flow simulation and generates the bus voltage vector results.

The methodology computes first the admittance matrices for the three-phase line section using equations (3.14) and (3.16), and for the Δ-Y_g connected transformer using equation (3.26). Taking the line parameters of the primitives impedance matrices listed in the EMTP-RV Netlist file of Appendix A, we get:

$$Y_{abc}^{line} = Z_{abc}^{line\,-1} = \begin{bmatrix} 0.4576 + j1.078 & 0.156 + j0.5017 & 0.1535 + j0.3849 \\ 0.156 + j0.5017 & 0.4666 + j1.0482 & 0.1580 + j0.4236 \\ 0.1535 + j0.3849 & 0.1580 + j0.4236 & 0.4615 + j1.0651 \end{bmatrix}^{-1} \quad \textbf{(4.1)}$$

$$Y_{abc}^{line} = \begin{bmatrix} 0.4866 - j1.0090 & -0.2364 + j0.3463 & -0.0853 + j0.2250 \\ -0.2364 + j0.3463 & 0.5441 - j1.0455 & -0.1448 + j0.2746 \\ -0.0853 + j0.225 & -0.1448 + j0.2746 & 0.4372 - j0.9737 \end{bmatrix} \quad \textbf{(4.2)}$$

$$Y_{Bus}^{Line} = \begin{bmatrix} Y_{abc}^{line} & -Y_{abc}^{line} \\ -Y_{abc}^{line} & Y_{abc}^{line} \end{bmatrix} = \begin{bmatrix} y_{aa} & y_{ab} & y_{ac} & -y_{aa} & -y_{ab} & -y_{ac} \\ y_{ba} & y_{bb} & y_{bc} & -y_{ba} & -y_{bb} & -y_{bc} \\ y_{ca} & y_{cb} & y_{cc} & -y_{ca} & -y_{cb} & -y_{cc} \\ -y_{aa} & -y_{ab} & -y_{ac} & y_{aa} & y_{ab} & y_{ac} \\ -y_{ba} & -y_{bb} & -y_{bc} & y_{ba} & y_{bb} & y_{bc} \\ -y_{ca} & -y_{cb} & -y_{cc} & y_{ca} & y_{cb} & y_{cc} \end{bmatrix} \quad \textbf{(4.3)}$$

Thus, the impedance values expressed in ohms [Ω] of the equivalent positive-sequence representation of figure 3.2 for the three-phase line in figure 4.4 are given by:

$$z_{ab} = -z_{ab'} = z_{a'b'} = -\frac{1}{y_{ab}^{r}} = -\frac{1}{-0.2364 + j0.3463} = 1.3446 + j1.9698 \quad \textbf{(4.4)}$$

$$z_{bc} = -z_{bc'} = z_{b'c'} = -\frac{1}{y_{bc}^{r}} = -\frac{1}{-0.1448 + j0.2746} = 1.5025 + j2.9494 \quad \textbf{(4.5)}$$

$$z_{ac} = -z_{ac'} = z_{a'c'} = -\frac{1}{y_{ac}^{r}} = -\frac{1}{-0.0853 + j0.2250} = 1.4732 + j3.8859 \quad \textbf{(4.6)}$$

$$z_{aa'} = \frac{1}{y_{aa}} = \frac{1}{0.4866 - j1.009} = 0.3878 + j0.8041 \quad \textbf{(4.7)}$$

$$z_{bb'} = \frac{1}{y_{bb}} = \frac{1}{0.5441 - j1.045} = 0.3917 + j0.7526 \quad \textbf{(4.8)}$$

$$z_{cc'} = \frac{1}{y_{cc}} = \frac{1}{0.4372 - j0.9737} = 0.3837 + j0.8547 \quad \textbf{(4.9)}$$

The shunt capacitive admittances expressed in siemens [*S*] are computed with equation (3.21).

$$b_{ag} = b_{aa} - b_{ab} - b_{ac} = 5.6712 + 1.8362 + 0.7034 = 8.2198 \quad \textbf{(4.10)}$$

$$b_{bg} = b_{bb} - b_{ab} - b_{bc} = 5.9774 + 1.8362 + 1.169 = 8.8926 \quad \textbf{(4.11)}$$

$$b_{ag} = b_{cc} - b_{ac} - b_{bc} = 5.3911 + 0.7034 + 1.169 = 7.2635 \quad \textbf{(4.12)}$$

The transformer impedance values z_1, z_2 and z_3 of figure 3.4 are easily computed with equations (3.27), and the results expressed in ohms [Ω] are:

$$y_t = \frac{1}{z_t} = 0.03433 + j0.17164 \quad \textbf{(4.13)}$$

$$z_1 = \frac{1}{y_1} = \frac{3}{y_t} = 3.36135 + j16.80676 \quad \textbf{(4.14)}$$

$$z_2 = \frac{1}{y_2} = \frac{1}{y_t} = 1.12045 + j5.6022 \quad \textbf{(4.15)}$$

$$z_3 = \frac{1}{y_3} = \frac{\sqrt{3}}{y_t} = 1.9407 + j9.7034 \quad \textbf{(4.16)}$$

The impedance values computed above correspond to the same values listed in the LFNetfile of Appendix A, for the three-phase line section and the Δ-Y_g connected transformer. The admittance matrix for the three-phase Δ-Y_g connected transformer is show in equation (4.17):

$$Y_{abc}^{tranf} = \begin{bmatrix} \frac{2y_t}{3} & \frac{-y_t}{3} & \frac{-y_t}{3} & \frac{-y_t}{\sqrt{3}} & 0 & \frac{y_t}{\sqrt{3}} \\ \frac{-y_t}{3} & \frac{2y_t}{3} & \frac{-y_t}{3} & \frac{y_t}{\sqrt{3}} & \frac{-y_t}{\sqrt{3}} & 0 \\ \frac{-y_t}{3} & \frac{-y_t}{3} & \frac{2y_t}{3} & 0 & \frac{y_t}{\sqrt{3}} & \frac{-y_t}{\sqrt{3}} \\ \frac{-y_t}{\sqrt{3}} & \frac{y_t}{\sqrt{3}} & 0 & y_t & 0 & 0 \\ 0 & \frac{-y_t}{\sqrt{3}} & \frac{y_t}{\sqrt{3}} & 0 & y_t & 0 \\ \frac{y_t}{\sqrt{3}} & 0 & \frac{-y_t}{\sqrt{3}} & 0 & 0 & y_t \end{bmatrix} \quad \textbf{(4.17)}$$

With these impedance matrices the total system admittance matrix $\boldsymbol{Y_{Bus}}$ is formed as follows:

$$Y_{Bus} = \begin{bmatrix} [Y_{abc}^{line}] & [-Y_{abc}^{line}] & [0] \\ [-Y_{abc}^{line}] & [Y_{abc}^{line} + Y_{abc}^{transf}] & [-Y_{abc}^{transf}] \\ [0] & [-Y_{abc}^{transf}] & [Y_{abc}^{transf}] \end{bmatrix}_{9x9} \quad \textbf{(4.18)}$$

The 9x9 system matrix $\boldsymbol{Y_{Bus}}$ of (4.18) is formed using the 3x3 line and transformer $\boldsymbol{Y_{abc}}$ sub-matrices obtained from (4.2) and (4.17) respectively.

The load values as well as the power generation are entered multiplied by three into the LFNetfile. Finally, the positive-sequence algorithm is performed and the bus voltage results are compared with the results obtained by EMTP-RV as is shown in table 4.1.

Table 4.1 3-Bus illustrative case voltage results

Bus Code	Voltage Magnitude [pu]					
	EMTP	Method	EMTP	Method	EMTP	Method
	Phase A	Phase A	Phase B	Phase B	Phase C	Phase C
BUS1	1.000	1.000	1.000	1.000	1.000	1.000
BUS2	0.993	0.993	0.996	0.996	0.996	0.996
BUS3	0.962	0.961	0.977	0.976	0.954	0.953

5 TEST SYSTEMS AND RESULTS VALIDATION

In addition to the simple 3-Bus system presented at the end of chapter 4, three more complex test systems were used to compare the accuracy, performance, and robustness of the proposed methodology. The first test case corresponds to a modified IEEE 34-Bus unbalanced distribution system presented by Ciric in [22]. The objective of this test case is to validate the accuracy of a simple unbalanced radial distribution networks against EMTP-RV and to compare also the results with the fast iterative unbalanced distribution load-flow software CYMDIST.

The second case presented corresponds to a 40-bus system developed with the purpose of validating most of the devices and complexities found in distribution and transmission systems such as, generators, transformers, meshed and radial networks, coupled and uncoupled lines, different load representations, single-, double-, three- and four-wire lines, three-phase, phase-to-phase, and phase-to-neutral loads, and fixed shunt capacitor banks. Many of these characteristics are hardly ever modeled in either conventional positive sequence load-flow or in fast iterative radial distribution applications. That is the main reason for using the EMTP-RV load-flow package for accuracy and robustness validation purposes.

The last test system presented in this chapter corresponds to a large meshed and ideally-transposed distribution network of 2,600 buses. The purpose of including this case is to validate the performance and robustness of the methodology presented in comparison with EMTP-RV and the fast iterative software CYMDIST.

5.1 Modified IEEE 34-Bus Distribution Test Case

The modified IEEE 34-bus unbalanced radial distribution feeder is shown in figure 5.1. Its loads and line parameters were obtained from reference [47]. This test case pursues to validate the multi-phase load-flow methodology presented against EMTP-RV, and to compare also the results with the iterative forward-backward sweep distribution solver CYMDIST. Since the purpose of this first test is to validate the accuracy of the methodology, a perfect line transposition was assumed in the system.

Even though similar simulation times were obtained in comparison with EMTP-RV, the fast iterative sweep solver is still faster than the standard Newton's methodology used in the proposed methodology. This IEEE 34-bus version has been modified with regards to its original version since neither transformer nor capacitor banks were included.

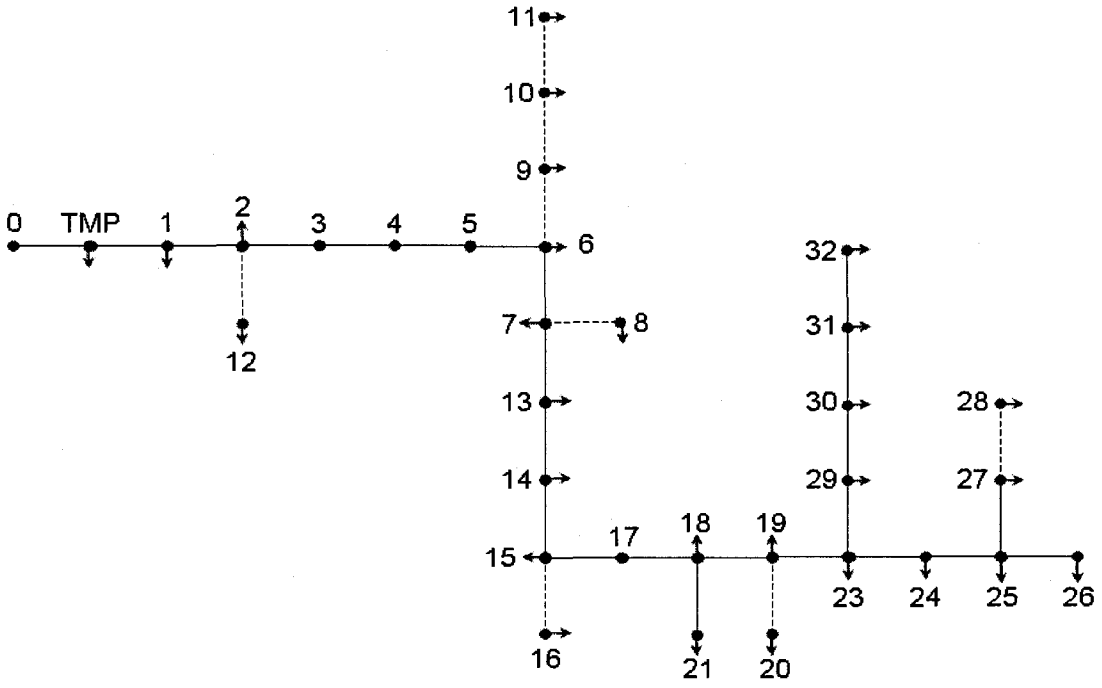

Figure 5.1 Modified IEEE 34-Bus distribution model

The results for the voltage magnitudes and angles obtained by each solver are listed in Table 5.1 and 5.2 respectively for a convergence criterion of 10^{-6} MVA.

Table 5.1 Modified IEEE 34-Bus Test system voltage magnitude results

Bus Name	Voltage Magnitud [pu]								
	EMTP	CYMDIST	Method	EMTP	CYMDIST	Method	EMTP	CYMDIST	Method
	Phase A	Phase A	Phase A	Phase B	Phase B	Phase B	Phase C	Phase C	Phase C
0	1.000	1.000	1.000	1.000	1.000	1.000	1.000	1.000	1.000
TMP	0.996	0.996	0.996	0.996	0.996	0.996	0.996	0.996	0.996
1	0.993	0.993	0.993	0.994	0.994	0.994	0.993	0.993	0.993
2	0.944	0.944	0.944	0.948	0.948	0.948	0.944	0.944	0.944
3	0.886	0.886	0.886	0.896	0.896	0.897	0.885	0.885	0.886
4	0.840	0.841	0.840	0.855	0.855	0.856	0.839	0.839	0.840
5	0.840	0.841	0.840	0.855	0.855	0.856	0.839	0.839	0.840
6	0.839	0.840	0.840	0.855	0.855	0.856	0.839	0.839	0.839
7	0.828	0.829	0.829	0.840	0.840	0.840	0.823	0.823	0.824
8	-	-	-	0.840	0.840	0.840	-	-	-
9	0.839	0.840	0.839	-	-	-	-	-	-
10	0.839	0.840	0.839	-	-	-	-	-	-
11	0.837	0.838	0.838	-	-	-	-	-	-
12	-	-	-	0.948	0.948	0.948	-	-	-
13	0.827	0.829	0.828	0.838	0.838	0.839	0.822	0.822	0.823
14	0.806	0.807	0.807	0.810	0.810	0.811	0.790	0.790	0.791
15	0.805	0.807	0.806	0.810	0.810	0.810	0.789	0.789	0.790
16	-	-	-	0.810	0.810	0.810	-	-	-
17	0.768	0.769	0.768	0.760	0.760	0.761	0.734	0.734	0.735
18	0.768	0.769	0.768	0.760	0.760	0.761	0.734	0.734	0.735
19	0.764	0.766	0.765	0.755	0.755	0.756	0.729	0.729	0.730
20	-	-	-	0.755	0.755	0.756	-	-	-
21	0.765	0.766	0.766	0.757	0.757	0.758	0.731	0.731	0.732
23	0.761	0.762	0.762	0.750	0.750	0.751	0.722	0.722	0.724
24	0.760	0.762	0.761	0.749	0.749	0.750	0.722	0.722	0.723
25	0.760	0.761	0.761	0.749	0.749	0.749	0.721	0.721	0.723
26	0.760	0.761	0.761	0.749	0.749	0.749	0.721	0.721	0.723
27	0.760	0.761	0.761	0.749	0.749	0.749	0.721	0.721	0.723
28	-	-	-	0.748	0.748	0.749	-	-	-
29	0.761	0.762	0.761	0.750	0.750	0.750	0.722	0.722	0.724
30	0.760	0.761	0.761	0.749	0.749	0.750	0.722	0.722	0.723
31	0.760	0.761	0.761	0.748	0.748	0.749	0.721	0.721	0.723
32	0.760	0.761	0.761	0.748	0.748	0.749	0.721	0.721	0.723

From the table above, it can be observed that the largest voltage magnitude error is only 0.28%, even though the voltage in some nodes is quite low, which shows also the convergence robustness of the methodology.

Table 5.2 IEEE 34-Bus Test system voltage angle results

Bus Name	Voltage angle [degrees]								
	EMTP	CYMDIST	Method	EMTP	CYMDIST	Method	EMTP	CYMDIST	Method
	Phase A	Phase A	Phase A	Phase B	Phase B	Phase B	Phase C	Phase C	Phase C
0	0.0	0.0	0.0	-120.0	-120.0	-120.0	120.0	120.0	120.0
TMP	0.0	0.0	0.0	-120.0	-120.0	-120.0	120.0	120.0	120.0
1	0.0	0.0	0.0	-120.0	-120.0	-120.0	120.0	120.0	120.0
2	0.0	0.0	0.0	-119.9	-120.0	-120.0	120.2	120.1	120.1
3	0.1	0.0	0.0	-119.8	-119.9	-119.8	120.4	120.3	120.3
4	0.1	0.0	0.0	-119.7	-119.8	-119.7	120.6	120.5	120.5
5	0.1	0.0	0.0	-119.7	-119.8	-119.7	120.6	120.5	120.5
6	0.1	0.0	0.0	-119.7	-119.7	-119.7	120.6	120.5	120.5
7	0.2	0.1	0.1	-119.6	-119.7	-119.7	120.6	120.5	120.5
8	-	-	-	-119.6	-119.7	-119.7	-	-	-
9	0.1	0.0	0.0	-	-	-	-	-	-
10	0.1	0.0	0.0	-	-	-	-	-	-
11	0.0	0.0	0.0	-	-	-	-	-	-
12	-	-	-	-119.9	-120.0	-120.0	-	-	-
13	0.2	0.1	0.1	-119.6	-119.7	-119.7	120.6	120.5	120.5
14	0.3	0.2	0.2	-119.4	-119.5	-119.5	120.6	120.5	120.5
15	0.3	0.2	0.2	-119.4	-119.5	-119.5	120.6	120.5	120.5
16	-	-	-	-119.9	-119.5	-119.5			
17	0.6	0.5	0.5	-119.0	-119.1	-119.0	120.6	120.5	120.5
18	0.6	0.5	0.5	-119.0	-119.1	-119.0	120.6	120.5	120.5
19	0.6	0.5	0.6	-118.9	-119.0	-119.0	120.6	120.5	120.5
20	-	-	-	-119.9	-119.0	-119.0	-	-	-
21	0.6	0.5	0.5	-119.0	-119.1	-119.1	120.5	120.4	120.5
23	0.7	0.6	0.6	-118.8	-118.9	-118.9	120.6	120.5	120.5
24	0.7	0.6	0.6	-118.8	-118.9	-118.9	120.6	120.5	120.5
25	0.7	0.6	0.6	-118.8	-118.9	-118.9	120.6	120.5	120.5
26	0.7	0.6	0.6	-118.8	-118.9	-118.9	120.6	120.5	120.5
27	0.7	0.6	0.6	-118.8	-118.9	-118.9	120.6	120.5	120.5
28	-	-	-	-118.8	-118.9	-118.9	-	-	-
29	0.7	0.6	0.6	-118.8	-118.9	-118.9	120.6	120.5	120.5
30	0.7	0.6	0.6	-118.8	-118.9	-118.9	120.6	120.5	120.5
31	0.7	0.6	0.6	-118.8	-118.9	-118.9	120.6	120.5	120.5
32	0.7	0.6	0.6	-118.8	-118.9	-118.9	120.6	120.5	120.5

The results for voltage magnitude and phase angle are quite similar for the three methodologies. This first validation test corresponds to an unbalanced radial system with constant single-to-ground and three-phase constant power loads. The next case allows comparing and validating results for a more complex composed Transmission-Distribution system.

5.2 40-Bus Transmission and Distribution Test Case

Most load-flow solvers are able to model and simulate either balanced transmission or unbalanced line-transposed distribution networks, but few can integrate and simulate both systems at the same time. Large R/X ratios, line transposition, load unbalancing, meshed distribution networks, neutral wire representation, phase-to-phase, phase-to-neutral and phase-merged loads are among the typical features and devices found in real electrical networks which are not modeled by commercial load-flow software. EMTP-RV load-flow package is the exception and that is the reason for choosing it as the validation tool. The main difference between EMTP-RV and the proposed methodology is that EMTP-RV is a tool which has been developed as a multi-phase load-flow solver and the developed methodology, on the other hand, utilizes a positive-sequence solver. In fact, it could utilize any positive-sequence load-flow solver existing in the power energy industry. Figure 5.2 shows the 40-Bus EMTP-RV test case developed for validation purposes.

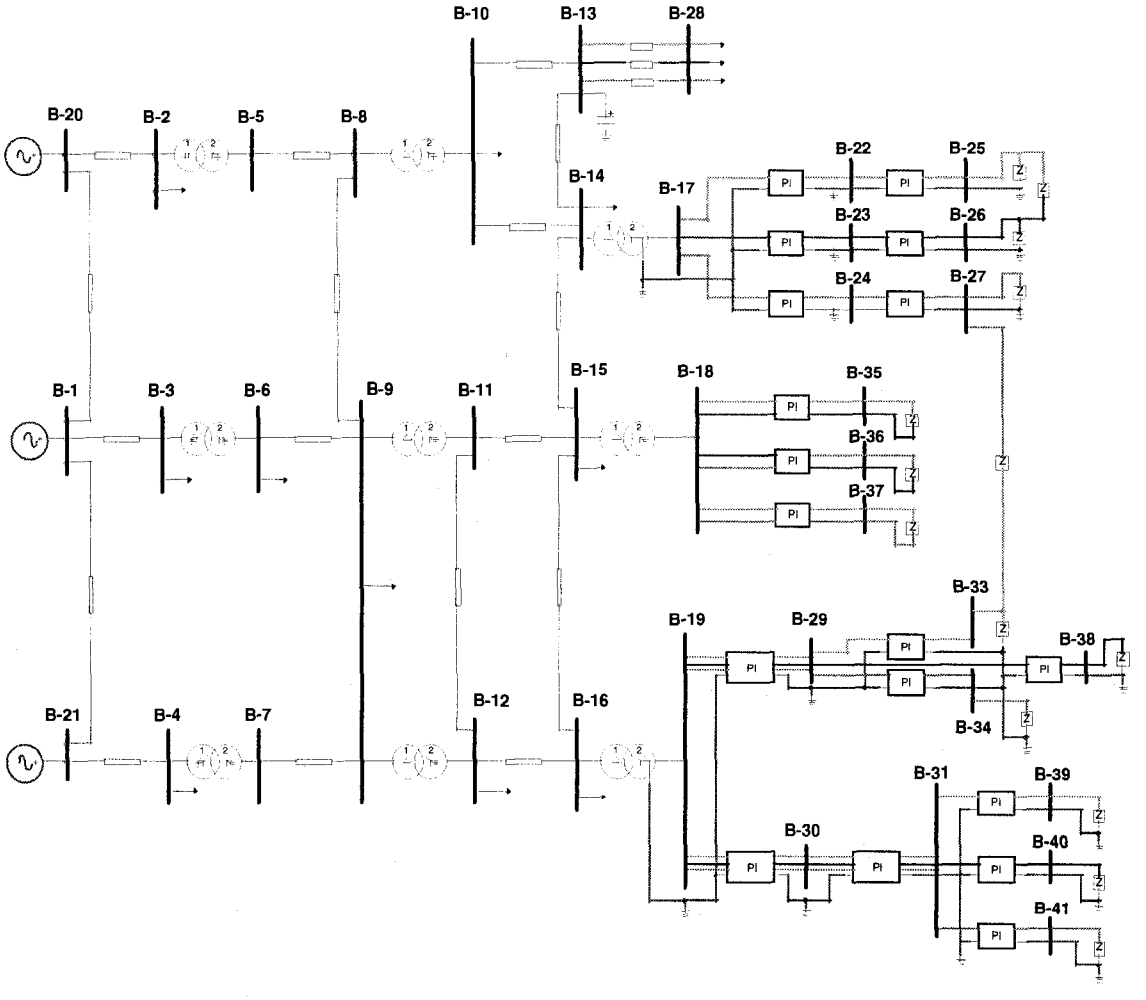

Figure 5.2 40-Bus Transmission-Distribution EMTP-RV model

The 40-Bus test case is composed of three areas defined as transmission, primary and secondary distribution networks. The system network includes:

- One slack and two PV generators feeding the system in 135 kV.
- Non-transposed coupled three-phase lines and three-phase constant power loads.
- Two 50 MVA grounded wye-grounded wye three-phase transformers to step down the voltage from 135 kV to 24.9 kV
- Three 10 MVA delta-grounded wye connected transformers to step down the voltage from 24.9 kV to 13.8 kV.

- One fixed three-phase 300-kVAR capacitor bank
- Three 5 MVA distribution transformers which step down the voltage from 13.8 kV to 400 V and 280 V.
- Both radial and meshed networks as well as phase-to-phase, phase-to-neutral RL loads were modeled in the distribution area, and the neutral wire was explicitly included in the distribution line models.

The results for the voltage magnitudes and angles obtained are listed in Table 5.3 and 5.4 for a convergence criterion of 10^{-6} MVA. The fast iterative backward-forward sweep solver is not included in this validation test due to its convergence and capability restrictions.

Table 5.3 40-Bus Test system voltage magnitude results

Bus Name	Voltage Magnitud [pu]					
	EMTP	Method	EMTP	Method	EMTP	Method
	Phase A	Phase A	Phase B	Phase B	Phase C	Phase C
BUS1	1.000	1.000	1.000	1.000	1.000	1.000
BUS2	1.000	1.000	1.000	1.000	1.000	1.000
BUS3	1.000	1.000	1.000	1.000	1.000	1.000
BUS4	1.000	1.000	1.000	1.000	1.000	1.000
BUS5	0.998	0.998	0.998	0.998	0.998	0.998
BUS6	0.997	0.997	0.997	0.997	0.997	0.997
BUS7	0.998	0.998	0.998	0.998	0.998	0.998
BUS8	0.987	0.987	0.991	0.991	0.989	0.989
BUS9	0.985	0.985	0.990	0.990	0.988	0.988
BUS10	0.983	0.983	0.984	0.984	0.979	0.979
BUS11	0.985	0.985	0.986	0.986	0.982	0.982
BUS12	0.984	0.984	0.986	0.985	0.981	0.981
BUS13	0.981	0.981	0.978	0.978	0.973	0.973
BUS14	0.980	0.980	0.979	0.979	0.974	0.974
BUS15	0.979	0.979	0.980	0.980	0.975	0.974
BUS16	0.978	0.978	0.980	0.980	0.975	0.975
BUS17	0.981	0.981	0.978	0.978	0.974	0.974
BUS18	0.980	0.980	0.978	0.978	0.974	0.974
BUS19	0.980	0.980	0.979	0.978	0.974	0.974
BUS20	1.000	1.000	1.000	1.000	1.000	1.000
BUS21	1.000	1.000	1.000	1.000	1.000	1.000
BUS22	0.951	0.954	-	-	-	-
BUS23	-	-	0.932	0.932	-	-
BUS24	-	-	-	-	0.943	0.945
BUS25	0.923	0.928	-	-	-	-
BUS26	-	-	0.885	0.887	-	-
BUS27	-	-	-	-	0.913	0.918
BUS28	0.980	0.980	0.976	0.976	0.970	0.970
BUS29	0.959	0.960	0.986	0.986	0.973	0.972
BUS30	0.976	0.976	0.976	0.976	0.969	0.969
BUS31	0.972	0.973	0.973	0.974	0.963	0.964
BUS33	0.903	0.905	-	-	-	-
BUS34	-	-	-	-	0.963	0.963
BUS35	0.961	0.961	0.948	0.948	-	-
BUS36	-	-	0.960	0.959	0.944	0.944
BUS37	0.950	0.949	-	-	0.955	0.955
BUS38	-	-	0.972	0.974	-	-
BUS39	0.947	0.950	-	-	-	-
BUS40	-	-	0.953	0.955	-	-
BUS41	-	-	-	-	0.935	0.938

Table 5.4 40-Bus Test system voltage angle results

Bus Name	Voltage angle [degrees]					
	EMTP	Method	EMTP	Method	EMTP	Method
	Phase A	Phase A	Phase B	Phase B	Phase C	Phase C
BUS1	0.0	0.0	-120.0	-120.0	120.0	120.0
BUS2	0.0	0.0	-120.0	-120.0	120.0	120.0
BUS3	0.0	0.0	-120.0	-120.0	120.0	120.0
BUS4	0.0	0.0	-120.0	-120.0	120.0	120.0
BUS5	-0.2	-0.2	-120.2	-120.2	119.8	119.8
BUS6	-0.4	-0.4	-120.4	-120.4	119.6	119.6
BUS7	-0.2	-0.2	-120.2	-120.2	119.8	119.8
BUS8	-0.9	-0.9	-120.9	-120.9	119.0	119.0
BUS9	-1.0	-1.0	-121.0	-121.0	118.9	118.9
BUS10	28.4	28.4	-91.8	-91.8	148.0	148.0
BUS11	28.6	28.6	-91.6	-91.6	148.4	148.4
BUS12	28.6	28.6	-91.6	-91.6	148.3	148.3
BUS13	28.1	28.1	-92.1	-92.1	147.4	147.4
BUS14	28.1	28.1	-92.1	-92.1	147.6	147.6
BUS15	28.1	28.1	-92.1	-92.1	147.7	147.7
BUS16	28.1	28.1	-92.1	-92.1	147.7	147.7
BUS17	58.0	58.0	-62.4	-62.4	177.9	177.9
BUS18	58.0	58.0	-62.3	-62.3	177.9	177.9
BUS19	58.0	58.0	-62.3	-62.3	178.0	178.0
BUS20	0.0	0.0	-120.0	-120.0	120.0	120.0
BUS21	0.0	0.0	-120.0	-120.0	120.0	120.0
BUS22	55.7	55.6	-	-	-	-
BUS23	-	-	-62.6	-62.9	-	-
BUS24	-	-	-	-	175.6	175.4
BUS25	53.4	53.1	-	-	-	-
BUS26	-	-	-62.9	-63.4	-	-
BUS27	-	-	-	-	173.1	172.8
BUS28	28.0	28.0	-92.3	-92.3	147.2	147.2
BUS29	57.1	57.1	-62.7	-62.7	178.3	178.3
BUS30	57.6	57.6	-62.5	-62.5	177.4	177.4
BUS31	57.1	57.1	-62.7	-62.7	176.9	176.8
BUS33	56.5	56.1	-	-	-	-
BUS34	-	-	-	-	177.9	177.9
BUS35	56.6	56.6	-62.1	-62.1	-	-
BUS36			-63.8	-63.8	178.2	178.2
BUS37	58.3	58.3	-	-	176.5	176.5
BUS38	-	-	-63.2	-63.2	-	-
BUS39	56.2	56.1	-	-	-	-
BUS40	-	-	-63.4	-63.5	-	-
BUS41	-	-	-	-	175.9	175.7

The results obtained with the proposed methodology are quite similar to those obtained with EMTP-RV. The maximum voltage magnitude mismatch found was 0.6% for the buses involving phase-merged loads. This small round-off errors exhibited can be significantly minimized by considering a small convergence tolerance, and large

numerical precision for loads and impedances parameters, above all for systems with large nominal voltage ratio defined as the division between the maximum and the minimum voltage level in the system. Voltage ratios for isolated transmission or distribution systems can vary by 10 to 30 times, but a composed transmission-distribution systems such as the 40-Bus test case presented above can reach voltage ratios between 500 and 3,000 times. Another way to minimize this round-off error is by using an intermediate system base voltage for the per-unit data calculation.

Only two iterations are required to reach the solution for both EMTP-RV and the proposed methodology.

5.3 2,600-Bus Distribution Test Case

The purpose of this test case, whose diagram is shown in figure 5.3, is to compare the performance and robustness of the methodology with EMTP-RV and CYMDIST. As it was mentioned before, this test system corresponds to a large meshed, ideally-transposed, and load unbalanced distribution network. The performance has been tested on a Pentium 4, 2GHz.-speed processor and 512MB-memory computer. The simulation time and number of iteration for each solver are presented in table 5.5.

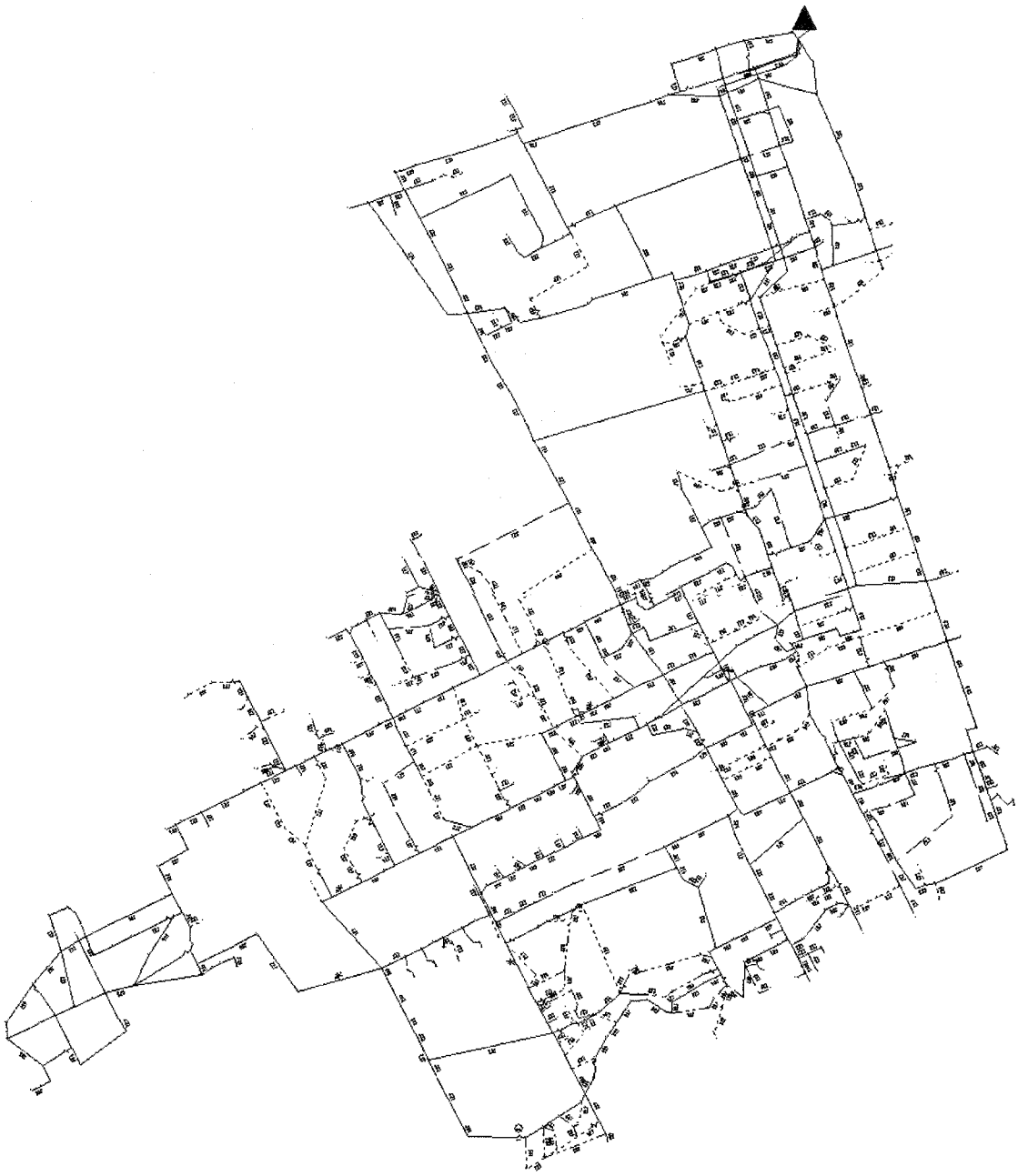

Figure 5.3 2,600-Bus Distribution Test Case System

Table 5.5 2,600-Bus Distribution test performance results

Solver	Simulation time [Sec.]	Number of iterations -
CYMDIST	8.0	77
EMTP- RV	19.0	3
Method	27.0	4

The simulation time presented in table 5.5 includes the data reading time, which is not minor for large networks. Considering this and taking into account that the proposed methodology has not been optimized in terms of programming, the simulation time seems to be quite reasonable. The fast iterative sweep solver presents the lowest simulation time, but a largest number of iterations. EMTP-RV takes a smaller amount of time on data reading, but a longer time for the iteration process in comparison with the proposed methodology, which seems to be an advantage for the latter taking into account that the data reading process can be easily optimized. The robustness of EMTP-RV and the proposed methodology is quite similar and much better than that of the fast solver taking into account the high number of iterations required for the latter to converge. The largest mismatch found for voltage magnitudes was lower than 0.1%.

6 CONCLUSIONS AND FUTURE DEVELOPMENTS

The present research work has involved the development of a methodology for solving multi-phase load-flow analysis using an existing positive-sequence load-flow solver based on the Newton's methodology with a direct numerical solver and optimal ordering. The proposed methodology has been presented in previous works, but none of them has been implemented in a positive-sequence based load-flow program.

The integration of both transmission and distribution systems in one simulation as well as the ability of accurate modeling all typical devices found in real transmission and distribution systems are the major contributions of this research work. The principal advantages of the proposed methodology can be summarized as follows:

- The inherent capability of solving multi-phase systems, which is very attractive for distribution networks applications involving explicit neutral wire and ground representation. Multi-phase systems include line sections with any combination of phase conductors and neutral wires such as single-phase, single-phase plus neutral, two-phase, two-phase plus neutral, three-phase, three-phase plus neutral, and so on.
- The capability of modeling parallel multi-phase circuits with their corresponding electromagnetic couplings.
- Explicit representation of different types of loads such as single, double or three-phase are accepted.
- Delta- or wye-connected loads being either balanced or unbalanced can be modeled.
- Ideally transposed and non-transposed lines can be modeled with this methodology due to its ability of representing electromagnetic couplings existing between phases and nearby circuits.
- The capability of simulating large systems including both radial and highly meshed networks thanks to its matrix formulation and robust convergence properties.

- All kinds of transformers connection can be represented with this methodology including unusual connection found in distribution networks such as open wye or delta connection, and mid-tap transformer.
- Large voltage ratios (V_{max}/V_{min}) as well as large X/R ratios for the line parameters are also supported.
- The capability of modeling and simulating large composed transmission and distribution systems, and complex configuration such as phase-merged loads, which are loads connected between phases of different branches or feeders.
- Other devices such as shunt and series compensation and voltage-controlled devices can be also represented.

The simulation results presented in chapter 5 have shown to be the very accurate. The highest voltage mismatch found is under the 0.2% and it could rise up to 0.5% for large voltage ratios in the simulated systems. Nonetheless, this small mismatch can be eliminated by considering a larger precision in the per-unit parameters computing, minimizing the round-off numerical errors. The number of iterations is low and very similar to what is obtained by EMTP-RV, showing the high robustness of the presented methodology. The test performed for the 2,600-bus case has shown that the simulation time reached by the developed algorithm close to the time exhibited by EMTP-RV. The simulation time measured for all the test cases included both the data reading and the simulation time.

Future developments can be conducted on several topics. One of them is the modeling of voltage-controlled devices that, although excluded from this work, can be easily added by the means of an iterative process. In addition, much more efficient programming algorithms could be investigated and implemented in order to improve the performance of the proposed methodology for large systems simulations.

7 REFERENCES

[1] J. Mahseredjian, S. Dennetière, L. Dubé, B. Khodabakhchian, L. Gérin-Lajoie, "On a new approach for the simulation of transient in power systems", International Conference on Power Systems Transients (IPST'05), Montréal, Canada, June, 2005.

[2] W. Kersting, "Distribution systems modeling and analysis", CRC Press LLC, CA, USA, 2002.

[3] J. D. Duncan and M. S. Sarma, "Power System Analysis and Design", Brooks/Cole, 3rd edition, California, USA, 2003.

[4] L. Powell, "Power Systems Load Flow Analysis", McGraw-Hill, 1st edition, NY, USA, 2005.

[5] B. Stott and O. Alsac, "Fast Decoupled Load Flow", IEEE Transactions on Power Apparatus and Systems, Vol. PAS-93, N°3, May 1974, pp. 859-869.

[6] A. Keyhani, A. Abur, and S. Hao, "Evaluation of power flow techniques for personal computers", IEEE Transactions on Power Systems, Volume 4, N°2, May 1989, pp. 817-826.

[7] M. H. Haque, "Efficient load flow methods for distribution systems with radial or mesh configuration", IEE Proceedings Gener. Trans. Distrib., Vol. 143, N°1, January 1996, pp. 33-38.

[8] D. Shirmohammadi, H. Hong, A. Semlyen, and G. Luo, "A Compensation-Based Power Flow Method for Weakly Meshed Distribution and Transmission Networks", IEEE Transactions on Power Systems, Vol. 3, May 1988, pp. 753-762.

[9] B. Stott, "Review of load-flow calculation methods", Proceedings of the IEEE, Volume 62, N°7, July 1974, pp. 916-929.

[10] S. Ghosh and D. Das, "Method for load-flow solution of radial distribution networks", IEE Proceedings Gener. Trans. Distrib., Vol. 146, N°6, November 1999, pp. 641-648.

[11] E. O. I. Elgerd, "Electric energy system theory", McGraw-Hill, 2nd edition, NY, USA, 1982.

[12] W. F. Tinney and C. E. Hart, "Power Flow Solution by Newton's Method", IEEE Transaction on Power Apparatus and Systems, Vol. PAS-86, N°11, November 1967, pp. 1449-1460.

[13] W. F. Tinney and J. W. Walker, "Direct Solutions of Sparse Network Equations by Optimally Ordered Triangular Factorization", Proceeding of the IEEE, Vol. 55, N°11, November 1967, pp. 1801-1809.

[14] M. Crow, "Computational Methods for Electric Power Systems", CRC Press LLC, Florida, USA, 2003.

[15] P. R. Amestoy, T. A. Davis, and I. S. Duff, "An Approximate Minimum Degree Ordering Algorithm", SIAM J. Matrix Analysis and Applications, Vol. 17 N°2, June 1985, pp. 141-153.

[16] F. de Leon and A. Semlyen, "Iterative solvers in the Newton power flow problem: preconditioners, inexact solutions and partial Jacobian updates", IEE Proceedings Gener. Trans. Distrib., Vol. 149, N°4, July 2002, pp. 479-484.

[17] Y. Saad, "Iterative Methods for Sparse Linear Systems", Society for Industrial and Applied Mathematics, 2nd edition, PA, USA, April 2003.

[18] K. A. Birt, J. J. Graffy, J. D. McDonald, and A. H. El-Abiad, "Three phase load flow program", IEEE Transactions on Power Apparatus and Systems, Vol. 95, N°1, Part 1, January 1976, pp. 59-65.

[19] B. C. Smith and J. Arrillaga, "Improved three-phase load flow using phase and sequence components ", IEE Proceedings Gener. Trans. Distrib., Vol. 145, N°3, May 1998, pp. 245-250.

[20] H. Le Nguyen, "Newton-Raphson method in complex form", IEEE Transactions on Power Systems, Vol. 12, N°3, August 1997, pp. 1355-1359.

[21] A. V. Garcia and M. G. Zago, " Three-phase fast decoupled power flow for distribution networks", IEE Proceedings Gener. Trans. Distrib., Vol. 143, N°2, March 1996, pp. 188-192.

[22] R. M. Ciric, A. P. Feltrin, L. F. Ochoa, "Power flow in four-wire distribution networks-general approach", IEEE Transactions on Power Systems, Vol. 18, N°4, November 2003, pp. 1283-1290.

[23] C. S. Cheng and D. Shirmohammadi, "A three-phase power flow method for real-time distribution systems analysis", IEEE Transaction on Power Systems, Vol. 10, N°2, May 1995, pp. 671-679.

[24] V. M. da Costa, N. Martins, J. L. R. Pereira, "Developments in the Newton Raphson power flow formulation based on current injections", IEEE Transactions on Power Systems, Vol. 14, N°4, November 1999, pp. 1320-1326.

[25] P. A. N. Garcia, J. L. R. Pereira, "Three-Phase Power Flow Calculations Using the Current Injection Method", IEEE Transactions on Power Systems, Vol. 15, N°2, May 2000, pp. 508-514.

[26] D. R. R. Penido, L. R. Araujo, J. L. R. Pereira, P. A. N. Garcia, S. Carneiro, "Four wire Newton-Raphson power flow based on the current injection method", Power Systems Conference and Exposition, 2004. IEEE PES 10-13, Vol. 1, October 2004, pp. 239-242

[27] M. Monfared, A. M. Daryani, M. Abedi, "Three Phase Asymmetrical Load Flow for Four-Wire Distribution Networks", Power Systems Conference and Exposition, 2006, IEEE PES, October-November 2006, pp. 1899-1903.

[28] A. G. Bhutad, S. V. Kulkarni, S. A. Khaparde, "Three-phase load flow methods for radial distribution networks", TENCON 2003. Conference on Convergent Technologies for Asia-Pacific Region, Vol. 2, October 2003, pp. 781-785.

[29] B. K. Chen, M. S. Chen, R. R. Shoults, C. C. Liang, "Hybrid three phase load flow", IEE Proceedings-Generation, Transmission and Distribution, Vol. 137, N°3, May 1990, pp. 177-185.

[30] J. H. Teng, "A Modified Gauss-Seidel Algorithm of Three-phase power flow Analysis in Distribution Networks", Electrical Power and Energy Systems, Vol. 24, 2002, pp. 97-102.

[31] A. F. Glimn and G. W. Stagg, "Automatic Calculation of Load Flows", AIEEE Transactions on Power Apparatus and Systems, Vol. 76, pt. III, 1957, pp. 817-828.

[32] J. Mahseredjian, "Multiphase Load-flow Method", Power systems graduate course notes, École Polytechnique de Montréal, Winter 2005.

[33] M. Abdel-Akher, K. Mohamed, and A. H. Abdul Rashid, "Improved Three-Phase Power-Flow Methods Using Sequence Components", IEEE Transactions on Power Systems, Vol. 20, N°3, August 2005, pp. 1389-1397.

[34] J. H. Teng, "A network-topology-based three-phase load flow for distributions systems", Proceedings Natl. Sci. Counc. ROC(A), Vol. 24 N°4, 2000, pp. 259-264.

[35] F. L. Alvarado, "Formation of Y-node using the primitive Y-node concept", IEEE Transaction on Power Apparatus and Systems, PAS-101:12, December 1982, pp. 4563-4572.

[36] T. H. Chen, M. S. Chen, K. J. Hwang, P. Kotas, and E. A. Chebli, "Distribution system power flow analysis: a rigid approach", Power Delivery, IEEE Transactions on Vol. 6, N°3, July 1991, pp. 1146-1152.

[37] H. A. Smolleck, and R. R. Shoults, "A straightforward method for incorporating mutually-coupled circuits into the bus admittance matrix using the concept of artificial branches", IEEE Transactions on Power Systems, Vol. 5, N°2, May 1990, pp. 486-491.

[38] W. H. Kersting, and W. H. Phillips, "Distribution feeder line models", IEEE Transactions on Industry Applications, Vol. 31, N°4, July-August 1995, pp. 715-720.

[39] T. H. Chen, M. S. Chen, T. Inoue, P. Kotas, and E. A. Chebli, "Three-phase cogenerator and transformer models for distribution system analysis", IEEE Transactions on Power Delivery, Vol. 6, N°4, October 1991, pp. 1671-1681.

[40] Z. Wang, F. Chen, and J. Li, "Implementing transformer nodal admittance matrices into backward/forward sweep-based power flow analysis for unbalanced

radial distribution systems", IEEE Transactions on Power Systems, Vol. 19, N°4, November 2004, pp. 1831-1836.

[41] P. Xiao, D. C. Yu, Y. Wei, "A unified three-phase transformer model for distribution load flow calculations", IEEE Transactions on Power Systems, Vol. 21, N°1, February 2006, pp. 153-159.

[42] T. H. Chen, J. D Chang, "Open wye-open delta and open delta-open delta transformer models for rigorous distribution system analysis", IEE Proceedings-Generation, Transmission and Distribution, Vol. 139, N°3, May 1992, pp. 227-234.

[43] T. H. Chen, J. D Chang, Y. L. Chang, "Models of grounded mid-tap open-wye and open-delta connected transformers for rigorous analysis of a distribution system", IEE Proceedings on Generation, Transmission and Distribution, Vol. 143, N°1, January 1996, pp. 82-88.

[44] T. H. Chen, W. C. Yang, "Modeling and analysis of three-phase four-wire distribution transformers with mid-tap on the secondary side", International Conference on Energy Management and Power Delivery, Vol. 2, March 1998, pp. 723-727.

[45] R. Bijwe, "Power systems equivalent for distribution power flows", Indian Institute of Technology Delhi, ND, India, Paper intended for IEEE Transactions, 2006.

[46] IEEE Working Group, "Common Data Format for the Exchange of Solved Load Flow Data", Transactions on Power Apparatus and Systems, Vol. PAS-92, No. 6, November/December 1973, pp. 1916-1925.

[47] W. H. Kersting, "Radial distribution test feeders", IEEE Transaction on Power Systems, Vol. 6, August 1991, pp. 975-985.

APPENDIX A: Data for illustrative case of section 4.6

EMTP-RV Nest list data file

```
Circuit.Diagram=Sample Test 4_6.ecf;
steadystate=0;
LoadFlow=1;
TestAbsCorrection_x=1;
TestAbsDxOverx=0;
! Subcircuit definitions
<xfmr_DYg_p30_unitO_ecf686ce;4;i,j,k,m,
_RLC;RL1;2;2;i,s36,
#R1#,#L1#,0,0,0,
#W1_scope#,
_RLC;RL2;2;2;s31,k,
#R2#,#L2#,0,0,0,
#W2_scope#,
_Tr0;Tygyg;4;4;s36,j,s31,m,
#Ratio#,,,
_x_Lnonl;Lmag;2;2;s36,j,
1,#Phi0#,1e-08,
#Lmag_scope#,
#ILnonl# #PhiLnonl#
_x_Rmag;R1;2;2;s36,j,
#Rm#,,,,,
<DYgp30_O_b34e1b4e;6;DELTAa,DELTAb,DELTAc,Ya,Yb,Yc,
@xfmr_DYg_p30_unitO_ecf686ce;xfmr_A;4;DELTAa,DELTAb,Ya,,
Phi0=Phiss01
@xfmr_DYg_p30_unitO_ecf686ce;xfmr_B;4;DELTAb,DELTAc,Yb,,
Phi0=Phiss02
@xfmr_DYg_p30_unitO_ecf686ce;xfmr_C;4;DELTAc,DELTAa,Yc,,
```

Phi0=Phiss03
@DYgp30_O_b34e1b4e;DYg_1;6;BUS2a,BUS2b,BUS2c,BUS3a,BUS3b,B
US3c,
R1=3.02342544;
L1=0.039696078294873566;
Rm=0;
PhiLnonl=[0];
ILnonl=[0];
Lnonl='Exclude';
Rmag='Exclude';
R2=0.021167999999999992;
L2=0.00027792535388135233;
Phiss01=0;
Phiss02=0;
Phiss03=0;
Ratio=0.25102185616940253;
Lmag_scope='';
W1_scope ='';
W2_scope ='';
_PI;PI1a;6;2;BUS1a,BUS2a,
3,1,0,1Ohm,0,1uS,0,1,1,1,1,
_PI;PI1b;6;2;BUS1b,BUS2b,
_PI;PI1c;6;2;BUS1c,BUS2c,
0.4576 0.1560 0.1535
0.1560 0.4666 0.1580
0.1535 0.1580 0.4615
1.0780 0.5017 0.3849
0.5017 1.0482 0.4236
0.3849 0.4236 1.0651

5.6712 -1.8362 -0.7034

-1.8362 5.9774 -1.1690

-0.7034 -1.1690 5.3911

0 0 0

0 0 0

0 0 0

_PQload;Load1;1;1;BUS3a,

6kVRMSLL,500kW,0,250kVAR,0,60,1,0,

_PQload;Load5;1;1;BUS3b,

6kVRMSLL,350kW,0,150kVAR,0,60,1,0,

_PQload;Load6;1;1;BUS3c,

6kVRMSLL,620kW,0,300kVAR,0,60,1,0,

_Slack;LF1a;3;1;BUS1a,

60,13.8kVRMSLL,0,1,1,1Ohm,1,,

_Slack;LF1b;3;1;BUS1b,

_Slack;LF1c;3;1;BUS1c,

0.1 0.1 0.1

0.1 0.1 0.1

_Vsine;AC1a;3;1;BUS1a,

13.8kVRMSLL,60,0,-1,1E15,

_Vsine;AC1b;3;1;BUS1b,

13.8kVRMSLL,60,-120,-1,1E15,

_Vsine;AC1c;3;1;BUS1c,

13.8kVRMSLL,60,120,-1,1E15,

Ref=Slack:LF1

Modified IEEE Multi-phase data file

****NEW CASE COMES FROM SAMPLE TEST CHAP 4-6.NET FILE****

BUS DATA FOLLOWS 9 ITEMS

1 BUS1 A 1 3 3 13.8 1.00000 0.00000 0.0000 0.0000 10.0000 5.0000

2 BUS1 B 1 3 3 13.8 1.00000 -120.000 0.0000 0.0000 10.0000 5.0000

3 BUS1 C 1 3 3 13.8 1.00000 120.000 0.0000 0.0000 10.0000 5.0000

4 BUS2 A 1 3 0 13.8 1.00000 0.00000 0.0000 0.0000 0.0000 0.0000

5 BUS2 B 1 3 0 13.8 1.00000 -120.000 0.0000 0.0000 0.0000 0.0000

6 BUS2 C 1 3 0 13.8 1.00000 120.000 0.0000 0.0000 0.0000 0.0000

7 BUS3 A 1 3 1 13.8 1.00000 0.00000 0.5000 0.2500 0.0000 0.0000

8 BUS3 B 1 3 1 13.8 1.00000 -120.000 0.3500 0.1500 0.0000 0.0000

9 BUS3 C 1 3 1 13.8 1.00000 120.000 0.6200 0.3000 0.0000 0.0000

-999

BRANCH DATA FOLLOWS 1 ITEMS

BUS1 BUS2 LINE1 ABC 1 3 0.457600 0.156000 0.153500 0.000000
0.000000 0.156000 0.466600 0.158000 0.000000 0.000000 0.153500 0.158000
0.461500 0.000000 0.000000 0.000000 0.000000 0.000000 0.000000 0.000000
0.000000 0.000000 0.000000 0.000000 0.00000
1.078000 0.501700 0.384900 0.000000 0.000000 0.501700 1.048200 0.423600
0.000000 0.000000 0.384900 0.423600 1.065100 0.000000 0.000000 0.000000
0.000000 0.000000 0.000000 0.000000 0.000000 0.000000 0.000000 0.000000
0.0000
5.671200 -1.83620 -0.70340 0.000000 0.000000 -1.83620 5.977400 -1.16900
0.000000 0.000000 -0.70340 -1.16900 5.391100 0.000000 0.000000 0.000000
0.000000 0.000000 0.000000 0.000000 0.000000 0.000000 0.000000 0.000000
0.000000

-999

IMPEDANCE LOADS DATA FOLLOWS 0 ITEMS

-999

TRANSFORMER DATA FOLLOWS 1 ITEMS

BUS2 BUS3 Trasf1 ABC DYg 1 3 2.00000 13.8000 6.00000 0.06000

5.00000 1.00000 1.00000

-999

END OF DATA

Positive-Sequence solver LFNetfile data file

Ins_Bus,BUS1A,0,13.80,1.00000,0.000,1.1,0.9,0,0
Ins_Bus,BUS1B,0,13.80,1.00000,-120.000,1.1,0.9,0,0
Ins_Bus,BUS1C,0,13.80,1.00000,120.000,1.1,0.9,0,0
Ins_Bus,BUS2A,0,13.80,1.00000,0.000,1.1,0.9,0,0
Ins_Bus,BUS2B,0,13.80,1.00000,-120.000,1.1,0.9,0,0
Ins_Bus,BUS2C,0,13.80,1.00000,120.000,1.1,0.9,0,0
Ins_Bus,BUS3A,0,13.80,1.00000,0.000,1.1,0.9,0,0
Ins_Bus,BUS3B,0,13.80,1.00000,-120.000,1.1,0.9,0,0
Ins_Bus,BUS3C,0,13.80,1.00000,120.000,1.1,0.9,0,0
Ins_Load,load,BUS3A,1.5000,0.7500
Ins_Load,load,BUS3B,1.0500,0.4500
Ins_Load,load,BUS3C,1.8600,0.9000
Ins_SW,Gener,BUS1A,10.0000,13.8000,0.000,0.1,0.1,0
Ins_SW,Gener,BUS1B,10.0000,13.8000,-120.000,0.1,0.1,0
Ins_SW,Gener,BUS1C,10.0000,13.8000,120.000,0.1,0.1,0
Ins_Line,line3Ph,BUS1A,BUS2A,0.3878,0.8041,8.2108,0,0
Ins_Line,line3Ph,BUS1B,BUS2B,0.3917,0.7526,8.9826,0,0
Ins_Line,line3Ph,BUS1C,BUS2C,0.3837,0.8547,7.2635,0,0
Ins_Line,line3Ph,BUS1A,BUS1B,1.3443,1.9699,0,0,0
Ins_Line,line3Ph,BUS1B,BUS1C,1.5025,2.8497,0,0,0
Ins_Line,line3Ph,BUS1C,BUS1A,1.4733,3.8864,0,0,0
Ins_Line,line3Ph,BUS2A,BUS2B,1.3443,1.9699,0,0,0
Ins_Line,line3Ph,BUS2B,BUS2C,1.5025,2.8497,0,0,0
Ins_Line,line3Ph,BUS2C,BUS2A,1.4733,3.8864,0,0,0
Ins_Line,line3Ph,BUS1A,BUS2B,-1.3443,-1.9699,0,0,0
Ins_Line,line3Ph,BUS1A,BUS2C,-1.4734,-3.8864,0,0,0
Ins_Line,line3Ph,BUS1B,BUS2A,-1.3443,-1.9699,0,0,0
Ins_Line,line3Ph,BUS1B,BUS2C,-1.5025,-2.8497,0,0,0

Ins_Line,line3Ph,BUS1C,BUS2A,-1.4734,-3.8864,0,0,0

Ins_Line,line3Ph,BUS1C,BUS2B,-1.5025,-2.8497,0,0,0

Ins_Line,DYg3Ph,BUS2A,BUS2B,3.36135,16.80676,0,0,0

Ins_Line,DYg3Ph,BUS2B,BUS2C,3.36135,16.80676,0,0,0

Ins_Line,DYg3Ph,BUS2C,BUS2A,3.36135,16.80676,0,0,0

Ins_Line,DYg3Ph,BUS2A,BUS3A,1.94068,9.70339,0,0,0

Ins_Line,DYg3Ph,BUS2B,BUS3B,1.94068,9.70339,0,0,0

Ins_Line,DYg3Ph,BUS2C,BUS3C,1.94068,9.70339,0,0,0

Ins_Line,DYg3Ph,BUS2A,BUS3C,-1.94068,-9.70339,0,0,0

Ins_Line,DYg3Ph,BUS2B,BUS3A,-1.94068,-9.70339,0,0,0

Ins_Line,DYg3Ph,BUS2C,BUS3B,-1.94068,-9.70339,0,0,0

Ins_Shunt,DYg3PhShunt,BUS3A,6.53721,-32.68602

Ins_Shunt,DYg3PhShunt,BUS3B,6.53721,-32.68602

Ins_Shunt,DYg3PhShunt,BUS3C,6.53721,-32.68602